Huntingtin function during zebrafish (*Danio rerio)* development

A thesis submitted in requirement for the degree of Doctor of Philosophy, December 2009

Tanya L. Henshall, B.Sc (Hons)

School of Molecular and Biomedical Science, Discipline of Genetics,

ARC Special Centre for the Molecular Genetics of Development,

The University of Adelaide.

Table of Contents

List of Figures and Tables

*Many figures from this list contain data and/or images which are reproduced from [229]

Statement of Originality

This work contains no material which has been accepted for the award of any other degree or diploma in any university or other tertiary institution to Tanya Henshall and, to the best of my knowledge and belief, contains no material previously published or written by another person, except where due reference has been made in the text.

I give consent to this copy of my thesis when deposited in the University Library, being made available for loan and photocopying, subject to the provisions of the Copyright Act 1968. The author acknowledges that copyright of published works contained within this thesis (as listed below*) resides with the copyright holder(s) of those works.

I also give permission for the digital version of my thesis to be made available on the web, via the University's digital research repository, the Library catalogue, the Australasian Digital Theses Program (ADTP) and also through web search engines, unless permission has been granted by the University to restrict access for a period of time.

* Henshall, T. L., Tucker, B., Lumsden, A. L., Nornes, S., Lardelli, M. T. and Richards, R. I., Selective neuronal requirement for huntingtin in the developing zebrafish. *Hum Mol Genet* 2009 18: 4830-4842.

Tanya Lynn Henshall

Acknowledgements

Firstly, I would like to thank my supervisors, Professor Robert Richards and Dr Michael Lardelli for the support and encouragement throughout this PhD.

Many thanks to members of the Richards and Lardelli labs for all of their friendship and continued support. In particular I would like to thank Amanda Lumsden, Morgan Newman, Sonia Dayan and Saumya Samaraweera. I know we will always be great friends!

I would also like to acknowledge the help of my friends and family (especially my Mum and Dad) for all of their support. Without your love, I would most certainly not have achieved as much as I have. Thank you all so much.

Tanya xox

Abbreviations

aa	amino acid
acridine orange	acridine orange hemi (zinc chloride) salt
amp	ampicillin
BCIP	5-bromo-4-chloro-3-indolyl phosphate
bh	basihyal (cartilage)
bp	base pairs
BDNF	brain derived neurotrophic factor
cDNA	complementary DNA
ch	ceratohyal (cartilage)
*c*MO	standard control morpholino
Ct	cycle threshold
DASPEI	2-(4-(dimethylamino)styryl)-N-ethylpyridinium iodide
DEPC	diethylpyrocarbonate
DF	degrees of freedom
DiI	1,1'-dioctadecyl-3,3,3'3'-tetramethylindocarbocyanine perchlorate ($DiIC_{18}(3)$)
DMF	dimethylformamide
DMSO	dimethylsulphoxide
DNA	deoxyribonucleic acid
dNTPs	deoxynucleotide triphosphates
dpf	days post fertilization
EDTA	ethylenediamine tetra-acetic acid
ef1a	elongation factor 1a
EGFP	enhanced green fluorescent protein
emx3	empty spiracles homeobox 3
ES	embryonic stem (as in ES cells)
EtBr	ethidium bromide
fgf8	fibroblast growth factor 8
GABA	γ-aminobutyric acid
HAP	huntingtin associated protein
HD	Huntington's disease

*hd*MO	morpholino antisense to zebrafish htt mRNA (as in *hd*MO1 and *hd*MO2)
HIP	huntingtin interacting protein
htt	huntingtin
hpf	hours post fertilization
hs	hyosymplectic cartilage
Kb	kilobase pairs
kDa	kilodalton
m	Meckel's cartilage
*mc*MO1	5 base mismatch of the *hd*MO1 antisense sequence
μM	micromolar
ml	millilitre
MLK2	mixed lineage kinase 2
mM	millimolar
morpholino/MO	morpholino oligonucleotide
MQ	milli-Q
mRNA	messenger RNA
NBT	nitro blue tetrazolium chloride
ng	nanogram
nl	nanolitre
NMDA	*N*-methyl-D-aspartic acid
nM	nanomolar
ntl	no tail
oligo	oligonucleotide primer
omp	olfactory marker protein
ORF	open reading frame
OSN	olfactory sensory neuron
otx2	orthodenticle homolog 2
p(3-7)	pharyngeal arch (3-7)
PBS	phosphate buffered saline
PBS-T	PBS with 0.1% tween-20
pbx2	pre-B-cell leukemia transcription factor 2
PCR	polymerase chain reaction
pmol	picomoles
polyQ htt	huntingtin with a pathogenic number of glutamine repeats

pq	palatoquadrate (cartilage)
PTU	1-phenyl-2-thiourea
qPCR	quantitative real-time PCR
RA	retinoic acid
REST/NRSF	RE-1 silencing transcription factor/neuron-restrictive silencer factor
RNA	ribonucleic acid
rpm	revolutions per minute
SDS	sodium dodecyl sulphate
six1	sine oculis homeobox homologue
SSC	sodium chloride/sodium citrate buffer
TBS-T	tris-buffered saline with 0.1% Tween-20
TUNEL	terminal deoxynucleotide transferase (TdT)-mediated dUTP nick-end labeling
UTR	untranslated region

Abstract

Huntington's disease shares a common molecular basis with eight other neurodegenerative diseases: expansion of an existing polyglutamine tract. In each case, this repeat tract occurs within otherwise unrelated proteins. These proteins show widespread and overlapping patterns of expression in the brain and yet the diseases are distinguished by neurodegeneration in a specific subset of neurons that are most sensitive to the mutation. It has therefore been proposed that expansion of the polyglutamine region in these genes may result in perturbation of the normal function of the respective proteins, and that this perturbation in some way contributes to the neuronal specificity of these diseases. The normal functions of these proteins have therefore become a focus of investigation as potential pathogenic pathways. Here, synthetic antisense morpholinos have been used to inhibit the translation of huntingtin protein during early zebrafish development. The results obtained show the effects of huntingtin loss-of-function on the developing nervous system, including distinct defects in morphology of the lateral line neuromasts, olfactory placode and branchial arches. The potential common origins of these defects were explored, revealing impaired formation of the anterior-most region of the neural plate as indicated by reduced pre-placodal and telencephalic gene expression with no effect on mid- or hindbrain formation. These investigations demonstrate a specific 'rate-limiting' role for huntingtin in formation of the telencephalon and the pre-placodal region, and differing levels of requirement for huntingtin function in specific nerve cell types.

CHAPTER 1: INTRODUCTION

1.1 Polyglutamine diseases

The polyglutamine repeat diseases comprise a group of nine neurodegenerative diseases including Huntington's disease (HD), spinobulbar muscular atrophy (SBMA), dentatorubral pallidoluysian atrophy (DRPLA) and several forms of spinocerebellar ataxia (SCA1-3, 6, 7 and 17) [1, 2]. Each of these diseases is caused by the expansion of a CAG repeat region (encoding polyglutamine) within nine distinct and unrelated genes. In each case, expansion of the CAG repeat region beyond a pathogenic threshold number results in progressive neurodegeneration.

Typically, polyglutamine repeat disease symptoms manifest later in life. The reason why this occurs is still not clear. However, in all polyglutamine diseases, the severity of the disease is related to the length of the repeat expansion, as longer repeats cause a more severe phenotype and earlier age of onset [3].

1.2 Huntington's disease

HD is the most common of the polyglutamine repeat diseases, affecting approximately 1 in 10,000 individuals in most populations of European origin [4]. HD results from expansion of an unstable CAG repeat in the 5' region of a novel 4p16.3 gene called *huntingtin* (*HTT*) [5, 6]. The expanded CAG repeat region in the *HTT* gene encodes a long stretch of glutamine residues starting at amino acid 17 of the protein product known as huntingtin (htt; described further in Section 1.3.2). In the general population, glutamine repeats within htt number between 11 and 34, however a gene with greater than 40 repeats is termed an HD allele [7].

The mean age of onset of HD is around 40 years, which is termed adult onset. These patients usually have expansions ranging from 40-50 CAG repeats. As with other CAG repeat

diseases, HD shows anticipation. This means that transmission of the expanded HD allele to an offspring may result in expansion of the CAG repeat region. Expansion of the CAG region is more commonly seen upon paternal transmission than maternal, however the reason for this difference is not known [8]. Greater than 55 repeats generally cause the juvenile form of HD with symptoms beginning at less than 21 years of age [9].

1.2.1 Huntington's disease symptoms

Involuntary choreiform movement is a characteristic feature of HD, beginning with small movements in the fingers, toes and face. These involuntary movements develop gradually and eventually interfere with walking, speaking, chewing and swallowing. In addition to these symptoms, HD patients experience cognitive impairment, and dementia in advanced cases [10].

1.2.2 Huntington's disease cellular pathogenesis

Despite widespread expression of all nine genes within the brain, each polyglutamine disease shows a distinct neuronal pattern of vulnerability to pathology. In HD, pathology is associated with selective neuronal degeneration and gliosis of medium spiny neurons within the striatum [11-13]. This includes loss of the GABA-encephalin containing medium spiny neurons projecting into the globus pallidus and GABA-substance P containing medium spiny neurons projecting into the substantia nigra. Over time, these neurons are nearly totally destroyed. Interneurons in this region are however relatively preserved [12, 14]. The cerebral cortex also shows significant reduction in size; most affected are the large neurons in layer VI, and to a lesser extent layers III and V. In addition to neurons in the striatum and cortex, HD brains also show atrophy of the lateral tuberal nucleus of the hypothalamus and to a lesser extent the amygdala and some regions of the thalamus [13, 15, 16].

1.3 Huntingtin

Note that in order to maintain consistency with scientific literature [6], gene nomenclature will be described in a species specific manner, including *HTT* in human, *Htt* in mouse, and *htt* in zebrafish, or referred to collectively as *HTT* gene homologues. When describing previous models of mouse *Htt* knockout, the original nomenclature is used in this thesis for the mouse gene, *Hdh* in accordance with the original publications, in order to

clearly identify the particular model used. In addition, throughout this thesis, the typographical convention is used such that the names of genes are printed in italic type, whereas gene products are printed in regular type.

1.3.1 Tissue and cellular expression of huntingtin

Htt is widely expressed at both the tissue and cellular level at all stages of development. However in the adult, htt is more highly expressed within the brain and the testes. A similar regional distribution is also seen for polyglutamine-expanded htt (polyQ htt) [13]. The ubiquitous expression pattern of wild-type and polyQ htt within the brain in both normal individuals and HD individuals does not shed any light on the specificity of cellular pathology seen in HD [17-21].

Similar to its tissue distribution pattern, htt is widely distributed within the cell. Htt is found in cell bodies, dendrites, axon terminals and a variety of organelles including the nucleus, endoplasmic reticulum, golgi complex, mitochondria and synaptic vesicles. Htt is also associated with the cytoskeleton, microtubules and nerve endings [22-26].

1.3.2 Structure of huntingtin

The human *HTT* gene spans 167 Kb (67 exons) of DNA and encodes a 350 kDa cytoplasmic protein, htt [5, 13]. Despite the identification of the *HTT* gene over 16 years ago, the cellular functions of htt are still not clear. Due to the fact that proteins with similar functions often contain similar conserved domains and motifs, detailed knowledge of the htt gene can help to suggest some possible cellular functions by comparison with similarly structured genes. A discussion of htt's known structure and any information this provides about possible functions for htt is described below.

Throughout the length of htt a number of conserved motifs and structural domains have been identified. Most notable is the presence of a polymorphic glutamine repeat stretch in the amino-terminus of htt (starting at amino acid 17; Figure 1.1). Previous studies have shown that the polyglutamine region is able to regulate the interaction of htt with various proteins, including transcription factors that also contain a polyglutamine region [7, 27-30], suggestive of a role for htt in transcriptional regulation.

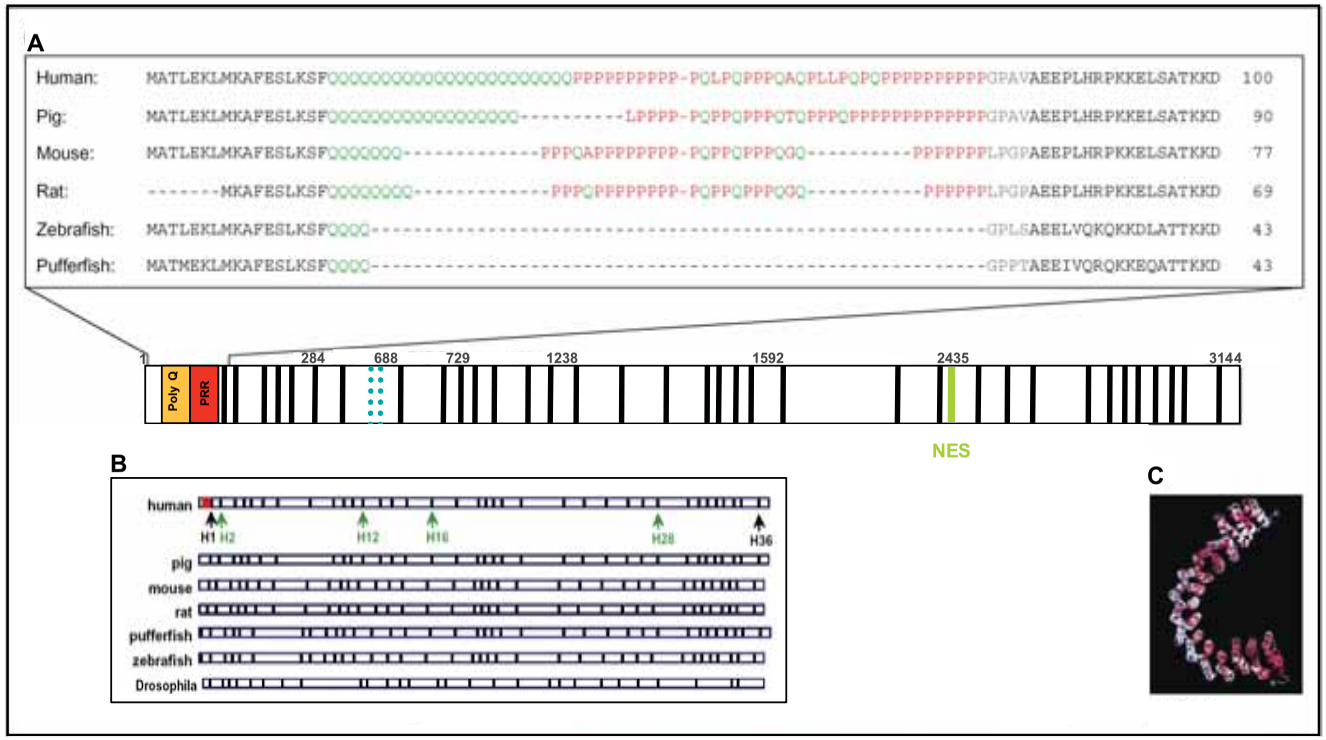

Figure 1.1 The structure of the htt protein and comparison to different species. Htt contains a glutamine repeat stretch (polyQ) and a proline-rich region (PRR) at the N-terminus (orange and red boxes). In addition, numerous HEAT repeats are found along the length of the protein (black bars). (A) Amino-acid-sequence comparison of htt polyQ and PRR regions between different species (NCBI Genbank Identifiers: human, 454415; pig, 4126796; mouse, 1708161; rat, 1708162; zebrafish, 2981138 and pufferfish, 804981) shows that this region is only partially conserved. (B) The distribution of HEAT repeats along the length of htt is highly conserved between different species. (C) The crystal structure of the PR65/A subunit of protein phosphatase 2A demonstrates that HEAT repeats form α helices, which assemble into an elongated superhelix containing a groove for protein–protein interactions. The 36 HEAT-repeats along the length of htt might adopt a similar structure suggesting a common conformational structure for htt and possibly similar functions. Blue dots show the location of caspase cleavage sites. Figure adapted from [29] and [39].

Immediately adjacent to the polyglutamine repeat region are two proline rich regions. A number of proteins have been shown to bind to these proline rich regions, such as SH3GL3, PACSIN 1, PSD-95 and p53. This finding may implicate htt in such functions as clathrin-mediated endocytosis, synaptic scaffolding and transcriptional regulation [18, 31-34]. An amino acid sequence comparison of htt from different species however shows that this polyproline region is poorly conserved. This suggests that the proposed functions that require the polyproline repeat are relatively newly acquired functions of htt (Figure 1.1 A).

Further downstream of the proline rich region, and distributed along the entire *HTT* gene, are 36 predicted HEAT repeats (Figure 1.1). HEAT repeats are degenerate 40aa long motifs, named according to four proteins in which they were first identified; Huntingtin, Elongation factor 3, the regulatory A subunit of protein phosphatase 2A and TOR1 [35]. The presence of these HEAT repeats suggests a specific conformational structure for htt [36, 37] as described below.

Individual HEAT motifs form a pair of anti-parallel helices that align next to each other in a linear manner. Multiple HEAT motifs within a protein, such as occurs within htt, results in a continuous, elongated interface structure (Figure 1.1 C). This structure supports protein:protein and RNA:protein interactions [36, 38] and suggests a role for htt as a scaffolding protein [39]. Cross species analysis of the *HTT* gene shows that these regions are evolutionarily conserved (Figure 1.1 B) and therefore are an important feature of the structure and function of htt [36, 39, 40].

A number of proteins have been found to bind to the HEAT repeat containing region of htt, including huntingtin interacting protein (HIP) 1, HIP14, and huntingtin associated protein (HAP) 1. These proteins are known to have roles in endocytosis, vesicle trafficking and cell survival, further suggesting a role of htt in these functions [29, 41-44]. The proposed functions of htt are discussed in more detail in Section 1.4 and Section 1.5.

1.4 Overview of the proposed cellular functions of huntingtin

Since identification of the *HTT* gene in 1993 [5], some insight has been gained into the biological functions of htt. Knowledge of htt's structure has helped to provide clues to htt's activities within the cell, based on the analysis of genes with a similar structure. In addition,

htt many binding partners also suggest a variety of functions for htt. Using this approach, htt's has been implicated in a variety of cellular functions including cell survival, endocytosis, axonal transport and neuronal transcription (reviewed in [45]).

More direct evidence of htt's functions however has been obtained by using *in vitro* cell culture or *in vivo* animal model systems. These two approaches are useful to identify functional relationships within the cell, including which signaling processes may require htt. The sections below (Section 1.4.1-1.4.4) provide an overview of what is currently understood about some of the better-known functions of htt, using *in vitro* and *in vivo* models while Section 1.5 provides more information about htt's possible functions during development using *in vivo* animal models.

1.4.1 Anti-apoptotic role of huntingtin

An understanding of htt's role in prevention of apoptosis is of great interest as neuronal apoptosis could play a role in neurodegeneration associated with HD [46]. Many studies have been carried out which support an anti-apoptotic a role for htt. The first study to suggest such a role was carried out by Rigamonti *et al*., (2000) [47]. This group found that when over-expressed, htt acts to protect cells from a variety of apoptotic stimuli including serum withdrawal and pro-apoptotic Bcl-2 homologues. Both full-length wild-type htt and an amino terminal truncation of the first 548 amino acids (N548) were shown to be equally protective for cells, whereas a shorter N terminus (N63) provided no protection from apoptosis. It was therefore concluded that the region of htt responsible for this anti-apoptotic activity lies within the first 548aa of the human htt protein.

One mechanism by which htt may be able to prevent apoptosis is by binding to HIP1. Through this interaction, htt is able to prevent HIP1 binding to another protein, HIPPI and forming a proapoptotic complex [48]. This finding not only suggests a role for htt in cell survival, but it also suggests a possible pathogenic mechanism for HD. The interaction between htt and HIP1 is polyglutamine length dependent [42]. Reduced binding of HIP1 to polyQ htt results in excess 'free' HIP1 available for interaction with proteins that mediate the apoptotic pathway, resulting in loss of htt mediated protection against apoptosis [43, 48].

HAP 1 is another htt interacting factor that suggests an anti-apoptotic role for htt. Htt has been shown to bind HAP1 in the cytoplasm and together they interact with Mixed Lineage Kinase 2 (MLK2) [49]. In the normal state, this interaction sequesters MLK2 away and prevents activation of the JNK apoptotic pathway. However, upon polyglutamine expansion, the interaction between htt and MLK2 is weak and the free MLK2 is able to

induce apoptosis via JNK activation, possibly contributing to neuronal loss observed in HD [49]. In addition to the benefits of sequestering MLK2 away from the apoptotic pathway, binding of htt to MLK2 enables activation of the transcription factor, NeuroD by phosphorylation. NeuroD has been shown to play an important role in neuronal survival and differentiation, therefore NeuroD activation is another mechanism by which htt can help prevent apoptosis [50].

Recently, htt has also been shown to mediate the apoptotic activity of a protein called p21-activated kinase 2 (pak2). Htt plays a direct role in this process by preventing cleavage of Pak2 into a constitutively active fragment capable of inducing apoptosis [51].

Support for the anti-apoptotic role of htt has also come from a number of *in vivo* studies. The Cre/LoxP site-specific recombination system was used to generate a null mutation of *Htt* in late stages (embryonic day 15, E15; and postnatal day 5, P5) of mouse forebrain development [52]. In these mice, absence of htt expression caused neurological deficits and progressive neurodegeneration in a similar pattern to that seen in HD patients, in the hippocampus, cortex and striatum.

A further role for htt in establishment and survival of neurons within these specific brain regions was suggested in work carried out by Reiner *et al*. (2001). Upon injection of $Htt^{-/-}$ ES cells into wild-type blastocysts, $Htt^{-/-}$ neurons were found in all brain regions except the striatum, cortex, hippocampus and Purkinje cells of the cerebellum. It therefore appears htt has a neuronal specific critical function within these specific brain regions in establishment and survival of neurons during early development [53].

Subsequent studies by Leavitt *et al*. (2004 and 2006) showed that over-expression of full-length htt in a yeast artificial chromosome (YAC) transgenic mouse model provided significant protection against NMDA induced acute excitotoxic stress. They also showed that wild type full-length htt was able to protect against neurodegeneration caused by mutant htt expression [54, 55].

1.4.2 Neuronal transcription

Htt has been shown to bind to a large number of transcription factors, as well as transcriptional co-activators and co-repressors [18, 56-59]. These include CREB binding protein (CBP), the co-activator CA150, REST/NRSF, Sin3a, the transcriptional co-repressor

C-terminal binding protein (CtBP), p53 and NcoR1. These interactions suggest that transcriptional regulation, both positive and negative, may be an important function of htt.

There are a number of mechanisms by which htt can regulate transcription. Firstly, htt acts as a protein interaction scaffold to promote stronger binding between transcription factors and their co-factors [60, 61]. Secondly, htt can sequester transcription factors in the cytoplasm to negatively regulate their activity, as occurs upon htt interaction with REST/NRSF transcriptional repressor [62]. Binding of htt to REST/NRSF is polyglutamine repeat-length dependent; the longer the repeat-length, the weaker the interaction. In the presence of mutant htt, there is a greater amount of REST/NRSF free to enter the nucleus to inhibit transcription [62], therefore this interaction may play an important role in HD pathology.

It has been previously stated that some 30 genes are regulated by REST/NRSF suppression [63, 64]. These genes have diverse functions in development and neuronal maintenance including neurotransmitter receptors, neurotrophins, synaptic vesicle proteins, cytoskeletal proteins, growth factors and ion channels [65]. Htt therefore has the ability to regulate the expression of many genes with a wide range of functions. Recently, research has focused on htt's relationship with Brain Derived Neurotrophic Factor (BDNF), a neurotrophin whose expression is regulated by the REST/NRSF system.

1.4.3 Axonal transport

Htt is predominantly localized in the cytoplasm. Here, htt is found to interact with vesicle structures, microtubules, and other associated proteins suggesting a possible role for htt in intracellular organelle and/or axonal transport [66]. Some of the proteins that bind to htt and have a known role in axonal transport include HAP1, HIP1, HIP14, HIP1 related protein (HIP1R), and protein kinase C and casein kinase substrate in neurons-1 (PACSIN1) [32, 41-44, 67, 68].

Htt and HAP1 function together as a scaffold to stabilize the interaction of selected cargo vesicles to molecular motors. This process facilitates the transport of many types of organelles along axon tracts including BDNF containing vesicles [29, 69-72]. Reduction in htt levels or expansion of the polyglutamine repeat region in htt can disrupt or slow axonal transport of BDNF containing vesicles resulting in inadequate trophic support to the striatum. Disruption in axonal transport may therefore be one contributing factor to pathology associated with HD [44, 72-76].

1.4.4 Dendrite formation and synaptic terminals

Htt has been shown to bind to many proteins that are involved in modulation of dendrite morphology and cytoskeletal organization, including PSD-95 and HAP1. PSD-95 has an important role in the organization of the post-synaptic cleft of neurons [77]. The interaction between htt and HAP1 helps to form a scaffold to allow PSD-95 to bind with other proteins, such as NMDR and kainate glutamate receptors (reviewed in [29]).

By yeast two-hybrid analysis, it was determined that upon expansion of the polyglutamine repeat region, the strength of the interaction between htt and PSD95 decreases. This suggests that dendrite formation may be affected in HD and that this may ultimately contribute to the overall pathology associated with the disease. This hypothesis is supported by the observation of decreased dendritic spine density and dendritic spine length in the medium striatal neurons and cortical pyramidal neurons of a transgenic HD mouse model [78].

In addition to this pathway, htt's interaction with HAP1 has been shown to contribute to dendritic morphology through their interaction with MLK2. The interaction of htt and HAP1 with MLK2 facilitates the phosphorylation and activation of NeuroD, a transcription factor that is shown to be important for neuronal survival and differentiation. However NeuroD also plays an important role in generation and maintenance of dendrites [50, 79]. The expansion of the polyglutamine repeat region of htt interferes with the interaction between htt and MLK2. However it is yet to be determined whether NeuroD levels are decreased in HD neurons [49]. If NeuroD levels are altered, then inhibition of this pathway is likely to be a contributing factor in the pathogenesis of HD affecting both neuronal survival and dendrite formation.

1.5 Huntingtin function during development - analysis of huntingtin knockout models

Htt is essential for early development. This has been demonstrated by three separate groups of researchers who have each shown that inactivation of both alleles of the *Htt* gene in mouse results in early embryonic lethality. Further work by these groups have identified that lethality occurs approximately during the onset of gastrulation and formation of the nervous

system (E8.5) [80-82], suggesting an important role for htt at this stage. These and other important *in vivo* studies of the normal functions of htt are described in more detail below.

In 1995, Zeitlin *et al*. generated a nullizygous mouse model by targeted mutagenesis of the promoter and exon 1 region of the mouse *Htt* gene (called Hdh^{prex1}) [81]. They observed lethality of homozygous mutant embryos between E8.5-E10.5. These embryos showed no obvious mutant phenotype by E6.5 compared to wild-type embryos, however at E7.5 *Htt* null mutants showed significant disorganization and developmental delay with many embryos having not yet reached the head fold stage.

Despite formation of three separate germ cell layers, many cells appeared to have abnormal morphology, were tightly packed, disorganized, and showed numerous pyknotic nuclei. This was particularly evident within the embryonic ectoderm. No morphological, behavioral or histological phenotype was observed for heterozygous mutant mice.

A similar study was carried out by Duyao *et al*. in 1995. A null mutation of the mouse *Htt* gene was made by insertion of a neomycin cassette to replace exons 4 and 5 (called $Hdh^{ex4/5}$) [80]. This group recorded very similar results to Zeitlin *et al*., in both heterozygous and homozygous null mutant embryos. Further detailed analysis of the $Hdh^{ex4/5}$ embryos was carried out using in *situ* hybridization [83]. It was discovered that compared to wild-type embryos, $Hdh^{ex4/5}$ embryos exhibited a number of patterning defects such as a shortened primitive streak, absence of a proper node and reduction of anterior streak derivates, including reduced neuroectoderm and the lack of head folds.

In a third study published in 1995, a *Htt* knockout mouse model was also generated by insertion of a neomycin cassette construct within the mouse *Htt* gene. However unlike the previously discussed model, this insertion resulted in deletion of intron 4 and half of exon 5 (called Hdh^{ex5}) [82]. This mutation resulted in production of a truncated 20 kDa polypeptide consisting of the first 4 exons of the mouse *Htt* gene. Like the two previously mentioned studies ($Hdh^{ex4/5}$ and Hdh^{prex1}), the homozygous Hdh^{ex5} mutation was embryonic lethal. However unlike these studies, heterozygous mutants of Hdh^{ex5} were not phenotypically normal, exhibiting cognitive defects, increased motor activity and a reduction in the size of the subthalamic nucleus [82]. It has been suggested that the heterozygous phenotypes observed may be due to a tissue-specific dominant negative effect of the truncated htt product over the full-length *Htt* allele [81].

Subsequent research, carried out by White *et al*. (1995) resulted in generation of a mouse htt knockdown model, expressing htt (with a pathogenic level of glutamine repeats; Q50) at one-third of normal levels [84]. Heterozygous Hdh^{neoQ50}/Hdh^{+} mice could not be distinguished from their wild-type littermates (in line with other *Htt* knockout models).

Homozygous *Hdh*^{neoQ50} mice however, die within two days of birth. Analysis of these pups revealed an abnormally shaped cranium, misplaced external ears and thickened, dehydrated skin. Histological analysis revealed abnormal CNS development including misshapen forebrain and midbrain, enlarged ventricles, and architectural abnormalities within the brain including ectopic striatal masses in the ventricles. Analysis of the brains of these embryos however showed no sign of striatal or cortical pathology to suggest any relationship to HD pathology in humans [84].

The research described above suggests a rate-limiting role for htt in early embryonic patterning just prior to the formation of the neural tube. More specifically, htt is shown to play an important role in CNS formation and organization, and in survival and normal functioning of post-mitotic neurons. Of note, htt has been shown to play a neuronal specific role in formation and survival of neurons within the hippocampus, cortex and striatum [52, 53].

1.6 Cause of pathogenicity in Huntington's disease

Toxicity of expanded polyglutamine

It is currently not clear how expansion of the polyglutamine repeat region within htt gives rise to the pathology seen in HD. There is much evidence to suggest that the polyglutamine expansion confers a toxic gain-of-function to the *HTT* gene (reviewed in [85, 86]). The first and most compelling evidence to support a theory of toxic gain of function is the autosomal dominant mode of inheritance of HD. Deletion of one allele of *HTT* (as seen in Wolf-Hirschhorn Symdrome) does not result in HD-like pathology in humans. This suggests that the expansion of the polyglutamine region within htt does not lead to loss of normal htt function [87]. Studies in two separate mouse models support this observation [80, 81]. In these models, 50% reduction in htt expression does not result in a phenotype, let alone pathology indicative of HD.

Further evidence shows that while homozygous knockout of *Htt* expression in mice results in embryonic lethality [80-82], this is not the case for homozygous repeat expansion within *HTT* in humans [88-90]. This data suggests that polyQ htt is able to fulfill the vital functions that wild-type htt plays in early development, and that the expanded polyglutamine

mutation associated with HD does not result in a complete loss of the normal function of htt [53].

In further support of the toxic gain of function theory, the polyglutamine expansion has been shown to be inherently toxic to cells as pathology is seen even when the CAG expansion is located within an unrelated gene [91].

Loss of normal function of huntingtin may contribute to pathology of HD

The evidence presented above strongly suggests that a toxic function acquired by polyQ htt contributes to HD pathology, and that a loss of normal htt function is not the cause of HD pathology. Despite this, there is some evidence to suggest that loss, or perturbation of normal function of htt may contribute in some way to the pathology of HD.

For a loss of function to contribute to HD, two conditions must be met. Firstly, the expanded polyglutamine region must cause htt to act in a dominant negative fashion [52]. PolyQ htt has been shown to form nuclear aggregates and can sequester wild-type htt within these aggregates [92]. This could result in a loss of function of wild-type htt [93].

Secondly, any loss of function phenotypes must occur in the adult, due to htt's critical functions in development [80-82, 84]. This is also possible, as HD pathology is associated with death of neurons that are very long-lived cells. If a dominant negative effect took place, it is likely to build up in neurons over time due to the lower rate of cell turn-over compared to other tissues [52]. Build up of this negative effect is likely to cause stress to the cells and/or result in reduced ability of the cell to withstand stress that may come from expression of polyQ htt, contributing to HD pathology [94]. For example, reduced trophic support due to a reduction in BDNF expression, suggested in various mouse models of HD and in post mortem HD patients brains [95-100].

One of the great mysteries about HD is the cellular specificity of neurodegeneration. Within nine neurodegenerative diseases, the same polyglutamine expansion is found in nine distinct and unrelated proteins, each with a characteristic neuronal pattern of vulnerability to pathology. This difference in pathological pattern has been proposed to indicate that loss or alteration of the unique normal functions of these proteins contribute in some way to the specificity of neuronal cell death [101].

A study of chimeric mice carried out in 2001, shows that htt expression is required for survival of neurons within the striatum, cortex and hippocampus specifically, however not in other regions of the brain tested, as mentioned in Section 1.4.1 [53]. This differing requirement of particular neurons for htt function provides a mechanism that can account for

the specificity of neuropathology in HD brains despite the widespread expression of htt in the brain.

Despite strong evidence to suggest an acquired toxic function of htt gives rise to pathology associated with HD, this does not rule out a contribution from a loss of wild-type htt function. In fact, the above data show that loss of any of the important functions of htt within the cell could sensitize the cell to stress and contribute to the pathology associated with HD. A greater understanding of the normal function of htt may help to provide some insight into the cause of pathology associated with HD.

1.7 Advantages of using zebrafish as a model system for investigation of gene function

Zebrafish (*Danio rerio*) is a well-characterized model system. It provides a wide range of advantages that have prompted many scientists to adopt this vertebrate model system for investigation of both normal development and disease pathogenesis [102, 103]. Some general advantages of using zebrafish as a model system include; small physical size, large clutch size, rapid development and relatively cheap housing costs. Other important advantages of the zebrafish model system include their easy genetic manipulation and external development.

One of the most exciting characteristics of zebrafish is that they are easily genetically manipulated. Embryos are fertilized and develop outside of the mother and therefore can be accessed for genetic manipulation at the one cell stage. A range of tools are available to alter the level of expression of genes in zebrafish. Genes of interest can be transiently blocked from expressing proteins using morpholino oligonucleotides (morpholinos). In addition, stable transgenic zebrafish lines can be made, or large-scale generation of zebrafish mutants carried out and easily screened due to their small size, transparency and rapid development [104-107].

External development of the embryo from the one cell stage is also a major advantage. Developing embryos can easily be visualized at any stage by using a dissection microscope (shown in Figure 1.2). In addition, transparency of the zebrafish embryos allows detailed analysis of specific body structures during development.

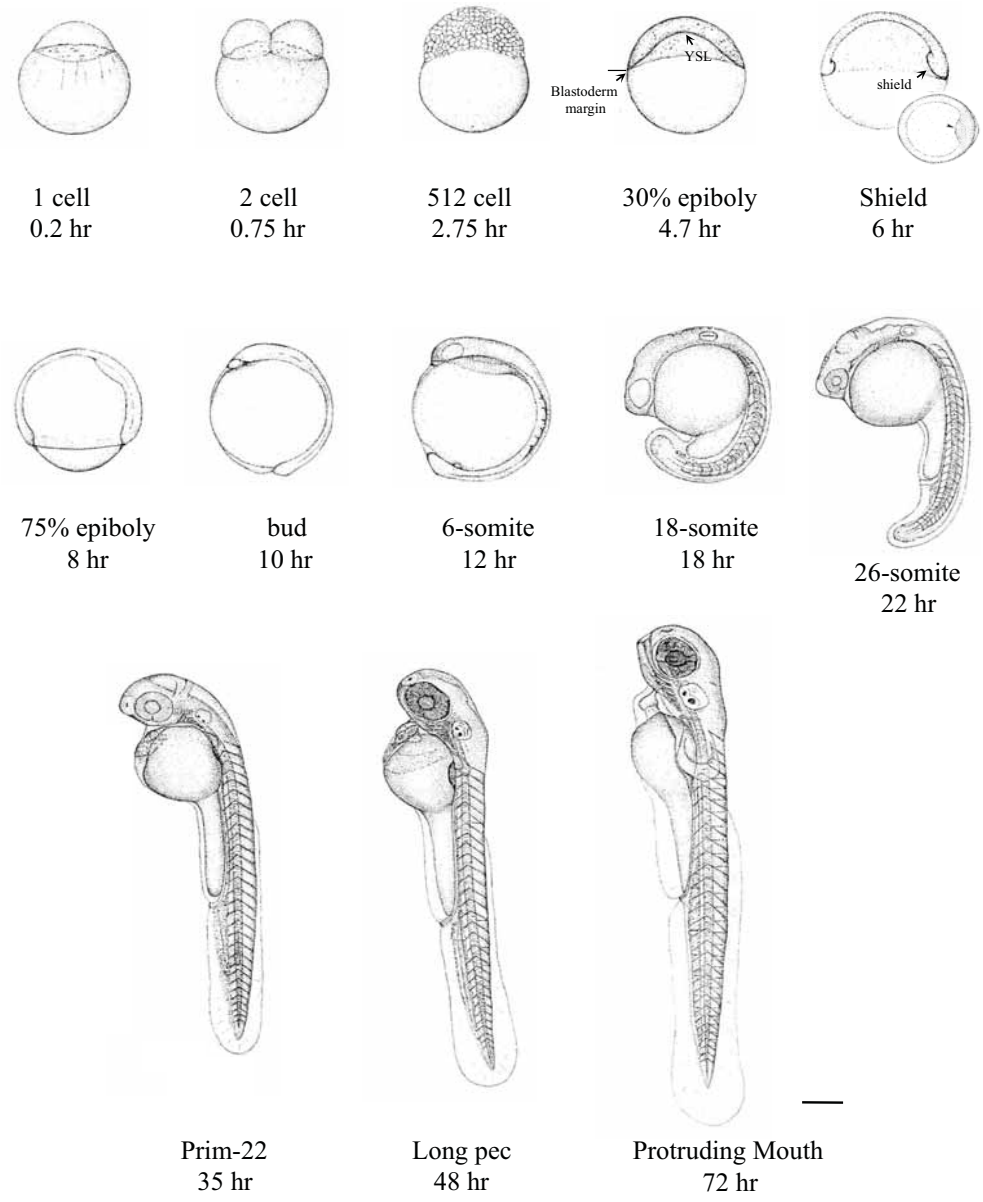

Figure 1.2 Camera lucida sketches of zebrafish embryonic development at selected stages. Zebrafish is a well characterized vertebrate model system. Development of the zebrafish has been investigated in detail from the one cell stage to adult. This figure shows selected stages throughout zebrafish development. External development from one cell stage is a great advantage of the zebrafish system for developmental analysis. Embryos are shown animal pole to the top at early stages, and anterior to the top at later stages. Figure reproduced from [102]. Scale bar = 250 μm.

Zebrafish also have a high level of genetic conservation to that of higher vertebrates, including human [108]. Initial characterization of the zebrafish *htt* gene was carried out in 1998 by Karlovich *et al*. [109]. The zebrafish htt gene encodes a 3121aa protein with a high level (70%) of amino acid identity to human htt. The zebrafish htt transcript is expressed ubiquitously at all developmental stages (Figure 1.3), with subsequent down-regulation in non-neural tissues consistent with htt mRNA expression in rodent development [80, 110-112].

1.8 Using development as a tool to assess gene function

The application of genetic analysis has transformed our understanding of developmental biology in the last decade. Much of this is due to the Nobel prize-winning research carried out by Drs. Christiane Nüsslein-Volhard, of Germany's Max-Planck Institute; and Eric Wieschaus, at Princeton [113]. The groups of Nüsslein-Volhard and Wieschaus used a new strategy to identify genes with an important role in embryonic development [114]. Their forward genetic approach was aimed at generating a screen of random mutations in the *Drosophila melanogaster* genome, then observing the mutant phenotypes to deduce the genes that have a particular important function in development. These studies were also successfully carried out in *Caenorhabditis elegans* and in *Danio rerio* (zebrafish). Importantly, this technique of genetic analysis identified many genes that regulate remarkably similar processes in the development of multiple model systems [106, 107, 115-117].

These studies were designed to take advantage of the strict spatial and temporal regulation of key processes in the development of embryos in these model systems. Reverse genetics works on the same principle, however it is conducted in the opposite direction to forward genetics. Reverse genetics is carried out by altering the expression of a specific gene by introducing a change or disruption, then observing the phenotype in the whole organism in an attempt to deduce its biological function.

This aim of the present research is to investigate the functions of htt using a reverse genetic approach. Morpholinos will be used as a tool to specifically alter the expression of htt in zebrafish embryos, and the resulting phenotype will be observed in an attempt to deduce the important functions of htt in development.

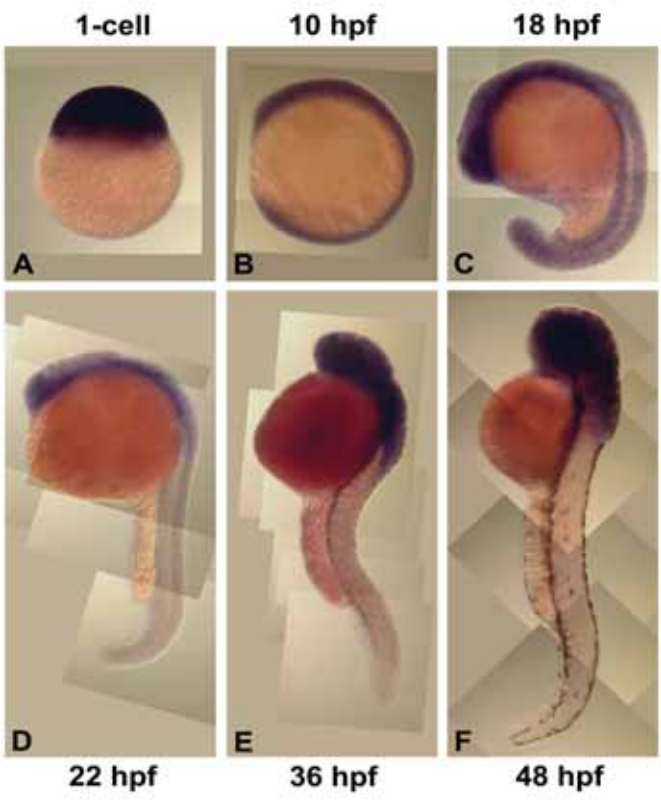

Figure 1.3 Htt mRNA expression in the zebrafish embryo at selected stages of development. *In situ* hybridization shows maternal deposition of htt mRNA (purple) at the one cell stage (A). Htt is ubiquitously expressed in early developmental stages becoming more highly expressed in the head after 18 hpf. Animal pole to the top in (A), and anterior to the top at all later stages (B-F). Experiment carried out by Amanda Lumsden. Figure reproduced from [112].

1.9 Project aims: Investigation of huntingtin function using zebrafish as a model system

Despite the identification of the *HTT* gene over 16 years ago there is still much to learn about the biological function of the htt protein. While much interest in the *HTT* gene is centered on how the mutation in this gene gives rise to HD pathology; htt itself, present in every person from the single-cell embryo stage, is being revealed as a key component in many cellular processes associated with cellular maintenance, survival and in normal embryonic development.

In vitro studies have identified a number of possible roles for htt in cell survival, endocytosis, axonal transport and neuronal transcription. Early mouse *Htt* knockout studies show that htt function at the level of the whole organism is vital, playing a critical role in normal development [80-82, 84]. However, limited information can be gained from these $Htt^{-/-}$ mouse embryos, with complete absence of htt, due to the early age of lethality and highly disorganized structure of the embryo.

The aim of this project is to investigate the proposed and novel functions of htt *in vivo*. We aim to overcome the limitations of the mouse $Htt^{-/-}$ system by investigating the normal functions of htt using an alternative animal model system, Zebrafish *(Danio rerio)*. The zebrafish model system provides a number of advantages for investigation of htt function (See Section 1.7). Arguably the most powerful advantage of the zebrafish system is easy genetic manipulation. In the zebrafish, gene expression can be reduced by injection of translation blocking morpholinos at the one cell stage. This laboratory has previously used morpholinos to inhibit translation of the htt protein from the one cell stage of development. Using this approach, the level of htt expression has been partially reduced in order to gain a milder phenotype than achieved with $Htt^{-/-}$ mice. This work has demonstrated dramatic effects on embryogenesis caused by reduction of htt expression, and also more specifically revealed a role for htt iron homeostasis in htt-reduced zebrafish (*hd*MO) [112]. Within the current research, further analysis of *hd*MO zebrafish has been carried out with the aim to uncover information on the cellular and/or developmental processes for which htt is a rate-limiting determinant (see previous section for discussion on using development as a tool to assess

gene function). Ultimately this approach has enabled a key question in HD pathology to be addressed: Do different neurons have differing functional requirements for htt? [118]

CHAPTER 2: MATERIALS AND METHODS

2.1 Materials

2.1.1 Enzymes

T4 DNA ligase	Roche
Restriction Endonucleases	New England Biolabs (NEB)
Taq DNA polymerase	Invitrogen
DNase I	Invitrogen
RNase H	Invitrogen
RNase OUT (RNase inhibitor)	Invitrogen
Superscript II reverse transcriptase	Invitrogen
Proteinase K	Sigma-Aldrich
SYBR green PCR master mix	Applied Biosystems
T7 RNA polymerase	Roche
T3 RNA polymerase	Roche
Sp6 RNA polymerase	Roche

2.1.2 Kits

QIAquick gel extraction kit	Qiagen
QIAquick PCR purification kit	Qiagen
Plasmid mini kit	Qiagen
RNeasy mini kit	Qiagen
SuperSignal® West Dura Extended Duration Enhanced Chemiluminescence (ECL) kit	Pierce
mMessage mMachine SP6 RNA transcription kit	Ambion
Expand long template PCR kit	Roche

pGEM-T Easy vector kit	Promega
Vector Red Alkaline phosphatase subrstate kit I	Vector laboratories

2.1.3 Plasmids

pGEMT	Promega
pCS2+	D. Turner (University of Michigan) [119]

2.1.4 Oligonucleotides

All Oligonucleotides (oligos) were obtained from Geneworks at standard PCR grade. DNA primers were designed using primer design software such as Primer Express (Applied Biosystems) or PerlPrimer (online), or taken from published papers where cited. All primers are designed to recognize zebrafish DNA. Primer sequences are shown 5'-3'. Primers were resuspended in MQ water at 50μM and stored at -20^{0}C until further use.

Oligos for PCR and sequencing:
M13-Fw 5'-GTAAAACGACGGCCAGT-3'
M13-Rv 5'-CAGGAAACAGCTATGAC-3'

Oligos for *in situ* probe cloning:
Specific oligos used for making clones for *in situ* probes are shown in Section 2.1.5.

Oligos for quantitative real-time PCR (qPCR):
All primers span introns where possible (exceptions are *omp*, and *val*).

Gene	Upstream primer (5' to 3')	Downstream primer (5' to 3')	Product (bp)
acta1	TGCCCAGAGGCCCTGTT	ACCGCAAGATTCCATACCCA	70
dlx3b	GAGGGCTGAGAACACGAACC	TCACCATTCTCAATGACCGCT	51
ef1a	CCAACTTCAACGCTCAGGTCA	CAAACTTGCAGGCGATGTGA	105
emx3	GATATCTGGGACACCGGTTTCA	AGCAGGTTTTCAGGGCTACTGT	52
fgf8	AAGATGGCGACGTTCATGC	TCCCAAATGTGTCCGTCTCTACTA	51
hoxb1	CAAAAGGAATCCCCCCAAAA	CGGCCCTAGTCCGTACTCAG	48
ntl	CACACCACAAACACTACCTCCAAC	TGACCACAGACTTGGGTACTGACT	51
omp	GAACCCACCGGACTCTTCTG	TTGGCCAGCTCTGCTATCCT	101
otx2	CCCTCCGTTGGATACCCAGT	TCGTCTCTGCTTTCGAGGAGTC	51
pbx2	GCGAAGATTCACCCCACACT	GAGAGAACGACCCTGAGCCA	51

six1	CTACCACACAAGTGAGCAACTGG	AGCGCCCGTGTTGTTGTT	99
sox32	CCTCAGCAAAATACTTGGCAAGA	TTATCTGCCAGAGACATTGCTTTC	95
val	CAGCTTGTGACCATGTCCGT	TGAAGCCCCGCAGGTGT	52

2.1.5 In situ *probes*

cDNA clones to make *in situ* probes, obtained from other labs:

Gene targeted	Plasmid	Antibiotic resistance	Endo-nuclease	Polymerase (antisense)	Insert size	Source Reference
krox20	unknown	Amp	XbaI	T3	2 Kb	Dr. Andy Oates, Princeton University, U.S.A. Now at Max Plank, Germany [120]
val	pGEMT	Amp	NcoI	SP6	750 bp	Dr. Michael Lardelli, Adelaide University, Australia [121]
otx2	pBluescript KS (+)	Amp	unknown	T7	2 Kb	Dr. Graham Lieschke, Walter and Eliza Hall Institute, Melbourne, Australia [122]
dlx3b	p373	Amp	EcoRV	T7	600 bp	Dr. Graham Lieschke, see above [123]
six1	pT3HBT7	Amp	HindIII	T7	700 bp	Dr Vladimir Korszh, Singapore [124]
dlx2	pBluescript SK (-)	Amp	BamHI	T7	1.7 Kb	Dr. Michael Lardelli, see above [123]
gsc	pBluescript K	Amp	EcoR1	T7	1.2 Kb	Dr. Michael Lardelli, see above [125]

ntl	T7TS	Amp	BamHI	T7	1.3 Kb	Dr. Andy Oates, see above [126]

cDNA clones for *in situ* hybridization, made by Tanya Henshall:

Gene target	Plasmid	Antibiotic resistance	Endo-nuclease	Polymerase (antisense)	Primer sequences	Reference
col2a1	pGEMT	Amp	NcoI	SP6	F:CAACAAGAAGATGACCAGGA R:TACCAGGCAAACCTCTAAGAC	[127]
hoxd4a	pGEMT	Amp	NcoI	SP6	F:TTCTCGGTTGATGAAGTCCC R:GTTGTGATCTCTGTCTGGCT	[128]

2.1.6 Antibiotics

Ampicillin	Sigma Aldrich
Kanamycin	Sigma Aldrich

2.1.7 Molecular weight markers

DNA: 1 Kb plus DNA ladder (Invitrogen). Sizes (in bp) 100, 200, 300, 400, 500, 650, 850, 1000, 1650, 2000 up to 12,000 in 1000 bp increments.

Protein: HiMark™ unstained high molecular weight protein standard (Invitrogen). Sizes (in kDa) 40, 5, 66, 97, 116, 160, 240, 290, 500.

Benchmark pre-stained protein ladder (Invitrogen). Sizes (in kDa) 8, 15, 20, 27, 38, 50, 65, 80, 115, 180 (sizes vary between batches, approximate sizes given).

2.1.8 Bacterial media

All media were prepared with distilled and deionized water and sterilized by autoclaving, except heat labile reagents, which were filter sterilized. Antibiotics were added from sterile stock solutions to the media after the latter had been autoclaved.

L-Broth (LB): 1% (w/v) amine A, 0.5% yeast extract, 1% NaCl, pH 7.0.
SOC: 2% bactotryptone, 0.5% yeast extract, 10mM NaCl, 2.5mM KCl, 10mM $MgCl_2$, 10mM $MgSO_4$, 20mM glucose.

Plates: L-Broth with 1.5% (w/v) bactoagar supplemented with ampicillin (100mg/L) or Kanamycin (50mg/L) where appropriate.

2.1.9 Morpholinos

All custom morpholinos used were designed by Gene Tools, LLC (www.gene-tools.com) from the zebrafish *htt* gene mRNA transcript.

Two htt morpholinos designed to non-overlapping sequences of zebrafish htt RNA were used:

*hd*MO1 - Complementary to the sequence between bases +5 to -19 of zebrafish htt RNA.

*hd*MO2 - Complementary to the sequence between -22 and -45 of the 5'UTR of the zebrafish htt RNA.

Two control morpholinos were also used;

*c*MO - A standard control morpholino used for earlier experiments. Stated to have no target and no significant biological activity in the zebrafish system (www.gene-tools.com; [129]).

*mc*MO1 - A 5-base mismatch of the *hd*MO1 antisense sequence. A more rigorous control for specificity, and used for experiments carried out in the later stages of the project (www.gene-tools.com).

Morpholino sequences are as follows (sequence complementary to the predicted start codon is underlined):

*hd*MO1: 5'-GCCATTTTAACAGAAGCTGTGATGA-3'

*hd*MO2: 5'-GATATAATCTGATCGGAGATAGGGT-3'

*c*MO: 5'-CCTCTTACCTCAGTTACAATTTATA-3'

*mc*MO1: 5'-GCgATTTcAACAcAAcCTGTcATGA-3'

(Mismatched bases are shown in lower case).

A stock solution of morpholinos was made in RNase free water to a concentration of 2 mM. 15 µl aliquots were stored frozen at -20ºC until use. Working stocks were made in RNase free water and heated to 65ºC for 10 minutes prior to use to dissolve any suspended particles. For injections, 2 nl of morpholino was injected into one cell stage embryos. Embryos were then incubated at 28.5ºC until reaching the required developmental stage.

2.1.10 Antibodies

Primary:

Anti-actin (beta) mouse monoclonal at 1/2000 (western)	Ab Cam
Anti-zebrafish htt rabbit polyclonal at 1/1200 (western)	[112]
Anti-Dig Alkaline phosphatase-conjugated Fab fragments 1/4000 (*In situ* hybridization)	Roche
Anti-FITC Alkaline phosphatase-conjugated Fab fragments 1/4000 (*In situ* hybridization)	Roche

Secondary:

horseradish peroxidase-conjugated donkey anti-rabbit IgG	Rockland
horseradish peroxidase-conjugated donkey anti-mouse IgG	Rockland

2.1.11 Solutions and Buffers

Solution/ buffer	Preparation
Diethylpyrocarbonate (DEPC) water	0.1% (v/v) DECP with distilled water mixed for 30 minutes at room temperature
DNA Loading buffer (6 x)	40% (V/V) guanidinium isothiocyanate, 10% (V/V) sodium citrate pH 7.0, 10% N-lauroysarcosine, 0.1% (V/V) β-mercaptoethanol in DEPC water.
Embryo medium	13.72 mM NaCl, 0.54 mM KCl, 0.025 mM Na_2HPO_4, 0.044 mM K_2HPO_4, 1 mM $CaCl_2$, 1 mM $MgSO_4$, 0.35 g/L $NaHCO_3$
Fix	4% Formaldehyde in 1x PBS
Formamide loading dye (25 x stock)	250 mM EDTA pH 8.0, 25 mg/ml bromophenol blue (w/v), 25 mg/ml xylene cyanol (w/v). Kept in dark at room temperature

Formamide loading dye (2 x)	10 µl formamide loading dye (25 x stock), 190 µl deionised formamide. Kept in dark at 4°C
NBT/BCIP equilibration buffer	100 mM Tris-HCl, 100 mM NaCl, 50 mM MgCl2, pH 9.5
Prehybridization solution	50% formamide (deionised), 5 x SSC, 2% Blocking reagent, 0.1% Tween-20, 0.5% CHAPS (Sigma), 50 µg/ml yeast RNA, 5 mM EDTA, 50 µg/ml heparin, (stored as 50 ml aliquots at -20°C)
PBS	7.5 mM Na2HPO4, 2.5 mM NaH2PO4, 145 mM NaCl
PBS-T	PBS, 0.1% Tween-20
SDS sample buffer (2 x)	250 mM Tris pH 6.8, 4% sodium dodecyl sulfate (SDS), 10% glycerol, 0.006% bromophenol blue, 2% β-mercaptoethanol
TAE electrophoresis buffer	40 mM Tris-acetate, 20 mM sodium acetate, 1 mM EDTA, pH 8.2
TBS-T	10 mM Tris pH 7.5, 100 mM NaCl, 0.1% Tween-20
TE	10 mM Tris-Cl, 1 mM EDTA, pH 7.5
Tricaine stock [130]	400 mg tricaine powder, 97.9 ml double distilled water, 2.1 ml of 1M Tris (pH 9). Adjust to pH 7. Stored at -20°C
Tricaine solution (1 x)	1/25 dilution of tricaine stock in embryo medium
Western blocking buffer	5% skim milk powder in 1 × TBS-T
Western transfer buffer (1 x)	25 mM Tris, 192 mM glycine. No methanol was added

2.1.12 Chemicals

The following standard chemicals and reagents were used in this study. All chemicals were of analytical grade:

Acetone	Ajax, Australia
Acridine orange hemi (zinc chloride) salt	Sigma-Aldrich, USA
Acrylamide, bis-acrylamide	Bio-Rad Laboratories, USA
Agarose	Progen, Australia
Alcian blue	AnaSpec, USA
Blocking reagent	Roche, Germany
CHAPS	Sigma, USA
2(4(dimethylamino)styryl)Nethylpyridinium iodide (DASPEI)	Fluka, Switzerland
Diethylpyrocarbonate (DEPC)	Sigma, USA
DiI [DiIC18(3)]	Invitrogen, USA
Dimethylformamide (DMF)	BDH, Australia
Dimethyl Sulphoxide (DMSO)	Ajax, Australia
EDTA (ethylenediamine tetra-acetic acid)	Sigma, USA
Ethanol	BDH, Australia
Ethidium bromide (EtBr)	Sigma, USA
Formaldehyde solution (40%)	BDH, Australia
Heparin	Sigma, USA
Methanol	Ajax, Australia
TEMED	Promega, USA
Tween-20 (10%)	Bio-Rad Laboratories, USA
Sodium Hydrogen Carbonate	Ajax, Australia
Sodium Hydroxide	Ajax, Australia
Tricaine (3-amino benzoic acidethylester)	Sigma, USA
Tris Hydrochloride	Sigma, USA
Tryptone	Oxoid, UK

2.1.13 Other

SYBR Green PCR master mix	Applied Biosystems
NuPage® 4-12% Bis-Tris acrylamide pre-poured gradient gel	Invitrogen
Deoxyribonucleoside triphosphate set (dATP, dCTP, dGTP, dTTP)	Roche
Ribonucleoside triphosphate set (rATP, rCTP, rUTP, rGTP)	Roche
Trypsin	Invitrogen
Dig-11-UTP	Roche
Fluorescein-12-UTP	Roche
Nanosep 30K omega columns	PALL life sciences
4-Nitro blue tetrazolium chloride (NBT)	Roche
5-bromo-4-chloro-3-indolyl-phosphate (BCIP)	Roche

2.2 Methods

Standard molecular genetic techniques were performed as described in Sambrook *et al*., 1989 [131]

2.2.1 Zebrafish maintenance

Wild-type stocks of *Danio rerio* were bred and maintained under standard conditions at 28.5ºC [130]. Morphological features were used to determine the stage of the embryos in hours (hpf) or days (dpf) post fertilization according to Kimmel *et al*. [102]. For *in situ* hybridization analysis of embryos older than 20 hpf, embryos were raised in 40 μM PTU from gastrula stage (5.5 hpf) to inhibit pigment formation.

2.2.2 Western blotting

Western blotting was used to detect the presence of htt protein in wild-type and *c*MO embryos, and to show reduction of htt expression in *hd*MO embryos. Dechorionated and deyolked embryos (48 hpf) were lysed in SDS sample buffer [130] (1 μl per embryo) and

homogenized with a pestle, on ice. Lysates were boiled for 5 minutes and centrifuged at 55,000 × g. for 20 minutes at 4°C in a TL-100 Ultracentrifuge (Beckman). The supernatant was removed and stored at -80°C. An equal volume of each sample was run on a polyacrylamide gel and transferred to a nitrocellulose membrane that was then stained with Ponceau S solution (Sigma). A digital image (.tif) of the membrane was created by scanning into Photoshop (Adobe), and band densitometry was performed using QuantityOne (Bio-Rad) software. Information of the relative band intensities was used to normalize subsequent protein loading. For western blot analysis, equal quantities of protein were separated by electrophoresis on a 4-12% Bis-Tris acrylamide gel (Invitrogen) at 200 Volts, and transferred to a nitrocellulose membrane in 1 x western blot transfer buffer. Protein transfer was carried out in a mini-PROTEAN 3 apparatus (Bio-Rad), at 30 Volts overnight (4°C). The membrane was blocked for 3 hours at room temperature with blocking buffer prior to overnight incubation at 4°C with polyclonal anti-htt antibody [112] diluted in the same buffer. After three 15 minute washes in blocking buffer the membrane was incubated for 1 hour with horseradish peroxidase-conjugated donkey anti-rabbit IgG secondary antibody. The membrane was then washed three times in 1 × TBS-T for 15 minutes before detection of the htt band by chemiluminescence using Super Signal West Dura ECL Substrate (Pierce). Immediately following htt detection, β-actin was detected on the same membrane, as a protein loading control, using the same western blot method as described above except that anti-beta Actin (Abcam) primary antibody and horseradish peroxidase-conjugated donkey anti-mouse IgG secondary antibody (Rockland) were used.

2.2.3 Acridine Orange staining

Detection of apoptosis in whole embryos was assessed by staining with the vital dye, acridine orange (AO) [132]. The acridine orange protocol was adapted from Li *et al*., 1997 [133]. A stock solution was made up to 1 mg/ml in water and stored in the dark at 4ºC. Embryos were dechorionated and placed in 1/1000 dilution of the Acridine orange stock solution in embryo medium. Staining was carried out in the dark at room temperature for 30 minutes. Embryos were then washed 2 x 5 minutes in 10 ml of embryo medium, then placed into anaesthetic (1 x tricaine solution; see Section 2.1.11) and viewed immediately using a green fluorescence filter.

2.2.4 Alcian blue staining

Alcian blue was used to stain cartilage to visualize the structure of the craniofacial skeleton of zebrafish. Five to eight day old larvae were fixed in 4% formaldehyde in 1 x PBS overnight at 4ºC. Embryos were washed 2 x 5 minutes in PBS-T then bleached in 0.5 ml 30% hydrogen peroxide for about 2 hours. 25 µl of 2M KOH was added to enhance the bleaching process. Embryos were checked every 15 minutes. When eyes appeared sufficiently translucent embryos were rinsed in PBS-T, transferred to a filtered Alcian blue solution (1% concentrated hydrochloric acid, 70% ethanol, 0.1% alcian blue), and left to stain overnight. Embryos are cleared in acidic ethanol (5% concentrated hydrochloric acid, 70% ethanol) for approx 4 hours then rehydrated in a graded ethanol series (50%, 25% then PBS) for approx 5-10 minutes each. Embryos were then washed in PBS-T and placed in 80% glycerol and left overnight a -20ºC. Craniofacial cartilage was visualized under a Ziess axiophot light microscope and photographed using a 10 x objective.

2.2.5 DiI staining

DiI was used to label mature olfactory sensory neurons in live zebrafish embryos. The procedure was carried out as described in [134]. DiIC18(3) powder was made up to 5% stock solution in Dimethylformamide (DMF; keep in the dark at 4ºC). To stain the embryos, 1 µl of DiI stock was added to 5 µl DMF and 4 µl 70% glycerol (to make 10 µl total of working DiI stock). 96 hpf zebrafish embryos were placed in a 35 mm tissue culture petri dish in 4 ml of embryo medium. The 10 µl working stock of DiI solution was added and fish left to swim in this solution for 15 minutes. The fish were then transferred to a clean 48 well dish and rinsed three times for 5 minutes each. To enable easier washing, fish were placed in a sieve, made from the top half of an eppendorf tube with gauze placed over the bottom. This sieve enabled the embryos to be easily transferred between washes in clean wells. For viewing, fish were anesthetized in 2 x working concentration of tricaine then mounted in three drops of 3% methylcellulose and one drop of 2 x tricaine. DiI stained olfactory receptor neurons were initially viewed on a dissecting microscope using a rhodamine cube or filter suitable for 550 nm emission and 565 nm excitation. Images were captured on a Leica SP5 spectral scanning confocal microscope.

2.2.6 DASPEI staining

DASPEI specifically stains hair cells within lateral line neuromasts [135] of live zebrafish embryos. The procedure was carried out as described in [136]. 120 hpf live zebrafish embryos were immersed in 1 mM DASPEI in embryo media for 5 minutes (supernatant only). The embryos were then rinsed thoroughly in embryo media before anaesthetizing and viewing as described above for DiI. For quantitation, presence or absence of each lateral line neuromast was recorded with reference to the previously described pattern of neuromast deposition along the lateral side of the embryo [137]. Statistical analysis was performed using a Students t-test.

2.2.7 Preparation of RNA from zebrafish embryos

RNA was extracted from 24 hpf zebrafish embryos for qPCR (Section 2.2.9) or probe generation for *in situ* hybridization (Section 2.2.8). The following procedure was used; 30-100 dechorionated embryos were staged and collected into a 1 ml plastic tube (Eppendorf). Excess embryo medium was removed. Embryos were then snap frozen in liquid nitrogen and placed immediately at -80ºC. RNA was extracted using an 'RNeasy Mini Kit' from Qiagen according to the manufacturers instructions with the following changes: Upon addition of buffer RLT, the embryos were homogenized by passing through a 20 gauge needle at least 10 times. RNA was eluted in 40 µl of water and run through the column twice. Recovered RNA was stored at -80ºC.

2.2.8 In situ hybridization

In situ hybridization analysis allows spatial visualization of the mRNA transcripts of a specific gene in the whole embryo by binding of a labeled probe complementary to a portion of the specific gene of interest. As certain genes are expressed in specific populations of cells, the presence of the mRNA message is often used as a 'marker' of these cells to show their presence, abundance and spatial distribution in the whole embryo.

In situ hybridization probes used in this project are specified in Section 2.1.5. The *in situ* hybridization probes were made in our lab by synthesizing the RNA probes from cDNA clones that were either constructed within the lab or obtained from other labs. These cDNA clones contained both M13 primer sites for amplification and for sequencing, and T7 or T3 RNA polymerase sites for RNA transcription.

In situ hybridization was carried out according to the protocols published by Jowett, T. (2001) [138]. Protocols describing embryo fixation, pretreatment of zebrafish embryos, hybridization and post-hybridization washes, and subsequent alkaline phosphatase staining with chromogenic substrates on zebrafish embryos were followed as published with minor changes, described as follows: To allow chromogenic detection, alkaline phosphatase conjugated antibody was added at 1:4000 dilution in PBT + 1% BSA for 1 hour at 4°C; also in the case of two color *In situ* hybridization, NBT/BCIP was used to detect the first (and weakest) probe, prior to detection of the second probe with Vector red, as the blue product is easier to visualize than the red.

2.2.9 Construction of labeled probes for in situ hybridization

The insert of interest was amplified in a PCR reaction using M13 primers in RNase free water. The PCR reaction was cleaned using a Qiagen PCR clean up kit and resuspended in RNase free water. 1 µg of amplified DNA was used in a transcription reaction using the appropriate polymerase enzyme (T7 or T3 polymerase, Roche) to produce an antisense product according to the manufacturers instructions.

Digoxigenin or fluorescein labeled UTP was used in the transcription reaction as part of the ribonucleotide mixture to produce a recombinant RNA product with labeled UTP nucleotides incorporated within.

RNA produced in the transcription reaction was purified using Nanosep 30 K columns (Section 2.2.10). Correct transcription of RNA was assessed by three methods; agarose gel electrophoresis (Section 2.2.11) to determine that the correct size product was transcribed, spectrophotometric analysis used to quantitate the amount of RNA, and dot blot analysis to check for the presence of labeled RNA (Section 2.2.12). RNA probes were stored at -80°C.

2.2.10 Purifying RNA in situ probes

Nanosep 30K columns were used to purify RNA after *in vitro* reverse transcription. Firstly, the 20 µl RNA transcription reaction was made up to 500 µl in RNase free water then added to the Nanosep column and centrifuged at 7,000 rpm for 12 minutes at room temperature in a bench top centrifuge. Flow through was discarded and the column by adding 400 µl of 1 x TE to the top of the column and centrifuged at 7,000 rpm for 12 minutes. After

two TE washes, RNA was collected from the top of the column by resuspending gently in 20 µl of RNase free water using a pipette. Another 20 µl of water was added to collect the remaining RNA and pooled with the first wash to give a final volume of 40 µl.

2.2.11 Agarose/formaldehyde electrophoresis (RNA)

Gel electrophoresis apparatus (including tank, glass plates and comb) was washed with 1% SDS in RO water to remove RNases then rinsed in milliQ water (DEPC treated). 2% agarose was prepared fresh by melting the required amount of agarose in 1 x TAE made with DEPC treated water. 1 µl of 10 mg/ml ethidium bromide was added to the molten agarose to aid visualization of RNA after electrophoresis. 1 µl of RNA sample was added to 1 µl of 2 x formamide loading dye and heated to 75ºC for 5mins. Enough 1 x TAE buffer was added to the tank to cover the sides, but not cover the top of the gel. RNA/load dye mix was then loaded into the well of the agarose gel and band separated by electrophoresis at 150 volts for approximately 10 minutes. Visualization of RNA was achieved by irradiation with short wave (254 nm) UV light.

2.2.12 Dot blot

A dot blot was used to assess the level of incorporation of digoxigenin or fluorescein labeled UTP into RNA *in situ* probes. To do this, 1 µl of suitable dilutions (1/10, 1/100, 1/1000 and 1/10000) of labeled probe was spotted onto a Hybond nitrocellulose membrane. The RNA was UV cross linked to the membrane using a UV stratalinker (BioRad) and dried in a 65ºC oven for 1 minute. The membrane was then rinsed briefly in 2 x SSC and washed twice in 1 x PBS for 15 minutes at room temperature. Alkaline phosphatase conjugated anti-digoxigenin or anti-fluorescein antibodies were added to the membrane at 1/2000 or 1/5000 dilution in PBS respectively, for 30-60 minutes. The membrane was then washed twice for 15 minutes in PBS and then equilibrated in NBT/BCIP equilibration buffer (pH 9.5). Labeled RNA probes were visualized by staining in 10 ml of water with one tablet of NBT/BCIP. The alkaline phosphatase activity produced a purple color where the antibody was bound to labeled probe. Only probes which show a visible purple ‘dot’ at 1/1000 dilution or higher were used for *in situ* hybridization.

2.2.13 Quantitative real-time PCR

Synthesis of cDNA from total zebrafish RNA: 1µg of total RNA was treated with DNase I to remove genomic DNA contamination, according to the manufacturers instructions. Reverse transcription was then carried out on this RNA using oligo (dT) primers and Superscript II™ reverse transcriptase in a 20 µl reaction. The cDNA was diluted to 100 µl using autoclaved milliQ water, and 5 µl of this was used in the qPCR reaction.

qPCR: Each sample was analysed in triplicate in a 96 well plate. Each experiment was performed on three independent occasions except for val, which was performed twice. A 20 µl volume of 1 x SYBR Green PCR master mix and 1.26 pmol of each primer was added to each well with the template cDNA as described above. Two control samples were also included: A "no reverse transcriptase control" (no reverse transcriptase was added when synthesising cDNA) was used to determine whether genomic DNA contamination was present. A "no template control" (no cDNA template added to the final reaction) was also added to check for any DNA contamination. qPCR analysis was performed on an ABI PRISM 7000 sequence detection system (Applied Biosystems). The program used had the following cycle steps: 50ºC for 2 minutes, 95ºC for 10 minutes, then 40 cycles of 95ºC for 15 seconds and 60ºC for one minute. A dissociation curve was performed for each 96 well plate.

Statistical analysis of qPCR data: ABI prism 7000 SDS software was used to determine cycle threshold (Ct) values from the raw qPCR data. A standard curve for each primer pair was determined by amplification of serial dilutions of a cDNA sample of known concentration. The slope of the standard curve was used to calculate the expression level of the transcript of interest. This value was then normalised against the expression level of a reference gene, *elongation factor 1a* (*ef1a*) [139]. Normalization of qPCR data was used to obtain a more accurate reading of gene expression by accounting for any variance in RNA quantitation between samples. Statistical analyses on normalized data were performed using ANOVA and Student's t-tests using Excel (Microsoft) and 'R' statistical (www.r-project.org) software. Raw P-values were adjusted using the false discovery rate method. All primers used are shown in Section 2.1.4. Where possible, primers were designed to span an intron. Exceptions were *omp* and *val*.

CHAPTER 3: THE ZEBRAFISH MODEL OF REDUCED HUNTINGTIN EXPRESSION

3.1 Introduction

Use of the zebrafish system to investigate the function of huntingtin in development.

Htt has been shown to play an important role in early embryonic development (as discussed in Section 1.7). *In vivo* analysis of htt function however is made difficult due to early embryonic lethality of *Htt* null mouse embryos and lack of an observable phenotype in heterozygous embryos. The zebrafish model system provides unique advantages for investigation of the biological function of htt in development. Importantly for this project, morpholino oligonucleotides (morpholinos) have been used to easily allow controlled reduction, rather than elimination of htt protein in zebrafish embryos. In this project, antisense morpholinos designed to block htt expression have been injected into one-cell stage embryos. Analysis of the resultant phenotype was then carried out in an effort to determine key developmental processes for which htt plays a role.

Approach

Use of morpholinos: Investigation of the function of huntingtin in development by reducing huntingtin expression in the zebrafish model system.

Morpholinos are a tool used to reduce translation of specific genes either; *in vivo*, in animal model systems, such as zebrafish; or *in vitro*, in cell culture. Composed of a short chain of about 25 nucleotides, morpholinos act by blocking translation initiation in the cytosol (Figure 3.1). The sequence of the morpholino is chosen to allow it to hybridize specifically to

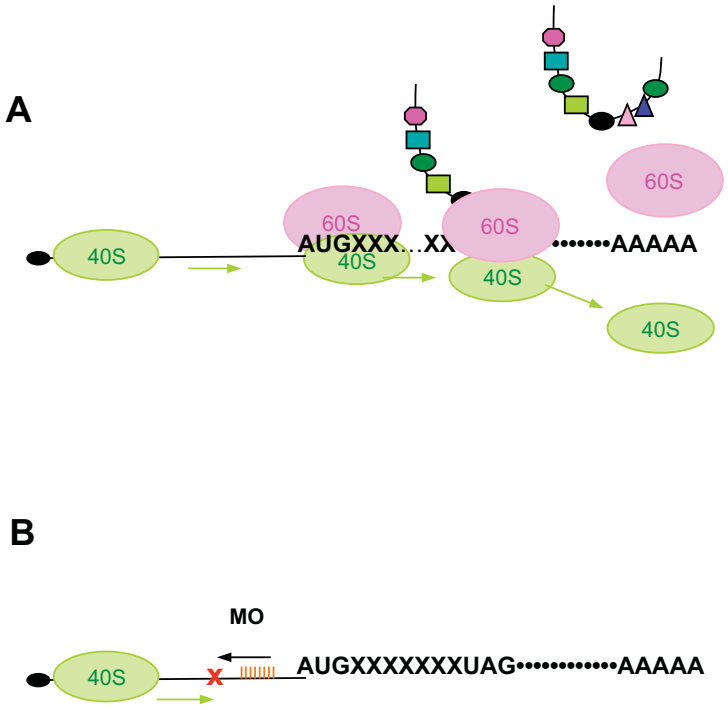

Figure 3.1 Morpholino oligonucleotides block translation initiation from target mRNA. (A) Cartoon showing the process of translation of an arbitrary gene, shown from left to right. The 40s ribosomal subunit scans the leader sequence of the RNA, identifies the start codon, and then recruits the 60s subunit for initiation of protein synthesis. (B) Binding of a morpholino to the 5'end of the gene inhibits the scanning and translation processes by blocking the 40s ribosomal subunit. Figure adapted from [139]. Abbreviations include; MO, morpholino.

the mRNA of a gene under investigation. It is optimal for the morpholino to bind somewhere within the 5' UTR, through to the first 25 bases of the mRNA coding sequence ([141]; www.genetools.com). By binding to this region, the morpholino is thought to block the RNA translation machinery from binding to the translation initiation region, thereby reducing the levels of the target protein [142].

In this study, two different morpholinos were used to reduce (or 'knockdown') the level of htt expression. Both were designed to be complementary to non-overlapping sequences in the 5'UTR of the zebrafish *htt* gene. The first morpholino (*hd*MO1) is targeted to the sequence between bases -19 to +5, therefore spanning the AUG translation start site. The second morpholino (*hd*MO2) is complementary to the sequence between -45 and -22 of the 5'UTR of the zebrafish htt RNA (Figure 3.2).

Control morpholinos are used to identify any effects on the embryos that are caused by injection of a morpholino, and not specific to reduction in htt expression. These control morpholinos are typically designed with sequences that are not complementary to any region of DNA in the genome. Two control morpholinos were used in this study. A standard control morpholino (*c*MO) [129] was used for earlier experiments and is stated to have no target, and no significant biological activity in the zebrafish system [www.gene-tools.com]. Later experiments were carried out using a 'mismatch' morpholino comprising the *hd*MO1 antisense sequence, interspersed with 5 mismatched bases (Figure 3.2). Throughout this thesis the *hd*MO1 mismatch morpholino will be abbreviated to *mc*MO1. Mismatch morpholinos provide a more rigorous test of specificity than the standard control morpholino. Mispair morpholinos are designed to have high sequence similarity to the translation blocking morpholino, but the incorporation of five mismatched bases along the length of the morpholino is sufficient to interfere with binding to the target RNA [143, 144]. In all experiments described within this thesis, very similar results were obtained for wild-type uninjected and control morpholino-injected embryos (either *c*MO or *mc*MO1). For simplicity only one control group (wild-type uninjected or control morpholino) image is shown. As injection of a control morpholino is a more stringent test of morpholino specificity than wild-type uninjected, *c*MO or *mc*MO images are shown where possible.

A

B

Morpholinos designed to block htt translation

•*hd*MO1:	5’-GCCATTTTAACAGAAGCTGTGATGA-3’
•*hd*MO2:	5’-GATATAATCTGATCGGAGATAGGGT-3’

Control morpholinos

•*c*MO: (Standard negative control)	5’-CCTCTTACCTCAGTTACAATTTATA-3’
•*mc*MO1: (5 base mispair)	5’-GCgATTTcAACAcAAcCTGTcATGA-3’

Figure 3.2 Morpholino oligonucleotides targeted against endogenous htt. Morpholinos were used as a tool to reduce the level of htt expression in developing zebrafish embryos by blocking translation from htt mRNA. (A) Two morpholinos were designed to bind to non overlapping sequences of the htt mRNA transcript. *hd*MO1 (blue) is complimentary to the 5’ AUG translation start site (bases -19 to +5) and *hd*MO2 (green) is complimentary to 5’UTR (bases -45 to -22). The AUG translation start site is shown in red uppercase letters. (B) Sequences of all morpholinos used in this project. In addition to the two *hd*MO morpholinos, two control morpholinos were used including a standard control morpholino (*c*MO) and a 5 base mispair of the *hd*MO1 antisense sequence (*mc*MO1). The 5 mismatched bases of *mc*MO1 are shown in red lower case letters.

3.2 Results

3.2.1 Confirmation of reduced huntingtin expression in hdMO embryos

One of the most powerful aspects of morpholino oligonucleotides lies within their ability to inhibit translation in a gene specific manner. For confident interpretation of the phenotypic results it is necessary to confirm the specificity when using a new morpholino oligonucleotide. A number of techniques can be used to do this. The most common of these is the use of an irrelevant (standard) and mispair control morpholinos, as described above (see Section 3.1). Another well-described technique is the use of two independent non-overlapping morpholinos targeted against the same mRNA which, when they achieve the same phenotype, are an indicator of the specificity of translation inhibition. *hd*MO1 and *hd*MO2 morpholinos have previously been shown to produce the same overall phenotype upon injection into zebrafish embryos [112]. As a result of the consistently similar phenotypic outcomes of *hd*MO1 and *hd*MO2 injection into zebrafish observed within this laboratory, many experiments described within this thesis were carried out with *hd*MO1 alone, unless stated otherwise.

One further measure commonly used to confirm the specificity of morpholino targeting is to assess the phenotypic severity in a 'dose-dependent' manner by injection of a morpholino at specific known concentrations. In many cases, a correlation between phenotypic severity and morpholino dose, similar to an allelic series, is used to demonstrate that the phenotype observed is a direct result of action of the morpholino to block gene expression, and less likely to be due to non-specific or toxic effects of a high dose of morpholino injection [129, 145].

Methods such as those described above have been used in this project to demonstrate gene specific inhibition of expression with *hd*MO morpholinos. The appearance of a similar phenotype upon injection of both *hd*MO morpholinos, and absence of a phenotype upon injection of *c*MO and *mc*MO1 morpholinos provides evidence for the specificity of each of the htt morpholinos, *hd*MO1 and *hd*MO2, to target and block translation from the same target RNA [112].

To further validate the *hd*MO model, this laboratory has previously demonstrated a reduction in htt protein expression upon injection of *hd*MO1 and *hd*MO2 morpholinos by two independent means, described in the following sections (Section 3.2.1.1 - 3.2.1.3).

3.2.1.1 Reduced huntingtin promoter-driven GFP expression in hdMO-injected embryos

In an experiment carried out by Amanda Lumsden [112], a construct was made that included ~1.2 Kb of the 5' UTR of the zebrafish *htt* gene sequence and the first 9 nucleotides of the htt ORF. Importantly, this region of the htt gene includes the htt promoter, and encodes both *hd*MO1 and *hd*MO2 binding sites. This DNA sequence was fused upstream and in frame of eGFP encoding Enhanced Green Fluorescent Protein. The resultant construct was injected into 1-cell stage embryos. At 10 hpf, these embryos showed a high level of GFP expression. When this *httpr*-GFP construct was injected along with *hd*MO1 or *hd*MO2 however, the level of GFP expression was significantly reduced. This result indicates that *hd*MO1 and *hd*MO2 were able to block GFP translation by binding to the appropriate region of mRNA originating from the *htt* promoter sequence (Figure 3.3).

3.2.1.2 Reduced endogenous huntingtin protein expression in hdMO-injected embryos (Western blot analysis)

Western blot analysis was used to visualize the effect of htt morpholino on the expression of htt protein in zebrafish embryos. Zebrafish embryos were injected at the one cell stage with *hd*MO1 or *c*MO. Protein lysate was collected at 48 hpf and separated on a polyacrylamide gel. Htt protein was detected using a polyclonal (rabbit) antibody directed against the amino terminus (aa1-17) of zebrafish htt [112]. Figure 3.3 shows that *hd*MO1 embryos have a reduced level of htt protein when compared to either *c*MO-injected or wild-type uninjected embryos. This demonstrates that *hd*MO1 morpholino is able to inhibit the translation of htt, while *c*MO does not.

3.2.1.3 Rescue of hdMO phenotypes

One further method to provide evidence for the specificity of a morpholino is by mRNA rescue. This method provides the most rigorous test of morpholino specificity by attempting to restore the phenotype of the morpholino-injected embryos to that seen in

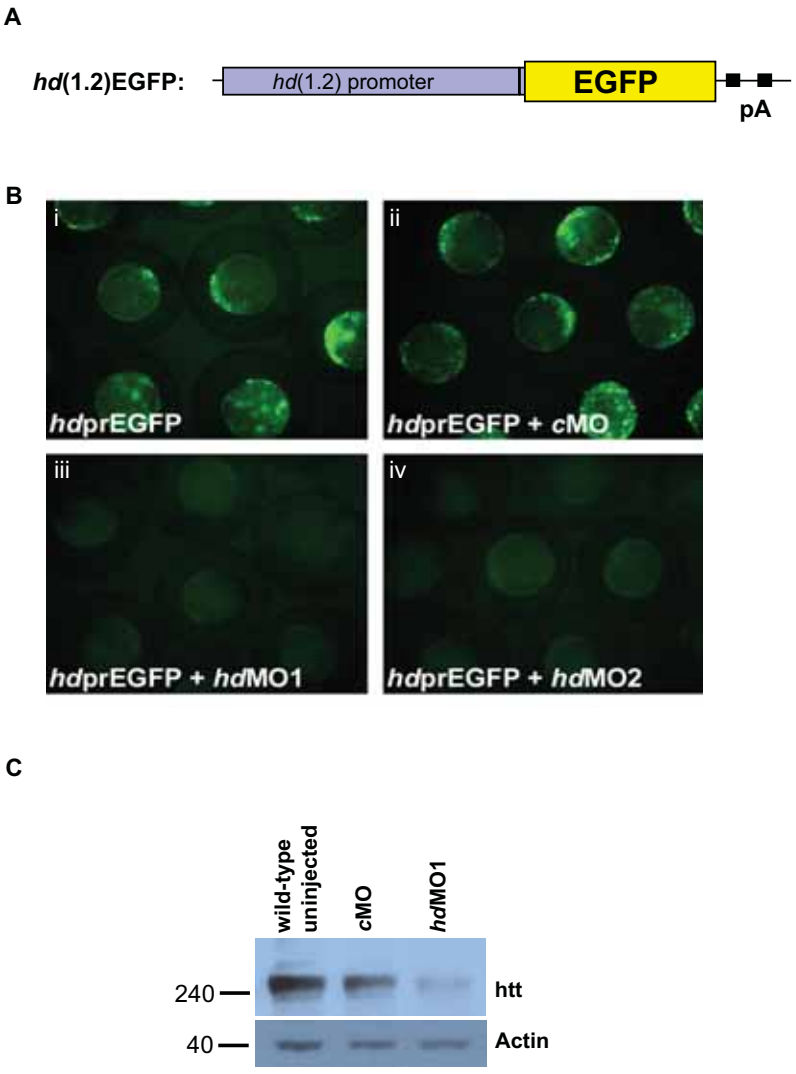

Figure 3.3 Analysis of the specificity of *hd*MO morpholinos. (A) The specificity of action of both *hd*MO morpholinos were analyzed by injecting a construct comprised of 1.2kb of the 5' untranslated region of the *htt* gene and 9 nucleotides of the *htt* ORF cloned upstream of GFP. This region of the *htt* gene includes the *htt* promoter, and encodes both *hd*MO1 and *hd*MO2 binding sites. (B) A transgenic line of zebrafish was created to express GFP driven by the *htt* promoter (i). Injection of *hd*MO1 or *hd*MO2 was able to block translation of GFP (iii and iv) while *c*MO injection did not (ii). GFP was expressed to a similar level in *c*MO-injected embryos (ii) as uninjected transgenic embryos (i). This experiment was carried out by Amanda Lumsden [112]. (C) Western blot analysis was used to show reduced htt expression in *hd*MO1embryos. 21.3ng of morpholino injected per embryo.

wild-type uninjected embryos. In an RNA rescue experiment, morpholino-injected embryos are co-injected with the same mRNA that the morphlino is targeted to bind to. The rescue mRNA therefore has the same gene sequence that the target mRNA does, however, the rescue mRNA has a modified 5'-UTR so that the morpholino cannot bind to it. Translation of the rescue mRNA replaces the production of the endogenous protein, which is knocked-down by the morpholino. Since the rescue mRNA will not alleviate phenotypic changes caused by off-target mRNA binding, RNA rescue can be a reliable test of the specificity of a morpholino.

RNA rescue was used in this project in an attempt to assess the specificity of *hd*MO activity. One major difficulty of the use of this method for the *hd*MO model is the size of the htt transcript. Zebrafish htt RNA is very large (~10 Kb) making both cloning and transcription of *htt* very difficult. One alternative approach was to clone only the amino terminal region of the htt protein. This particular fragment (the first 12 exons, or 548aa) has been shown to include nearly all of the interaction domains and modification sites of htt [146]. This N-terminal region of htt has also been shown to function in a similar manner to full-length htt in neural protection assays, including serum deprivation and 3NP addition to a variety of cell lines [47, 93]. Cloning of the amino terminal region was therefore carried out in an attempt to rescue the phenotype of *hd*MO zebrafish. A fragment of the zebrafish *htt* gene equivalent to the first 548aa of the human htt protein was amplified and cloned into an expression vector commonly used for zebrafish RNA expression, pCS2+. The insert of the resultant construct (htt548eq) was then transcribed, and the RNA injected into one cell stage zebrafish embryos.

No disturbance in development was observed after injection of htt548eq RNA alone. The high survival rate of embryos to 24 hours upon RNA injection showed that even large doses (400pg) did not cause any toxic effect to wild-type embryos. Unfortunately, injection of htt548eq RNA along with *hd*MO1 was not able to noticeably recover either of two *hd*MO phenotypes (the reduction in *sine oculis homeobox homologue (six1)* expression in the pre-placodal region or reduction of *no tail (ntl)* expression in the tail bud; see Chapter 5) by *in situ* hybridization analysis (results not shown).

Time constraints of this PhD did not allow further analysis of the ability of this construct to rescue *hd*MO phenotypes. It is possible that the use of *in situ* hybridization to identify changes in gene expression is not sensitive enough to detect any small changes in expression levels. For future work, it may be helpful to look at quantitative gene expression changes such as qPCR analysis of *olfactory marker protein (omp)* and *six1*. The clear and reproducible nature of these qPCR phenotypes may be helpful to highlight any small changes in gene expression (see below and Chapter 5 for a description of the olfactory and pre-placodal phenotypes).

It may also be helpful in future rescue experiments to use a vector construct which can increase expression of the htt construct, such as the *Tol2* transposon vector. The minimal *Tol2* vector and transposable element system has been shown to improve efficiency of DNA integration over plasmid microinjection by up to 14 fold [147]. Importantly for this project, the *Tol2* vector has also been shown to carry a DNA insert as large as 11 Kb without reducing its transpositional activity [148]. Since the *Tol2* vector is injected as DNA and has good integration efficiency, the full-length *htt* gene could be injected, enhancing the possibility of a successful phenotype rescue.

3.2.2 Analysis of hdMO phenotype

3.2.2.1 Apoptosis detection in hdMO embryos using acridine orange

Previous studies have suggested that htt has an important function in prevention of apoptosis (as discussed in Section 1.4.1). We therefore decided to look at the general pattern of apoptosis within the whole *hd*MO embryo at various stages of development. The aim of this experiment was to determine whether reduction in htt expression results in an increased level, or altered pattern of apoptosis within the developing embryo.

Acridine orange is widely used as a stain for the detection of apoptotic cells. Upon application to live embryos, acridine orange accumulates inside acidic granules that are formed primarily in cells undergoing apoptosis. These cells are visualized as bright green fluorescent spots visible under the dissecting microscope [149, 150]. Acridine orange has been shown to stain apoptotic but not necrotic cells in live *Drosophila* embryos [132] and is commonly used to identify apoptotic cells in whole zebrafish [151-157].

Acridine orange is easily applied to live embryos in embryo medium and results can be viewed immediately. One advantage of using this technique for apoptosis detection is that application to whole zebrafish provides information on the spatial distribution of apoptotic cells throughout the whole embryo. Due to htt's proposed role in neuronal survival and high level of expression within the brain, it was hypothesized that reduction in htt expression would result in an increase in the number of cells dying by apoptosis, and that this may occur most noticeably within the brain.

In order to visualize any change in apoptosis, various stages of zebrafish embryo development were analyzed from 10 hpf (the time of early neurogenesis) to 72 hpf (when the embryo has developed into a fully formed, free-swimming larvae; Figure 1.2 and Figure 3.4).

Using this technique, apoptosis within the wild-type uninjected embryo was found to occur at all time points, consistent with previous findings of apoptosis as part of normal zebrafish development [158]. For this reason, apoptosis in *hd*MO1 embryos was compared with that of wild-type uninjected and *c*MO-injected embryos from the same embryo batch.

No significant increase in apoptosis was detected in *hd*MO1 embryos prior to 36 hpf (Figure 3.4). Later time-points (after 36 hpf) revealed a number of interesting phenotypes, which are described below. Only one of these phenotypes was observed within the brain.

3.2.2.2 Optic tectum

The optic tectum (termed superior colliculus in mammals) is located within the midbrain on the dorsal side of the head. The function of the optic tectum is to process visual space and auditory information. It is the largest visual processing region in the brain [159, 160].

In *hd*MO1 embryos, the number of apoptotic cells in the optic tectum appeared to be greater than that observed in wild-type uninjected or *c*MO embryos (Figure 3.4 and 3.5). The increase in apoptosis was most visible at 48 hpf.

In each batch of embryos, a range of phenotypic severity was observed. The cause of this variation is not known, however it may be a result of small differences in the precise location of morpholino injection within the embryo, or small variations in injection volume. For this reason, apoptosis within the optic tectum was quantitated by scoring each embryo against a panel of standard images representing various amounts of apoptosis on a scale from 0 to 5 (see Figure 3.5). This scoring regime revealed an overall increase in the level of apoptosis in the optic tectum of *hd*MO1 embryos compared to wild-type uninjected and *c*MO embryos. Injection of half of the amount (4.25ng) of *hd*MO1 morpholino resulted in a milder increase in the level of apoptosis suggesting a dose dependent response to *hd*MO1 injection (Appendix A).

In a study of apoptosis in the developing wild-type zebrafish brain, Cole and Ross observed a high rate of apoptosis within the optic tectum that peaked between 48 and 60 hpf [158]. This burst of apoptosis coincides with growth of retinal axons, extending from the eye to make contact with the optic tectum. Any tectal cells with insufficient contacts with retinal axons are eliminated by apoptosis. Cole and Ross therefore concluded that this burst of

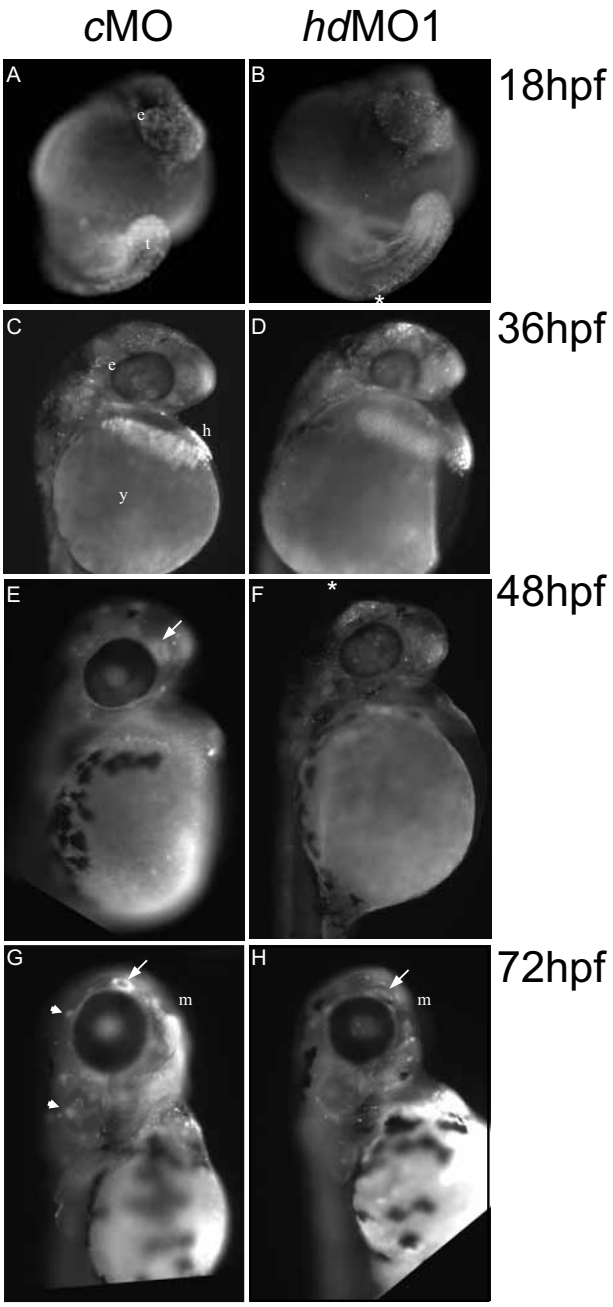

Figure 3.4 Apoptosis in whole *hd*MO1 embryos. Acridine orange staining of *hd*MO1 embryos at various stages of development. A high level of background staining was seen at 18 hpf throughout the embryo. The hatching glad also has high background staining (36 hpf). Some structures of interest include; olfactory placode, (E, G, H) arrow; lateral line neuromast, (G) arrow head; optic tectum, (F) asterix. Abbreviations include; e, eye; m, mouth; h, hatching gland; t, tail; y, yolk; (A-B) anterior view, (C-H) lateral view. 8.5ng of morpholino injected per embryo.

A

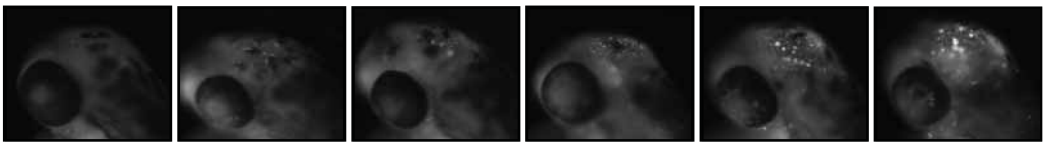

0 1 2 3 4 5

B

8.5ng MO		0	1	2	3	4	5	Total # of embryos
48hpf	WT uninj.	100	0	0	0	0	0	29
	*c*MO	94.1	5.9	0	0	0	0	34
	*hd*MO1	2.4	2.4	17.1	19.5	31.7	26.8	41
72hpf	WT uninj.	97.3	2.7	0	0	0	0	37
	*c*MO	73.6	26.4	0	0	0	0	53
	*hd*MO1	19.6	25.5	41.2	7.8	5.9	0	51
96hpf	WT uninj.	100	0	0	0	0	0	45
	*c*MO	100	0	0	0	0	0	40
	*hd*MO1	92.6	0	3.7	3.7	0	0	27

Figure 3.5 Apoptosis within the optic tectum of *hd*MO1 embryos. Reduction in htt expression results in increased apoptosis within the optic tectum. (A) Scoring table of representative embryos showing various amounts of apoptosis within the optic tectum scored from 0 (no apoptosis) to 5. (B) Results of scoring are displayed as a percentage, with the total number of embryos shown in the right-hand column. Green boxes indicate the scoring level with the greatest number of embryos for each treatment group and each time point. *hd*MO1 embryos have an increased level of apoptosis at 48 and 72 hpf as evidenced by the shift in green box to the right. (A, B) Representative embryos shown for each group (0-5). Dorsal/lateral views of embryos, anterior to the left; 48 hpf. 8.5ng morpholino injected per embryo. Half-dose response shown in Appendix A. Results pooled from 2 independent experiments for each time point.

apoptosis is due to the death of cells in the optic tectum that have not had contact with a retinal axon. The cause of the increase in apoptosis (above wild-type levels) in the optic tectum of *hd*MO1 embryos has not been determined. The increase in apoptosis was evident between approximately 48 and 72 hpf. This window of time corresponds to that when retinal axons are making contact with the optic tectum. Due to the similar time window, it is hypothesized that the increase in apoptosis observed in *hd*MO1 embryos, above wild-type levels, is a result of a reduction in the number retinotectal axons which make contact with the optic tectum. This phenotype may result from misguidance of retinal axons or possibly a reduction in the number of retinal neurons. Further discussion about this phenotype is included in Chapter 6.

3.2.2.3 Olfactory placodes

During development of wild-type embryos, the olfactory placodes have one of the highest rates of apoptosis compared to any other region of the brain [158]. This apoptosis begins at 22 hpf and continues throughout development. The continuous apoptosis observed in the olfactory placode occurs as an important part of maintenance of this sensory system. Olfactory sensory neurons (OSN) are continuously being replaced by newly differentiated olfactory neurons. It is thought that this process may be important for a number of reasons, including: to replenish ageing OSN, to replace OSN that have inappropriate contacts with the brain, or as a result of exposure to environmental toxins [161].

In the wild-type uninjected embryo, apoptosis within the olfactory placode can be easily visualized from 48 hpf onward after staining with acridine orange. With this staining it is revealed that between 48 and 72 hpf, the appearance of the olfactory placode changes and the level of apoptosis increases. At approximately 48 hpf, a pit is beginning to form in the centre of the placode, which appears as a loose group of cells just anterior to the eye (Figure 3.6 C). By 72 hpf, the olfactory pit has enlarged and the placode appears as a mature olfactory structure (Figure 3.6 A).

In *hd*MO1 embryos, the level of apoptosis within the olfactory placodes is diminished compared to that of *c*MO embryos at 72 hpf (Figure 3.6 A and B). *hd*MO1 embryos appear to also have a very small, immature olfactory pit, similar in appearance to that of a 48 hpf *c*MO embryo. This could suggest that the development of the olfactory placode may be delayed (for comparison see Figure 3.6 B and C). This is unlikely to be due to general developmental

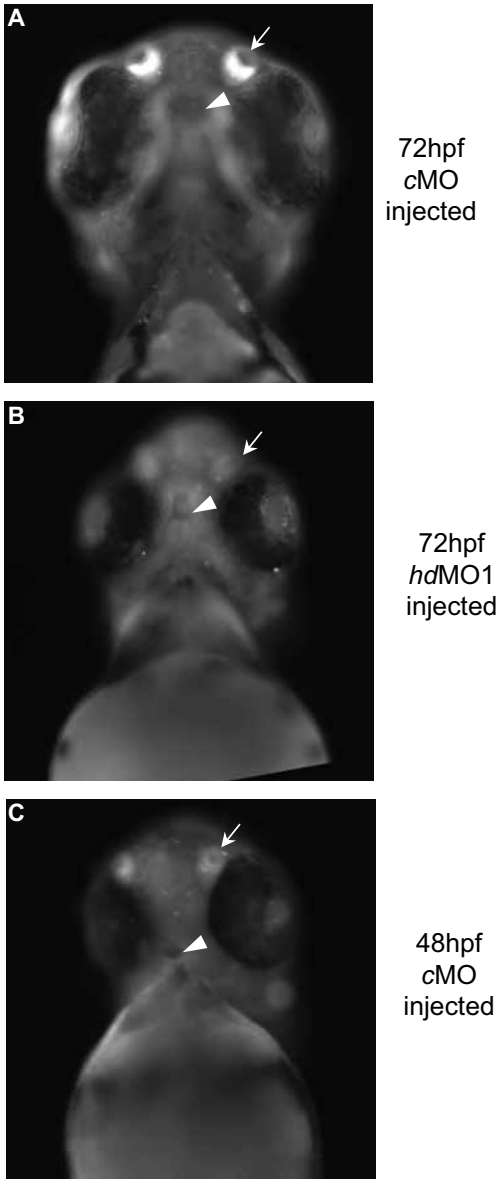

Figure 3.6 Apoptosis within the olfactory placode of *hd*MO1 embryos. (A, B) Show decreased level of apoptosis with the olfactory pit of *hd*MO1 embryos compared to *c*MO embryos. Also note lack of olfactory pit (arrow) suggestive of a delay in olfactory placode development. (B, C) The appearance of the *hd*MO1 embryo olfactory placode is similar to that of a 48hpf *c*MO embryo based on its shape and the small size of the olfactory pit. However the delay in olfactory placode development is unlikely to be due to general developmental delay as the mouth (arrowhead) of *hd*MO1 embryos (B) has progressed beyond that seen in a 48hpf *c*MO embryo (C). All embryos shown in ventral view, anterior to the top. Numbers of embryos displaying the described phenotypes were (A, B) wt uninjected 0/78, *c*MO1 0/93, *hd*MO1 40/64. 8.5ng morpholino injected per embryo. Representative embryos shown. Results pooled from 4 independent experiments.

delay, as development of the mouth in *hd*MO1 embryos has progressed beyond that seen in a 48 hpf *c*MO embryo, while the olfactory placode development has not. Therefore it appears that the reduced level of htt expression results in a decreased level of apoptosis and also inhibits the development of the olfactory placode specifically.

DiI, is a lipophillic dye that preferentially stains mature olfactory sensory neurons [134]. Staining with DiI shows that there is a near complete reduction in the number of mature olfactory sensory neurons in *hd*MO1 embryos, compared to *c*MO embryos (Figure 3.7 A). This result suggests that the lack of apoptosis within the olfactory placode is not due to failure of olfactory sensory neurons to undergo apoptosis, but rather due to absence of olfactory neurons in the placode of *hd*MO1 embryos. Similarly, quantitative PCR (qPCR) analysis of olfactory marker protein 2 (*omp*), expressed by mature olfactory sensory neurons [162], is significantly reduced in *hd*MO1 embryos compared to *mc*MO1 embryos. Figure 3.7 B shows that *hd*MO1 embryos have significantly reduced expression levels of *omp* RNA suggesting that htt plays a role in formation or survival of the olfactory sensory neurons.

3.2.2.4 Lateral line neuromasts

The lateral line sensory system is part of the peripheral nervous system of fish and amphibians, and is closely related (and possibly ancestral) to the human auditory system. It is used to detect mechanosensory stimuli such as water movement. The lateral line system is comprised of a number of discrete sensory units (neuromasts) arranged in a species-specific pattern on the surface of the body (Figure 3.8 A) [137]. Each neuromast is comprised of mechano-sensory hair cells surrounded by support cells and associated neurons which extend axons to make contact with the hindbrain [163]. Apoptosis within the lateral line system is a well-known phenomenon. Central hair cells of the neuromasts undergo a continuous high rate of cell death throughout zebrafish development and adulthood [158, 164] and are re-supplied by differentiation of supporting cells into new sensory hair cells.

Analysis of *hd*MO1 embryos after acridine orange staining revealed a reduced level of apoptosis within the lateral line neuromasts compared to wild-type uninjected and *c*MO embryos (Figure 3.8). Since apoptosis is an essential part of maintenance within the neuromasts, the absence of staining within the neuromasts could be a result of either; an inability of *hd*MO1 hair cells to undergo apoptosis, or to absence of either neuromasts or hair cells in *hd*MO1 embryos.

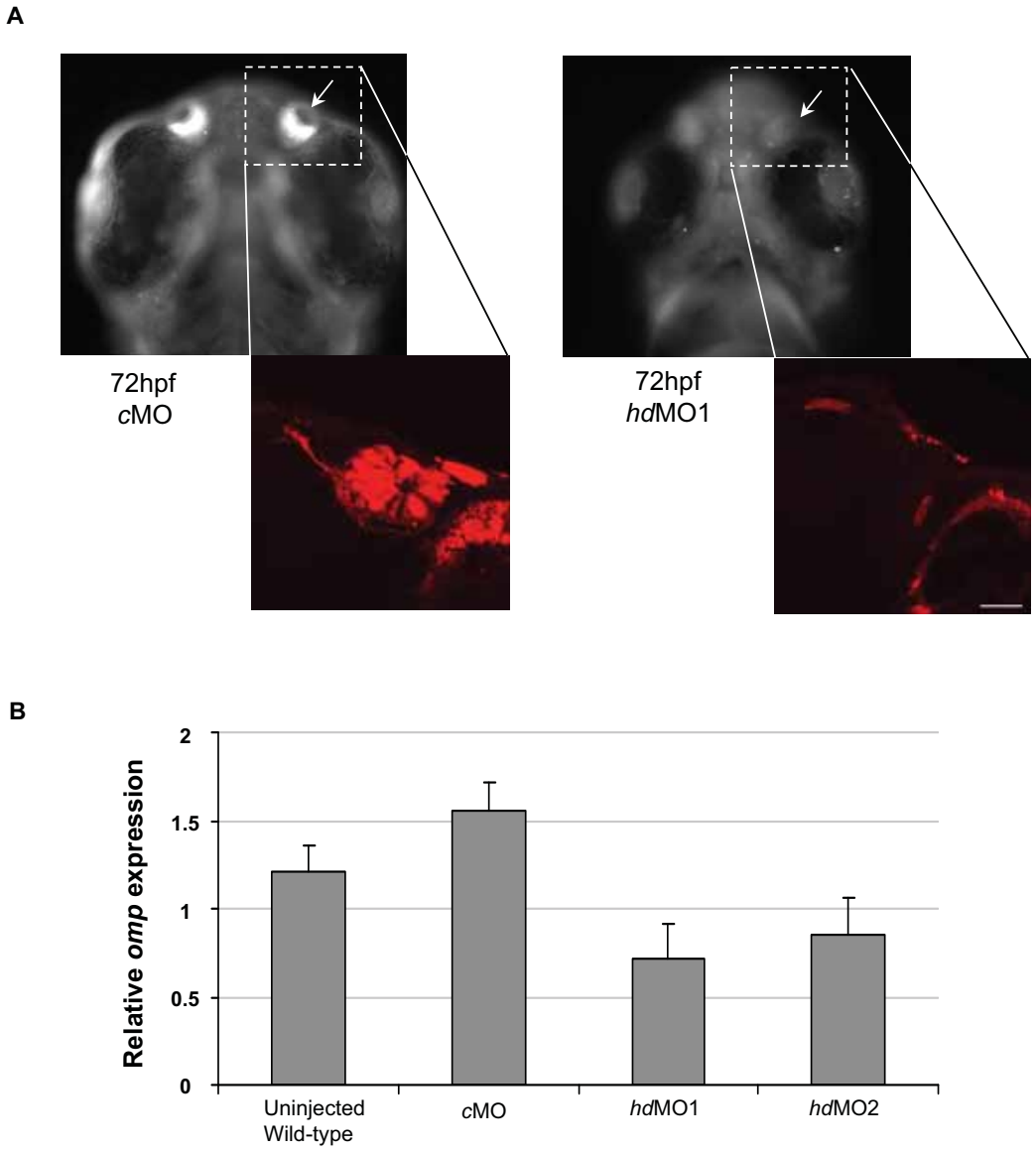

Figure 3.7 *hd*MO1 embryos have a reduced number of olfactory receptor neurons within the olfactory placode. (A) DiI staining revealed *hd*MO1 embryos have a reduced number of olfactory receptor neurons (red) in the olfactory placode. (B) qPCR analysis was used to quantitate the reduction in olfactory sensory neurons in *hd*MO1 embryos by analysis of *omp* mRNA expression levels. Graph shown is representative of three independent experiments. Data is expressed relative to *ef1a* gene expression. For all three experiments combined, *hd*MO1 vs *mc*MO1 P-value = <0.001 (see Table 5.1). (A) 8.5ng of morpholino injected per embryo. Ventral view, anterior to the top. (A) 72 hpf, (B) 48 hpf. Numbers of embryos displaying the described phenotypes were (A) *c*MO1 0/53, *hd*MO1 26/37. Representative embryos shown. Scale bar = 25 μm.

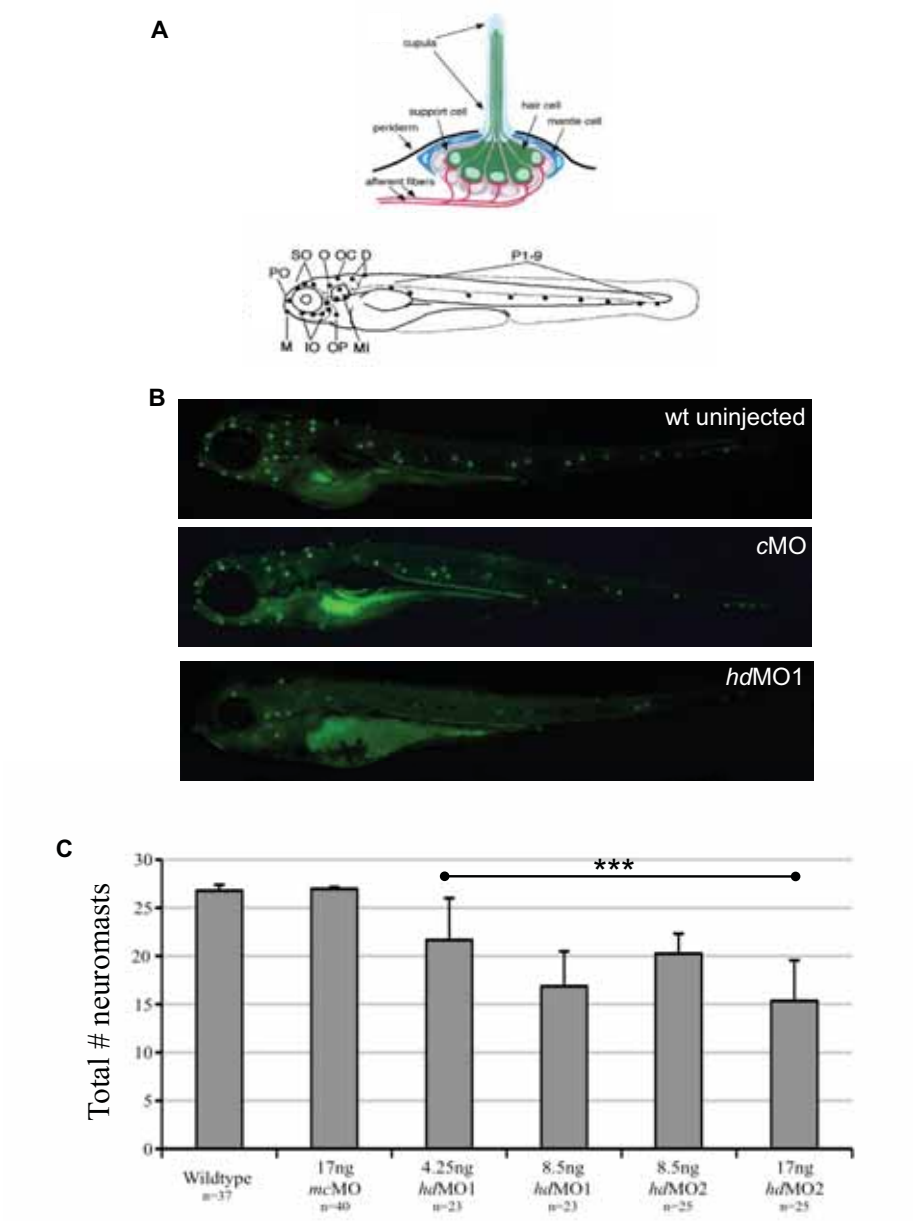

Figure 3.8 *hd*MO1 embryos have a reduced number of lateral line neuromasts. (A) Lateral line neuromasts are composed of hair cells (green) surrounded by support cells (pink) and are present in a specific, well characterized pattern along the lateral side of the embryo. Figure reproduced from [137] and [163]. (B) DASPEI staining reveals a reduced number of neuromasts (green) in *hd*MO1 embryos. Number of neuromasts quantitated in (C) and (D) in anterior and posterior regions respectively. All embryos shown anterior to the left. *** Significance is determined by P-value = < 0.001. P-values were determined by a Students t-test comparison of each group to wt uninjected. Wt uninjected vs. *mc*MO1 comparison showed no evidence of a significant effect due to *mc*MO1 injection. P-values = 17ng *mc*MO1, 0.10637499; 4.25ng *hd*MO1, $1.83991E^{-08}$; 8.5ng *hd*MO1 $5.16023E^{-21}$; 8.5ng *hd*MO2, $2.82275E^{-23}$; 17ng *hd*MO2, $5.56472E^{-21}$. (B) 8.5ng morpholino injected per embryo.

Like DiI, DASPEI staining is used to visualize sensory neurons, however DASPEI is specifically taken up by hair cells within the lateral line neuromast [135]. In the wild-type embryo, the number and pattern of lateral line neuromasts is well characterized [137]. DASPEI staining showed that *hd*MO1 embryos have fewer lateral line neuromasts compared to wild-type uninjected and *mc*MO1-injected embryos (Figure 3.8 B). Quantification of the total number of neuromasts in each embryo shows that this reduction occurs as a dose dependent response to *hd*MO1 injection (Figure 3.8 C).

3.2.2.5 Craniofacial skeleton

Gross analysis of the morphology of *hd*MO1 embryos revealed disruption in tissues of the mouth. This was especially evident after staining with acridine orange (Figure 3.6). Despite no obvious increase in cell death in this region, acridine orange staining provided some contrast within the transparent embryo, exposing the external pharyngeal morphology. As the structure of the branchial region lies over the cartilage skeleton, it seemed likely that *hd*MO1 embryos would have an altered cranioskeletal structure. Alcian blue was used to stain the cartilage of *hd*MO1 embryos in order to visualize this disruption.

The craniofacial skeleton of zebrafish has been well characterized. Schematic diagrams demonstrate the precise spatial plan of the bones that make up this region [165] as shown in Figure 3.9. In addition, a range of craniofacial mutations have been identified and characterized in zebrafish mutation screens [165-167]. These studies have provided knowledge of genes involved in formation of this region and their precise function. By comparing the craniofacial structure of *hd*MO1 embryos to wild-type uninjected embryos we can determine how reducing htt expression affects craniofacial formation, and possibly associate this disruption with genes involved in formation of the disrupted area. This information may then provide some suggestions as to the normal function of htt and pathways htt is involved in (this is discussed further in Section 4.2).

The lower jaw of the zebrafish craniofacial skeleton is comprised of 7 major pharyngeal arches (p1-7) from anterior to posterior (as shown in Figure 3.9). The first pharyngeal arch (p1, otherwise known as the mandibular arch) is composed of the Meckel's (m) and palatoquadrate (pq) cartilages. The second pharyngeal arch (p2, or hyoid) is composed of the ceratohyal (ch) and hyosymplectic (hs) cartilage. The remaining pharyngeal arches (p3-7, otherwise known as the branchial region) are gill-bearing arches. The basihyal (bh) cartilage is formed in the midline in an anterior-posterior direction. p3-7 cartilages radiate out from the bh cartilage to the lateral edges of the embryo (Figure 3.9).

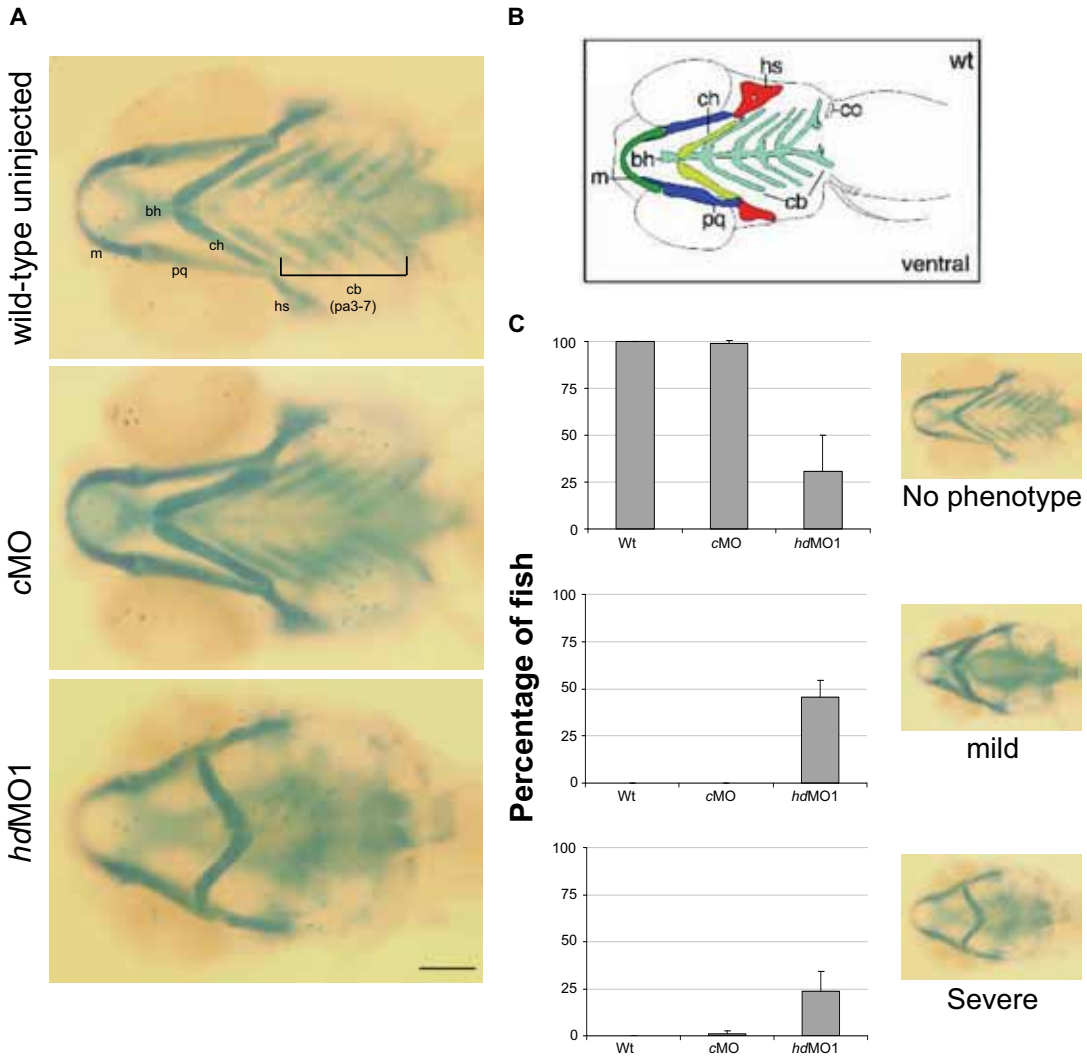

Figure 3.9 Reduced htt expression disrupts branchial arch formation in the developing zebrafish. (A) Alcian blue cartilage stain shows disruption in the pattern and formation of the pharyngeal cartilage. (B) Map of zebrafish craniofacial bones. Figure adapted from [165]. (C) Scoring of severity of craniofacial disruption. Number of embryos = 29 wt, 54 *c*MO, 47 *hd*MO1 embryos. All embryos are at 7 dpf. Results pooled from two independent experiments. All fish shown in ventral view, anterior/rostral to the left. 8.5ng morpholino injected per embryo. Abbreviations include; bh, basihyal; cb, ceratobranchial; ch, ceratohyal; hs, hyosymplectic; m, Meckel's cartilage; p3-7, pharyngeal arch 3-7; pq, palatoquadrate. Scale bar = 200 μm.

Alcian blue binds to proteoglycans of the extracellular matrix of cartilage. Upon addition of the stain, cartilage appears blue and can easily be visualized in the whole zebrafish embryo due to the transparency of the embryo (after bleaching of some pigment). Alcian blue staining showed that *hd*MO1 embryos have fully formed p1 and p2 cartilages. The most common phenotype of *hd*MO1 embryos was partial or complete loss of p3-7 cartilages compared to *c*MO embryos. Some embryos however also had a ceratohyal cartilage pointing in a caudal rather than a rostral direction. This appears to be a more severe phenotype as this disruption was not evident without the loss of p3-7 cartilage.

Each batch of *hd*MO1-injected embryos were scored in three groups (shown in Figure 3.9 C) including;

'No phenotype' - no disruption of any pharyngeal arch cartilage, and a rostral facing p2.
'Mild phenotype'- disruption of some or all p3-7 cartilage, with a rostral facing p2.
'Severe phenotype' - disruption in all p3-7 cartilage, and a caudal pointing p2.

All craniofacial cartilage is formed by 5 dpf. However, quantitation and analysis of the craniofacial structure was carried out on 7dpf embryos to eliminate the possibility of general developmental delay as a cause of this phenotype.

At a moderate dose of morpholino (8.5ng), alcian blue staining showed that the ceratohyal cartilage was pointing in a caudal rather than rostral direction in 25% of *hd*MO1 embryos. Approximately 70% of all *hd*MO1 embryos showed partial or complete loss of p3-7 cartilages. When a higher concentration of morpholino was injected (to deliver 21ng, instead of 8.5ng morpholino per embryo), a very similar phenotype was observed (Figure 3.10). The same pattern of bone formation was evident in both groups (21ng and 8.5ng-injected) with differentiation of the first two branchial arches and absence of the most posterior arches (p3-7). This suggests that htt at this low level is not a rate-limiting step in p1 and p2 cartilage differentiation, however they are grossly malformed. Analysis of the alcian blue stained *hd*MO1 neurocranium (Figure 3.10) shows little difference when compared with *c*MO-injected embryos however, in the most severe cases the neurocranium appears shorter than in *c*MO-injected embryos.

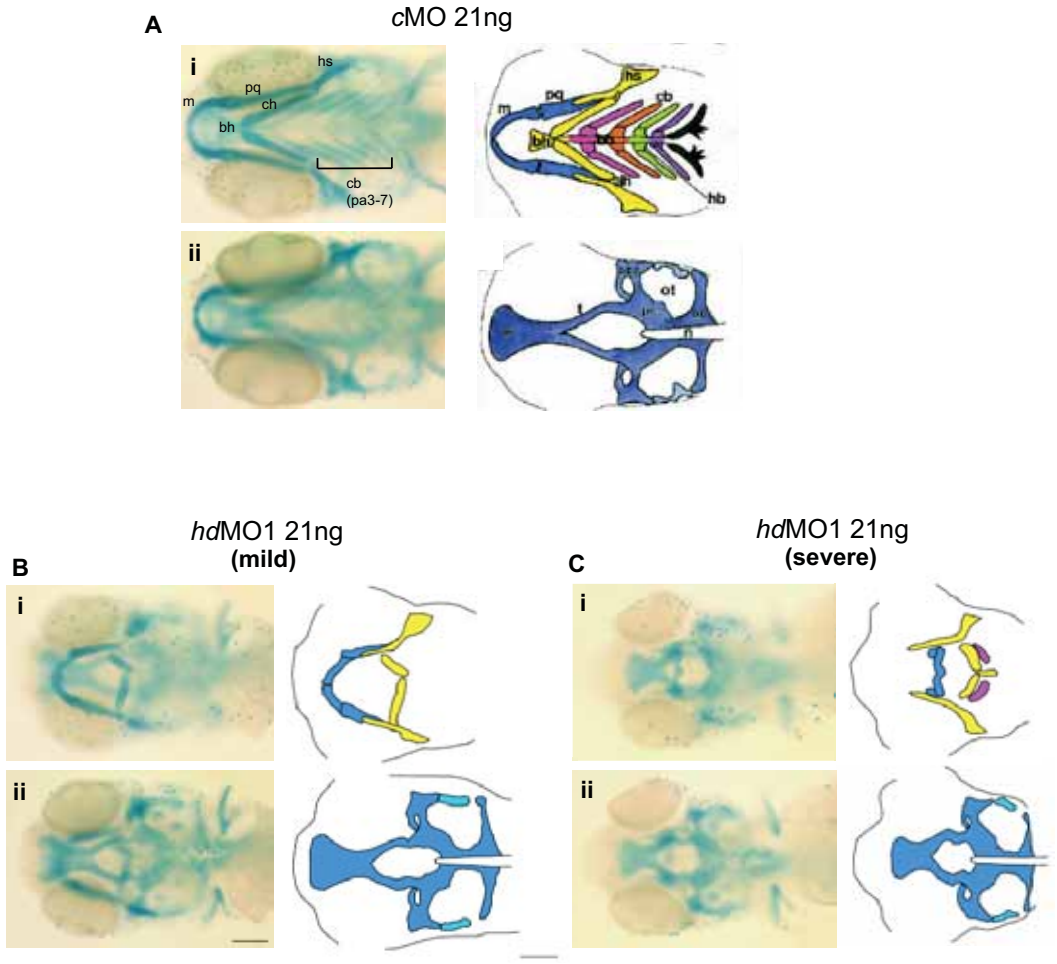

Figure 3.10 Htt plays a rate-limiting role in formation of all craniofacial bones. Injection of a high dose (21ng) of *hd*MO1 morpholino results in a similar yet more severe phenotype than 8.5ng. (B, C) Alcian blue staining shows that even at high doses of morpholino, *hd*MO1 embryos still form p1 and p2. No structural difference is evident in the neurocranium of *hd*MO1 embryos (Bii, Cii) compared to *c*MO embryos (Aii). All (i) show branchial arch cartilage, and all (ii) show neurocranium. (A-C) Alcian blue stained embryos (left column) and schematic diagrams of craniofacial bones (right column). (A) right column schematic adapted from [167]. Cartilages of the same segment share the same colour: pa1 (mandibular, blue), pa2 (hyoid, yellow), pa3 (pink), pa4 (orange), pa5 (green), pa6 (purple), and pa7 (black). All fish shown in ventral view, anterior to left, 7 dpf. 21ng morpholino injected per embryo. Abbreviations include; ac, auditory capsule; bb, basibranchial; bh, basihyal; c, cleithrum; cb, ceratobranchial; ch, ceratohyal; e, ethmoid plate; hb, hypobranchial; hs, hyosymplectic; ih, interhyal; m, Meckel's cartilage; n, notochord; ot, otic capsule; pa3-7, pharyngeal arch 3-7; pc, parachordal; pq, palatoquadrate; t, trabeculae cranii. Scale bar = 200 μm.

3.3 Conclusion

The primary aim of this project was to investigate htt's normal function(s) during development and the possible contribution of the perturbation of these functions to the pathology of HD. This aim was addressed by investigating the phenotypes caused by reduction of htt expression in a zebrafish model system.

This chapter has described the validation of two htt specific morpholino oligonucleotides (*hd*MO1 and *hd*MO2) by Western blotting and by inhibition of htt promoter-driven GFP expression (carried out by Amanda Lumsden). These two morpholinos were used to reduce the level of htt during zebrafish development in an attempt to identify the important, however as yet uncertain, functions of htt in development. It was proposed that observation of the *hd*MO1 embryos during development will help to identify critical stages in development in which htt plays a role, and may help to determine specific rate-limiting roles for htt in development.

Initial investigations focused on a proposed role for htt in prevention of apoptosis. It was hypothesized that if htt were involved in prevention of apoptosis then reduction in htt expression would result in an increased amount of apoptosis (as visualized by staining with acridine orange). Although some alteration in the level of apoptosis was observed, *hd*MO1 embryos did not show a significant increase in the amount of apoptosis within the brain, as was hypothesized. This result may suggest that htt does not play a significant role in cell survival in the brain. This possibility is supported by evidence that mouse embryonic stem cells and neurons lacking htt are able to survive in culture [80, 168, 169]. It is however also possible that the acridine orange staining technique was not sensitive enough to detect a minor change in apoptosis, or that acridine orange was not able to penetrate into the brain of zebrafish. For a more detailed analysis of brain apoptosis it may be necessary to dissect the skin and eyes off the embryo prior to staining to assist in penetration of the stain, or alternatively use another method for apoptosis detection, which can be carried out on formalin fixed brain sections, such as TUNEL stain.

Overall, acridine orange staining of *hd*MO1 embryos revealed a number of interesting phenotypes involving an alteration in the level of apoptosis. This investigation found that htt is important for formation of the olfactory sensory system, the lateral line sensory system, and proper formation of the facial cartilage. In addition, it was observed that *hd*MO1 embryos have an increased level of apoptosis within the optic tectum.

The following paragraphs describe each of the observed *hd*MO1 phenotypes and discuss a possible cause for the observed disruption. If a loss of normal htt function plays any role in the pathology of HD then there may be similarities between the disease pathology and the phenotypic outcome of a reduction in htt expression. For this reason, the following paragraphs also outline any disruption in olfactory, auditory or visual function in HD patients or in *in vivo* animal models of HD.

Olfactory sensory system

Results described in this chapter have demonstrated a possible role for htt in development of the olfactory sensory system. There are several possible explanations for the reduction in the number of mature olfactory sensory neurons including: a reduced number of olfactory precursor cells, dysfunction in migration of precursor cells, or a defect in differentiation from early precursor cells to olfactory sensory neurons. At this stage, the cause of the olfactory phenotype was unknown. Further investigation of this phenotype is described in Chapter 5.

Clinical observations of HD patients reveal some evidence of olfactory impairment. HD patients have been shown to have impaired olfactory detection [170-172], olfactory memory [172-174], identification [170, 171, 175, 176], and discrimination of quality and intensity of odors [170]. This dysfunction may occur by either of two mechanisms. Firstly, neurodegeneration within brain regions which are important for processing olfactory information is likely to be the cause of impaired olfactory memory, and odor identification and discrimination [173], while impaired odor detection is likely to be due to dysfunction of olfactory neurons. It is possible that perturbation of the normal function of htt could play a role in impaired olfactory function seen in HD patients.

Lateral line

DASPEI staining showed that *hd*MO1 embryos have fewer lateral line neuromasts, and therefore suggests a role for htt in formation of the lateral line system. The cause of this dysfunction has been investigated in greater detail and is described further in Chapter 5.

Hearing loss has not been described as a clinical feature of HD. Only one study linking HD to hearing impairment has been reported and is described online by the HD Advocacy Centre [177]. Despite the lack of evidence for hearing loss in HD patients, The National

Institute of Health states that a measurement of hearing is currently used as part of a panel of diagnostic tests for HD [178]

Optic tectum

Acridine orange staining of *hd*MO1 embryos revealed an increase in apoptosis within the optic tectum. As mentioned in Section 3.2.2.2, one likely cause may be due to inappropriate connection of retinal axons with the optic tectum. This suggests that htt may be involved in formation or survival of retinal cells, a theory supported by a *Drosophila htt* knockout model in which absence of htt leads to retinal degeneration in the eyes of adult flies [75]. The observed neurodegeneration is similar to that caused by overexpression of polyQ htt [75]. These results together support the theory that expansion of polyglutamine may result in loss of htt function.

Retinal degeneration is also seen in an HD transgenic mouse model, R6/2 [179, 180] and a human HD patient compared to age matched control, although only one HD patient was studied [181]. This evidence suggests a role for htt in survival of retinal cells, and for perturbation of htt function in the pathogenesis of HD.

Craniofacial

Alcian blue staining of *hd*MO1 embryos revealed disruption in the craniofacial structures of the lower jaw with predominantly more posterior branchial arches affected. There is some evidence from other *in vivo* animal model systems to suggest that bone formation is also affected when htt expression is reduced. For example, the homozygous transgenic *Htt* knockout mouse model ($Hdh^{neoQ50}/Hdh^{neoQ50}$) and the compound heterozygous *Htt* knockdown mouse model ($Hdh^{neoQ50}/Hdh^{ex4/5}$) both show abnormal cranial structure. The $Hdh^{neoQ50}/Hdh^{ex4/5}$ mouse model shows the most severe cranial phenotype with an abnormal, elongated, dome-shaped head and exencephaly [84].

A study of HD affected individuals and non-affected family members shows that HD patients have an altered cranial shape with a significantly longer face height and narrower head width compared with their non-affected family members [182]. Investigation into htt's role in craniofacial formation in the *hd*MO1 zebrafish model may therefore help to determine whether loss or perturbation of htt function results in the cranial phenotype seen in patients with HD.

The objective of this thesis is to use the zebrafish *hd*MO1 model to investigate the normal functions of htt. Each of the phenotypes described within this chapter were therefore

investigated further. The outcome of this analysis has been described in later chapters of this thesis. Further investigation of htt's role in craniofacial formation has been described in the following chapter (Chapter 4), while the olfactory, lateral line and optic tectum phenotypes are described in Chapter 5.

CHAPTER 4: HUNTINGTIN AND NEURAL CREST DERIVED STRUCTURES

4.1 Introduction

Chapter 3 described some of the phenotypes arising from morpholino-induced inhibition of htt translation in zebrafish embryos. The overall aim of this project was to investigate the normal functions of htt and how this might relate to the neuronal specificity of the disease. Subsequent work has therefore focused on detailed characterization of the phenotypic profile of *hd*MO1 embryos. Analysis of tissue specific markers (both absolute levels-by qPCR; and spatial distribution-by *in situ* hybridization) has been used to further analyze each of the structures described in Chapter 3. The aim of this work was to determine at which stage of development, and in which tissues, htt function is important. This chapter will focus on the role of htt in development of the craniofacial structure, while the olfactory and lateral line sensory systems, and the optic tectum will be described further in Chapter 5.

4.2 Results

The pharyngeal arch region is a highly organized structure, comprising the upper and lower jaws. This region is very well characterized in mouse and zebrafish. Schematic diagrams have been produced to communicate the detailed knowledge of the many bones that make up the pharyngeal arches (shown in Figure 3.9). Recently, a number of large mutation screens have been carried out [165-167]. In these studies, zebrafish were exposed to a mutagen and embryos were selected, which show alteration in their craniofacial structure. These investigations describe many different pharyngeal phenotypes and also identify the perturbed signaling pathways involved.

The pharyngeal phenotype of *hd*MO1 embryos was compared to these mutational screens in order to observe any similarities to published craniofacial mutants. A similar phenotype may suggest a similar process of disruption or perhaps a similar signaling pathway involved. This approach may help to indicate at which point in craniofacial development or in which pathways htt may play a rate-limiting role.

4.2.1 Investigating a role for huntingtin in retinoic acid signaling during development

The published craniofacial mutant screens have revealed many different pharyngeal phenotypes affecting the formation or differentiation of one or more different cartilage elements. Of these mutants, the no-fin (*nof*) zebrafish mutant had a craniofacial phenotype that appeared most similar to that of *hd*MO1 embryos (Figure 4.1). Both *nof* and *hd*MO1 embryos have a pharyngeal phenotype characterized by fully formed p1 and p2 cartilages with partial or complete loss of p3-7 cartilages. Approximately 25% of *hd*MO1 embryos exhibit a caudal facing p2, similar to *nof* mutants. It is possible that the same aberrant development of the craniofacial region in *nof* mutants may also occur in *hd*MO1 embryos and that htt may play a role in the same pathway as that which is perturbed within the *nof* mutant.

The *nof* phenotype is caused by a mutation in a gene called *retinaldehyde dehydrogenase 2* (*raldh2*), encoding an enzyme, Raldh2, involved in synthesis of retinoic acid from retinal (Vitamin A) [183]. Retinoic acid plays an important role in early development as a transcription factor, and is involved in anteroposterior patterning of the hindbrain and in organogenesis [128]. Retinoic acid regulated genes, such as *hox* genes, have previously been shown to play a role in patterning of the pharyngeal region (reviewed in [184]).

The role of retinoic acid in patterning of the pharyngeal region is of particular interest as htt has previously been suggested to play a role in regulating signaling from the retinoic acid receptor (RAR) [56, 185]. Further investigation was therefore carried out to determine whether htt plays a role in retinoic acid signaling.

4.2.2 Hindbrain patterning

During development, the brain forms into three distinct regions; the forebrain, midbrain and hindbrain. The hindbrain is further segmented into smaller units called rhombomeres. The rhombomeres are named from anterior to posterior, r1-7. In the case of the *nof* mutant, where

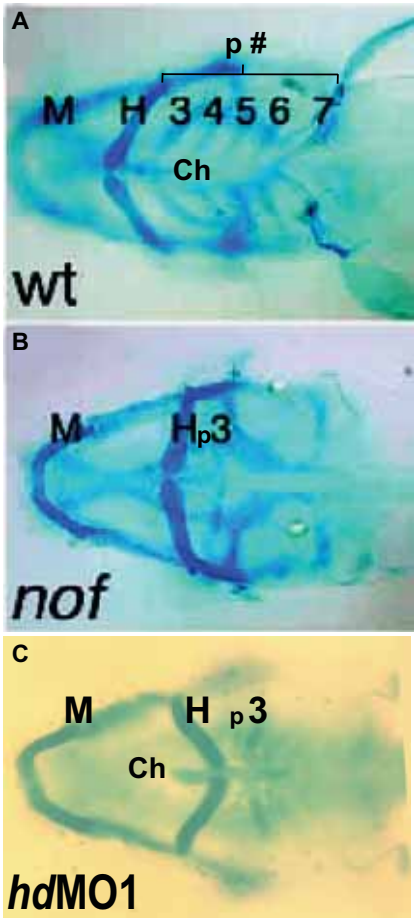

Figure 4.1 Craniofacial phenotype of *no-fin* (*nof*) mutant and *hd*MO1 embryos. *Nof* and *hd*MO1 embryos share a similar cranioskeletal structure including loss of posterior pharyngeal arches (p3-7) and a caudal pointing p2 cartilage. Alcian blue staining of (A) wild-type uninjected, (B) *nof* mutant and (C) *hd*MO1 embryo. (A and B) 5 dpf; Figure adapted from [182]. (C) 7 dpf. 8.5 ng of *hd*MO1 morpholino injected per embryo. All animals shown in ventral view, anterior toward the left. Representative embryos shown. Abbreviations: H, hyoid; M, mandibular; p3-7, pharyngeal arch 3-7; Cb, ceratobranchial. Abbreviations in this figure are slightly different to that used throughout the thesis text, as some abbreviations are in capital letters in this figure and lower case throughout the thesis text. Capital letters have been used in the original publication referenced above (see A and B), and were maintained within (C) to aid image comparison.

retinoic acid signaling is disrupted due to a mutation in the Raldh2 enzyme, hindbrain segmentation is disrupted [183]. Visualization of mRNA expression of specific rhombomeric markers (by *in situ* hybridization analysis) shows that the hindbrain of *nof* mutants is anteriorized in the absence of retinoic acid signaling. This phenotype is characterized by expansion of more anterior rhombomeres, and loss of more posterior rhombomeres. The same phenotype was demonstrated clearly in *raldh2*$^{-/-}$ mutant zebrafish (Figure 4.2 A-H). Treatment of zebrafish with DEAB (a potent retinaldehyde dehydrogenase inhibitor) also produces the same phenotype, confirming a role for retinoic acid in hindbrain segmentation.

Anteriorization of the hindbrain has been shown to have a significant effect on the craniofacial structure of the *nof* embryos. Cranial neural crest cells, which give rise to the facial cartilage, arise in the hindbrain in close association with the rhombomeric structure (described in Section 4.2.4). The most posterior population of neural crest cells (stream 3) eventually migrate and form the posterior pharyngeal arches (p3-7). Loss of the more posterior rhombomeres results in loss of the associated neural crest cell group(s). As a result, in the *nof* mutant, anteriorization of the hindbrain results in loss of the posterior pharyngeal arches [183].

To investigate whether the same dysfunction gives rise to both the *nof* and *hd*MO1 craniofacial phenotypes, we have used the same rhombomere-specific markers to investigate the hindbrain formation in *hd*MO1 embryos. Figure 4.2 shows that the hindbrain is patterned correctly in *hd*MO1 embryos with no apparent difference to the hindbrain pattern of *c*MO or wild-type uninjected embryos. Unlike the *nof* mutant therefore, anteriorization of the hindbrain does not give rise to the posterior pharyngeal arch deficiency seen in the *hd*MO1 craniofacial phenotype. This result suggests that dysfunction leading to the craniofacial phenotype in *hd*MO1 embryos is not the same as that of *nof* mutants and that it is unlikely that perturbation of retinoic acid signaling by htt is the cause of the *hd*MO1 craniofacial phenotype. The following sections of this chapter describe the continued investigation of the cause of the craniofacial phenotype seen in *hd*MO1 embryos by carrying out a more detailed analysis of the precursors of the pharyngeal cartilage, the cranial neural crest cells.

4.2.3 Neural crest cell formation in the hindbrain

Cranial neural crest cells are a pluripotent cell population that arise along the dorsolateral length of the neural plate during formation of the neural tube (Figure 4.3 A). Shortly after neurulation (neural tube closure), neural crest cells migrate away from the neural tube to distant regions of the embryo where they will give rise to many different cell types

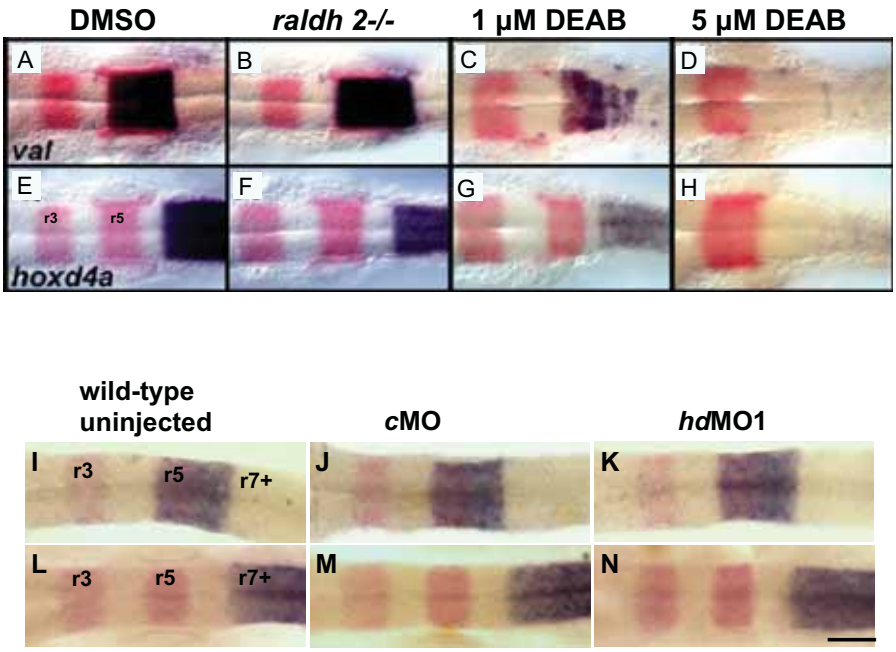

Figure 4.2 Htt does not play a rate-limiting role in patterning of the hindbrain region. (A-H) Shows loss of posterior rhombomeres in the absence of retinoic acid signaling in raldh2 mutant embryos and embryos exposed to DEAB (retinaldehyde dehydrogenase inhibitor). Figure reproduced from [128]. (I-N) *hd*MO1embryos show no disruption in hindbrain patterning. In all images, *krox-20* (red) is expressed in rhombomeres 3 and 5. (A-D and I-K) *val* (purple) is expressed in rhombomeres 5 and 6. (E-H and L-N) *hoxd4a* (purple) is expressed in rhombomere 7 and continues posteriorly. (I-L) Wild-type uninjected embryos. (J, M) *cMO* embryos. (K, N) *hd*MO1 embryos. (A-H) 11.6 hpf (5 somites), (I-N) 18-19 hpf (18-20 somites). 8.5 ng of morpholino injected per embryo. All emryos shown in dorsal view, anterior toward the left. n= 74 wt, 76 *c*MO, 76 *hd*MO1 embryos, approximately half in each of *val* and *hoxd4a* groups. Representative embryos shown. Abbreviations: r3/5, rhombomere 3/5; r7+, rhombomere 7 and continuing further to the posterior of the embryo. Scale bar = 200 µm.

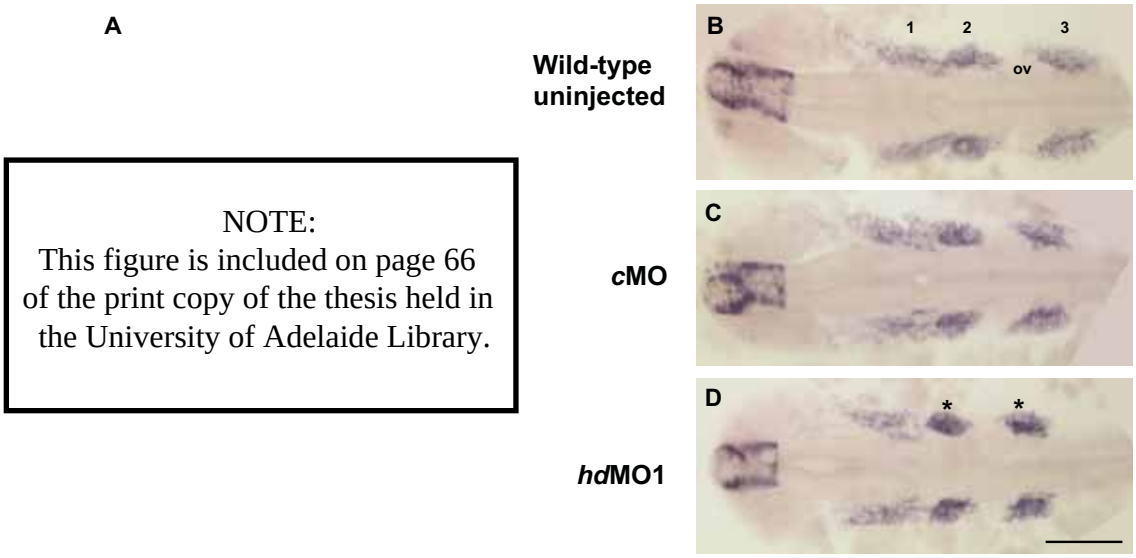

Figure 4.3 Htt does not play a rate-limiting role in specification of cranial neural crest. Cartoon of the developing vertebrate nervous system (A). During neurulation, the neural plate (purple) rolls up and the neural plate border (light blue) becomes the neural folds. Near the time of neural tube closure, the neural crest cells go through an epithelial to mesenchymal transition, delaminate from the neural folds or dorsal neural tube, and migrate along defined pathways. Anterior is to the top. Figure reproduced from [187]. (B-D) *In situ* hybridization analysis of *dlx2* expression shows no disruption in neural crest cell formation in *hd*MO1 embryos (1, 2 and 3 represents stream 1, stream 2 and stream 3). Astrix shows posterior groups of neural crest (stream 2 and 3) which appear aggregated in *hd*MO1 embryos (D) unlike in wild-type or *c*MO embryos (B, C). n = 48 wt, 59 *c*MO, 57 *hd*MO1 embryos. Representative embryos shown. All animals were at 19 hpf (20 somites). 21.2 ng of morpholino injected per embryo. Dorsal view, anterior toward the left. Representative embryos shown. Abbreviations: ov, otic vesicle. Scale bar = 500 μm.

including; chondrocytes, osteocytes, melanocytes, chromaffin cells, tendons and smooth muscle, neurons and glia of the peripheral nervous system, and hormone producing cells in certain organs (reviewed in [187]). Importantly, neural crest cells also form many of the cell types that make up the underlying tissue of the branchial region including skeletal and connective tissues of the arches [188, 189], musculature, and cells of the underlying pharyngeal endothelium [188-191].

In wild-type embryos, neural crest cells arise within the hindbrain in three small groups adjacent to the neural plate (as shown in Figure 4.3). The formation of neural crest cells in *hd*MO1 embryos was investigated by looking at the expression of branchial arch neural crest cell marker, *distal less 2* (*dlx2*) [123]. Figure 4.3 (B-D) shows that reduction of htt expression in *hd*MO1 embryos does not affect formation of neural crest cells, which appear to form in the same 3-group-pattern in the hindbrain as seen in wild-type uninjected and *c*MO embryos. The only observable difference appears to be aggregation of the two most posterior groups of neural crest cells in *hd*MO1 embryos. Despite their aggregated appearance, the neural crest cells appear to form correctly upon htt knockdown.

4.2.4 Migration and patterning of neural crest cells

Once formed in the hindbrain, neural crest cells migrate ventrally into the pharyngeal region to fill the pre-formed pouches within the pharyngeal endoderm, according to their rhombomeric origin (Figure 4.4 A). Since htt activity is not required for correct patterning of the hindbrain or formation of the neural crest, migration of neural crest cells into the pharyngeal region was investigated as the next step in pharyngeal arch development. Aggregation of neural crest cells has been suggested previously to interfere with neural crest cell migration [192], therefore it was hypothesized that aggregation of the posterior group of neural crest cells seen in 19 hpf *hd*MO1 embryos could impair the migration of these cells and result in absence of p3-7 as seen in the *hd*MO1 craniofacial phenotype.

In situ hybridization analysis of *dlx2* at a later stage (33 hpf), showed that the migration of neural crest cells was largely unperturbed in *hd*MO1 embryos. Figure 4.4 B shows that neural crest cells have migrated into the underlying pharyngeal pouches in a similar manner to that of wild-type uninjected and *c*MO embryos. To ensure the appearance of the craniofacial

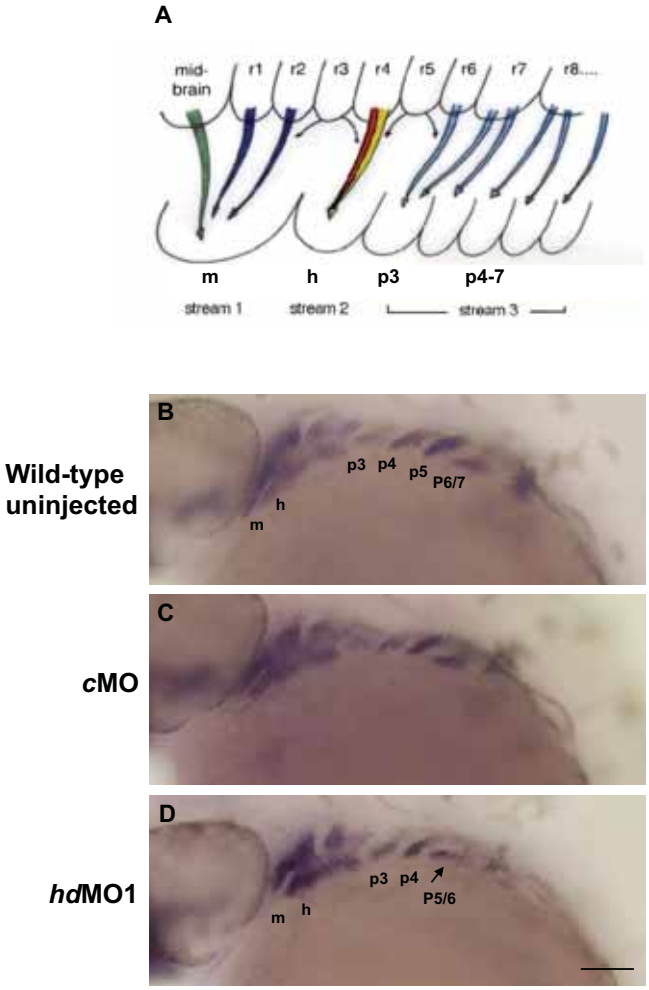

Figure 4.4 Htt does not play a rate-limiting role in migration of cranial neural crest. (A) Neural crest cells migrate as three distinct streams. Neural crest cells emigrate from distinct rhombomeres to populate particular arches and give rise to specific cartilages of the pharyngeal skeleton including the mandibular (m), hyoid (h) and pharyngeal (p) arches. Figure reproduced from [202]. (B) *In situ* hybridization analysis of *dlx2* expression shows that htt is not required for migration of the neural crest cells into the pharyngeal arches. At this time, neural crest cells have populated the arches, which are separated from each other by endodermal tissue (non-staining tissue between the arches). In wild-type and *c*MO embryos (B, C), arches p5-p6 have already been divided by the endoderm, while arches p6–p7 have not yet divided. Arches p5-p6 are currently dividing in *hd*MO1 embryo (D, arrow) suggesting a slight developmental delay of craniofacial formation. n = wt, 27; *c*MO, 23; *hd*MO1 embryos, 23. All animals were at 33 hpf (20 somites). 21.2 ng of morpholino injected per embryo. Lateral view, anterior toward the left. Representative embryos shown. Abbreviations: m, mandibular (p1); h, hyoid (p2); p3–p7, pharyngeal arches 3–7; r1–r8, rhombomeres 1–8. Scale bar = 100 μm.

*hd*MO1 phenotype in this batch of *hd*MO1 embryos, some embryos were allowed to develop to 7 dpf and alcian blue staining was carried out. The same group of embryos were then used for quantitation of the craniofacial phenotype seen in Figure 3.8.

The craniofacial phenotype of *hd*MO1 embryos is therefore not a result of perturbation of neural crest migration into the branchial arches. *In situ* hybridization for *dlx2* expression however does show some acute differences between *hd*MO1 and *c*MO embryos (Figure 4.4 B-D). Firstly, staining in p1 and p2 (mandibular and hyoid) regions appears darker in *hd*MO1 embryos than *c*MO embryos at 56 hpf. This maybe due to aggregation of neural crest cells or an increase in neural crest cell number. However, *in situ* hybridization for *dlx2* in 19 hpf *hd*MO1 embryos does not show any obvious increase in *dlx2* staining in the first (stream 1) group of cells, which will ultimately form the p1 and p2 arches (Figure 4.3 B-D). Aggregation of the cranial neural crest cells in *hd*MO1 embryos and its possible role in the craniofacial phenotype is discussed further in Section 4.2.5.

Secondly, the pharyngeal arches are separated from each other by pharyngeal endoderm (non-staining tissue between the arches). In 33 hpf wild-type uninjected and *mc*MO1 embryos (Figure 4.4 B and C), arches p1–p5 are divided by the endoderm, but p6 and p7 have not yet divided. In *hd*MO1 embryos, despite accurate staging of embryos, p5-p6 have not finished dividing (Figure 4.4 D, arrow). This suggests a slight developmental delay of craniofacial formation. At this time however, p3 and p4 have correctly separated in *hd*MO1 embryos, which suggests that this delay in segmentation is unlikely to result in the p3-7 deficiency phenotype of *hd*MO1 embryos (Figure 4.4 D).

4.2.5 Neural crest cell survival and differentiation

Investigations described within this chapter have so far revealed that htt does not play a role in formation or migration of cranial neural crest cells that make up the craniofacial skeleton. It is possible that the neural crest cells are either unable to undergo differentiation or are dying before differentiation begins. The next step therefore is to look at the survival of neural crest cells and their ability to differentiate into cartilage.

Cranial neural crest cells in the branchial region express *dlx2* from the time of their formation along the developing neural plate (around 19 hpf), until differentiation (around 48 hpf). *In situ* hybridization for *dlx2* was carried out on 48 hpf embryos to see whether neural crest cells are still present at the time of cartilage differentiation, as death of neural crest cells

in the posterior arches could be the cause of the lack of posterior pharyngeal arches seen in the *hd*MO1 embryos. Due to the fact that differentiation occurs over a period of time, and to account for any delay in pharyngeal development, 56 hpf embryos were also analyzed. Figure 4.5 shows that in *hd*MO1 embryos, *dlx2* expressing neural crest cells are present in the pharyngeal region at the time of differentiation (48 hpf) and still present at a high level at 56 hpf. Reduction in htt expression therefore does not cause death of neural crest cells prior to differentiation.

In situ hybridization of *dlx2* at 56 hpf reveals that the neural crest cells appear malformed and condensed (particularly of the pq, ch and p3 arches; abbreviations first described in Section 3.2.2.5). In addition to this, the ch bone appears to be fused to p3, another indication that reduction in htt expression results in aggregation of neural crest cells. It is possible that fusion of p3, or bh to the ch cartilage could give rise to the caudal pointing ch phenotype seen in *hd*MO1 embryos (Figure 4.1 and Figure 4.5). A schematic diagram of this hypothesis is shown in Figure 4.6. It is also possible however that the cause of this malformation may be lack of development of the underlying endoderm.

Around the time of cartilage differentiation, neural crest cells begin to express genes required for their differentiation such as *collagen type II alpha-1a* (*col2a1*) [193, 194]. *In situ* hybridization was carried out in order to examine whether the expression of *col2a1* mRNA is altered in post-migratory neural crest cells of *hd*MO1 embryos.

In the 48hpf *c*MO embryo, several cartilage elements have already started to differentiate (Figure 4.7 A). Strong *col2a1* expression can be seen in the ethmoid plate and the otic placode. Cartilage of the lower jaw is also shown to be expressing *col2a1* including the ch, bh and p3 cartilages. In *hd*MO1 embryos however, *col2a1* is only visible within ch cartilage, which is suggestive of a delay in differentiation at this time (Figure 4.7 B).

By 56 hpf, the most anterior pharyngeal cartilage is differentiating in wild-type uninjected and *mc*MO1 embryos, including the ethmoid plate (ep), pq, p2, and p3 cartilages (Figure 4.7 C). Differentiation has also begun in *hd*MO1 embryos, however *col2a1* is reduced in the pq and p2 cartilage, and absent in p3. This result suggests that the absence of many or all of the ceratobranchial cartilage elements (p3-7) is likely to be due to impaired differentiation of these cartilage elements in *hd*MO1 embryos (Figure 4.7 D).

Initial analysis of *col2a1* expression at 48 hpf appears to suggest that *hd*MO1 embryos are simply delayed in development, particularly the appearance of a smaller ethmoid plate. There are, however two reasons why a simple delay in development is not likely to give rise to this craniofacial phenotype. Firstly, the differentiation of the lower jaw cartilage of *hd*MO1

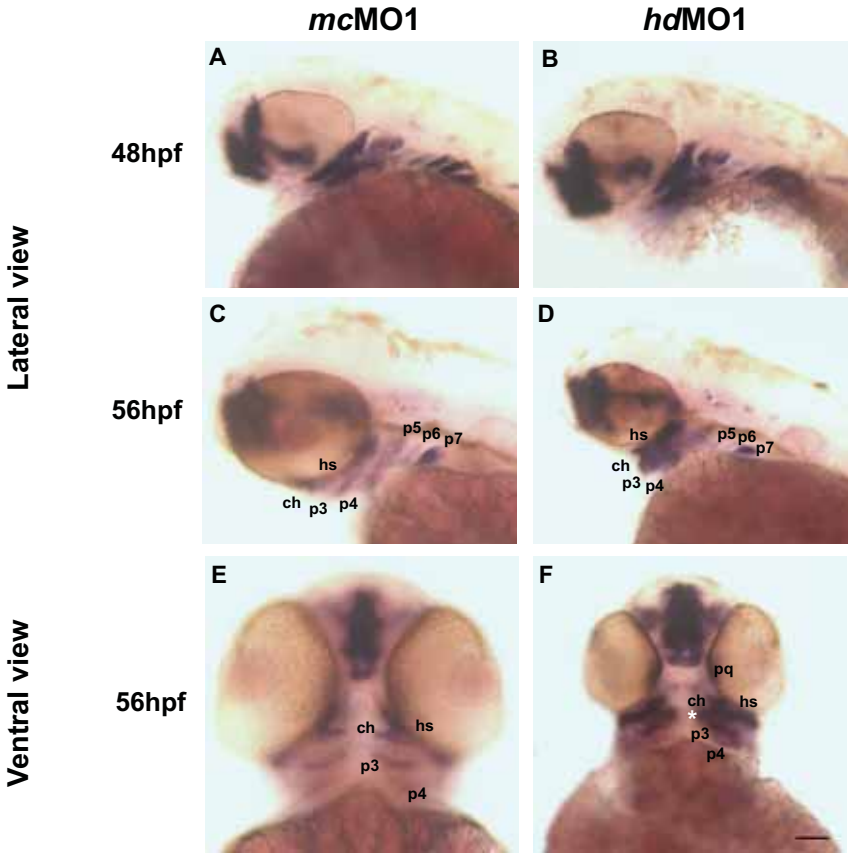

Figure 4.5 Htt does not play a rate-limiting role in survival of cranial neural crest.
In situ hybridization analysis of *dlx2* expression shows that htt is not required for survival of cranial neural crest cells in the pharyngeal arches. *Dlx2* expressing neural crest cells (purple), are present at the time of differentiation of neural crest cells and still present at a high level at 56 hpf. Asterix in (F) shows the site of possible fusion of ch and p3. 21.2 ng of morpholino injected per embryo. Lateral view shows anterior toward the left; ventral view shows anterior towards the top. Representative embryos shown. Abbreviations: ch, ceratohyal; p3-7, pharyngeal arch 3-7; pq, palatoquadrate. Scale bar = 100 μm.

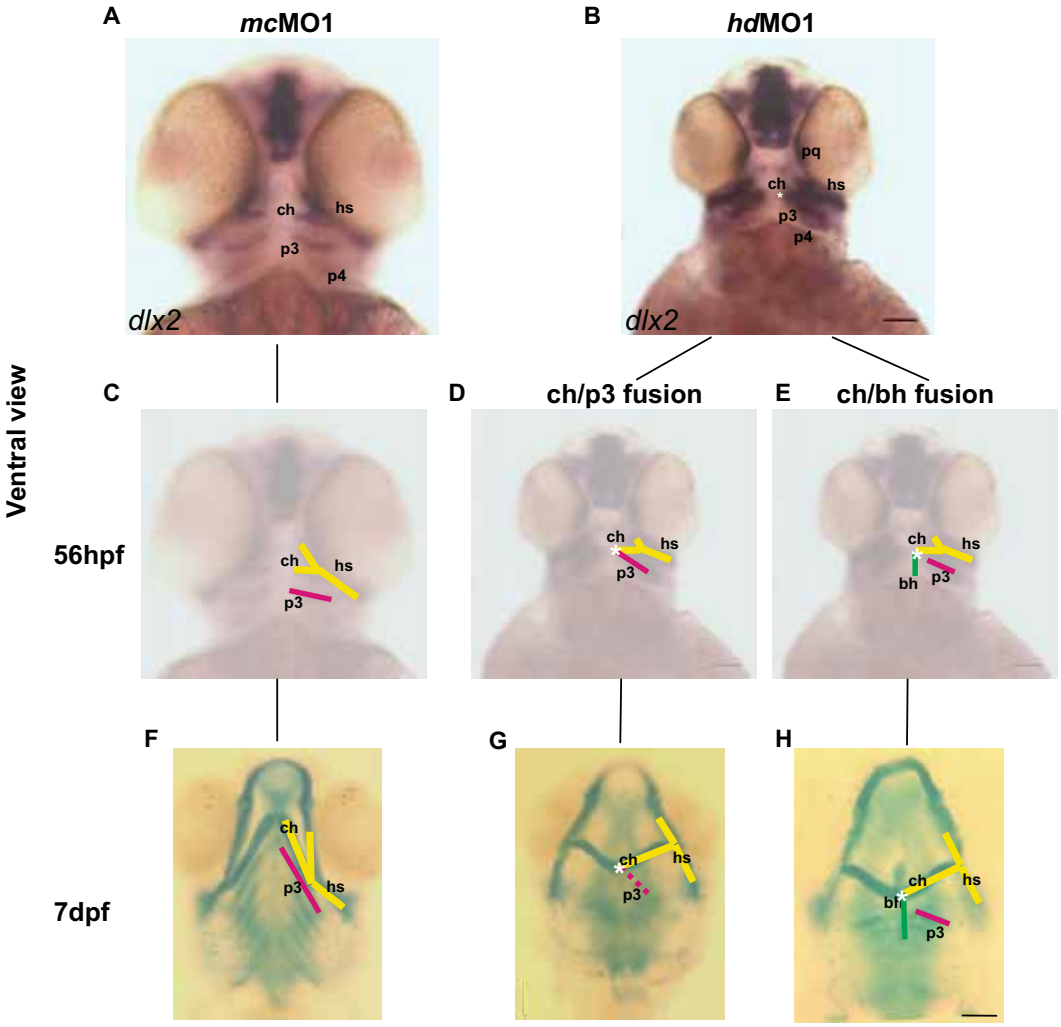

Figure 4.6 A proposed model for formation of caudal pointing ceratohyal cartilage in *hd*MO1 embryos. This flow chart is used to illustrate the developmental processes which may give rise to the malformation of the ch cartilage in *hd*MO1 embryos. (A, C, F) A *mc*MO1 embryo demonstrates the normal spatio-temporal development of craniofacial cartilage. Asterix shows site of possible fusion of ch and p3 (G), or ch and bh (H). Solid lines indicate either; neural crest cells ready to under go differentiation (56 hpf), or cartilage which has differentiated (7 dpf). Dashed lines indicate where the described cartilage elements have failed to differentiate as a result of reduced htt expression. Ventral view, anterior towards the top. Representative embryos shown. Abbreviations: bh, basihyal; ch, ceratohyal; p3-7, pharyngeal arch 3-7. Scale bar = (A, B) 100 µm; (F-H) 200 µm.

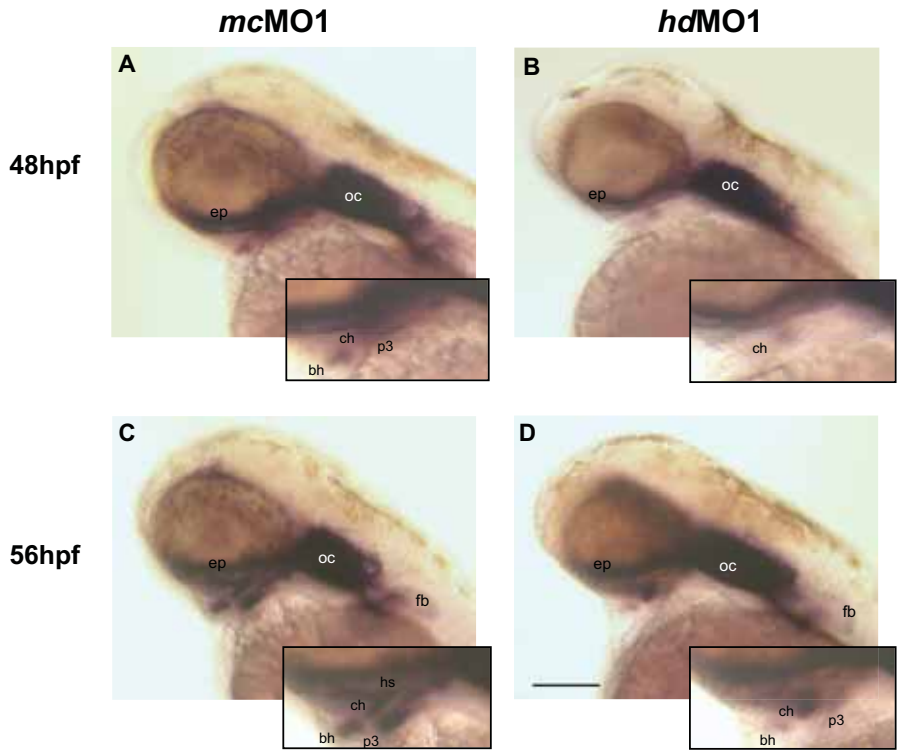

Figure 4.7 Perturbation in pharyngeal development of *hd*MO1 embryos possibly due to impaired cartilage differentiation. *In situ* hybridization analysis of *col2a1* (expressed by neural crest during chondrogenesis) shows that unlike *mc*MO1 embryos (A), *col2a1* expression is reduced in the pharyngeal region of *hd*MO1 embryos (B) at onset of differentiation (48hpf). Inset boxes show magnified view of the pharyngeal arch region. 8 hours later (56hpf), *hd*MO1 embryos (D) are expressing slightly more *col2a1* however the expression still appears reduced compared to *mc*MO1 embryos (C) of the same age. Numbers of embryos showing the described phenotype (56 hpf) = *mc*MO1, 0/17; *hd*MO1 embryos, 11/12. 21.2 ng of morpholino injected per embryo. Lateral view, anterior to the left. Representative embryos shown. Abbreviations: ch, ceratohyal; ep, ethmoid plate; hs, hyosymplectic; oc, otic capsule; p3-7, pharyngeal arch 3-7; pq, palatoquadrate. Scale bar = 200 μm.

embryos at 56 hpf is much less than that seen in the *c*MO embryos despite appropriate spatial development of the cartilage elements. Secondly, we have analyzed older embryos to account for a potential delay in differentiation. The phenotype remains the same at 7 dpf, which argues against a general delay in development, as this should allow enough time for any remaining cartilage elements to be formed.

4.3 Conclusion

Results shown in this chapter have focused on further investigation of one of the *hd*MO1 phenotypes, altered craniofacial structure. The aim of this work was to investigate in detail the developmental processes that take place during formation of the craniofacial structure, and to identify which of these processes is perturbed in *hd*MO1 embryos, ultimately indicating a limiting functional requirement for htt.

Investigation of the *hd*MO1 craniofacial phenotype was carried out by detailed analysis of each stage of development of the pharyngeal arches, including formation of neural crest cells at the lateral edge of the neural plate, migration into the pharyngeal region, and differentiation of neural crest cells to form cartilage. The formation and migration of neural crest cells was analyzed by *in situ* hybridization of *dlx2*, expressed by cartilage forming cranial neural crest cells. Analysis of *dlx2* expression revealed that a reduced level of htt expression does not affect the formation of neural crest cells in the hindbrain or migration of these cells into the pharyngeal region. At 33 hpf, neural crest cells were observed to form the appropriate pattern of identifiable arches (p1-7) within the pharyngeal region demonstrating that the lack of posterior pharyngeal arches is not due to inappropriate patterning of precursor cells.

The final step in development of the pharyngeal arches is differentiation of neural crest cells into cartilage. *In situ* hybridization analysis revealed reduced expression of *col2a1* in specific cartilage elements of *hd*MO1 embryos. This result suggests that dysfunction of differentiation is responsible for the craniofacial cartilage phenotype seen in embryos with reduced htt expression, therefore implicating a role for htt in differentiation of the craniofacial cartilage. During preparation of this thesis, Diekmann *et al*. (2009) [195] published an article describing the craniofacial phenotype of zebrafish embryos with reduced htt expression. In this model, zebrafish were injected with morpholinos of the same sequence as has been used in this thesis, and as used in a paper published earlier in this lab [112]. They describe a craniofacial phenotype almost identical to that found in this current work and suggest a rate-

limiting role for htt in cartilage differentiation. Diekmann *et al*. also showed that this function of htt requires BDNF signaling.

Specificity of phenotype

The experiments outlined above suggest that htt plays a role in differentiation of craniofacial cartilage. These results however do not reveal if this role for htt extends to all craniofacial cartilage elements (p1-7), or is limited only to the more posterior arches (p3-7). Even if htt is required for differentiation of all cartilage elements, due to the transient nature of morpholino knockdown, expression may return in time to allow differentiation of some arches (the ones which differentiate first such as p1, p2 and to a lesser extent p3). By this time, the opportunity may be lost for differentiation of the more posterior arches. If this was the case, then it may be expected that injection of a higher dose of morpholino would affect differentiation of more anterior cartilage elements including p1 and p2. Figure 3.10 shows that injection of a greater amount of *hd*MO1 (21ng) does not affect differentiation of p1 and p2 arches. Despite their severely malformed structure, p1 and p2 still differentiate as shown by alcian blue staining. The presence of p1 and p2 cartilage elements in *hd*MO1 embryos suggests that unlike p3-7, htt is not a rate-limiting factor in development of the p1 and p2 arches.

Intrinsic cellular issue or perturbed tissue interactions?

Neural crest cells are specified at an early stage by signals that they acquire from the neuroepithelium. This information, based on relative levels of *hox* gene expression, allows the cells to migrate into the pharyngeal region in a pattern according to their rhombomeric origin [188, 196]. Due to this important intrinsic ability, it was a long held theory that craniofacial anomalies arise due to a primary defect in neural crest cell development. Recent advances however, have highlighted the important influence of a complex interaction of neural crest cells with tissues such as mesoderm, ectoderm and endoderm (reviewed in [197]). For neural crest cells, these tissues are an important source of factors such as bone morphogenic protein (*bmp)*, sonic hedgehog (*shh)* and fibroblast growth factor (*fgf)* – all well known for their roles in embryonic patterning and morphogenesis.

The pharyngeal endoderm plays a major role in patterning of the branchial arches by establishing a three dimensional structure composed of several pouches. The underlying

endoderm expresses important factors critical for neural crest cell viability and differentiation into cartilage [166, 198-200]. Deficiency in the pharyngeal endoderm may inhibit differentiation of neural crest cells and therefore contribute to the pharyngeal phenotype seen in *hd*MO1 embryos. Time constraints of this PhD prevented further investigation of this phenotype. Analysis of the integrity of the pharyngeal endoderm (with monoclonal antibody, Zn-5) [201, 202] may help to determine whether htt is required for pharyngeal endoderm formation or maintenance, and ultimately may help to further clarify the cause of the *hd*MO1 craniofacial phenotype.

CHAPTER 5: A RATE-LIMITING ROLE FOR HUNTINGTIN IN ANTERIOR NEURAL PLATE FORMATION

5.1 Introduction

Initial investigations of *hd*MO1 embryos have revealed a number of interesting phenotypes, which have been described earlier in this thesis. All of the observed phenotypes arise as a result of blocking translation of htt during early development. While investigations into a possible role for htt in development of the craniofacial structure has been described in Chapter 4, research described within the current chapter was aimed at further characterization of the sensory neuron phenotypes.

Two sensory systems have been identified as having perturbed development in *hd*MO1 embryos. These include the olfactory and the lateral line sensory systems. Initial investigations described in Chapter 3 reveal that *hd*MO1 embryos have a reduced number of differentiated olfactory sensory neurons and a reduced number of lateral line neuromasts, respectively. The aim of the research carried out in this chapter was to investigate the mechanism of perturbation in sensory neuron development in an effort to determine where htt may play a role in their development.

5.2 Results

Both the olfactory and lateral line sensory systems arise from specialized regions of embryonic ectoderm termed the olfactory placode and lateral line placode respectively. The olfactory and lateral line placodes are among a number of cranial placode tissues formed in all vertebrates (other placodal tissues include adenohypophyseal, trigeminal, lens, profundal and a series of epibranchial and hypobranchial placodes).

All placodal tissues originate from a common precursor region, the pre-placodal region, early in gastrulation. The pre-placodal region is located around the anterior end of the neural plate, in the outer neural folds and adjacent ectoderm [203-206] (Figure 5.1). At early gastrula stage, cells in this precursor region have not yet committed to a specific placodal lineage. Therefore in the early stages of development, this region presents a common primordium for all placodes (reviewed in [207-212]).

Due to the common placodal origin of the olfactory and lateral line sensory systems, it was hypothesized that the reduction of htt in development may give rise to both of these phenotypes by dysfunction at the early pre-placodal stage. For this reason, further investigations were carried out into the formation of the pre-placodal region in *hd*MO1 embryos.

5.2.1 Early placode cell formation

By late gastrulation, or early neural plate stages of zebrafish development (8-9 hpf), cells of the once homogenous pre-placodal region begin to adopt a particular placodal fate. Fate maps show that precursors of each placode are located in a specific, however somewhat overlapping territory (reviewed in [210, 211, 213]; Figure 5.2). The cells in each territory begin to express specific transcription factors. These transcription factors can be used to trace the fate of cells from the pre-placodal regions during development. Fate and expression maps (such as those shown in Figure 5.2) demonstrate the current state of knowledge of gene expression and lineage fate within this region [205, 214].

Six1, orthologue of the *Drosophila* gene *sine oculis*, encodes a homeodomain transcription factor expressed throughout the pre-placodal region ([124] and reviewed in [210]). We analyzed the mRNA expression pattern of *six1* in an attempt to visualize the pre-placodal region in the developing zebrafish.

In situ hybridization analysis of *hd*MO1 embryos revealed a clear reduction in the level of *six1* expression, while no change was seen in the pattern of its expression (Figure 5.3 A). In 12 hpf wild-type embryos, placodal cells have formed at the anterior end of the neural plate and some of the placodal cells (the lateral line and otic placodes) have broken away and are migrating posteriorly toward their final destination. For this reason, *six1* expression can be seen in one anterior group and one posterior group of cells. Embryos in this experiment were scored according to the intensity of *six1* expression in both of these regions.

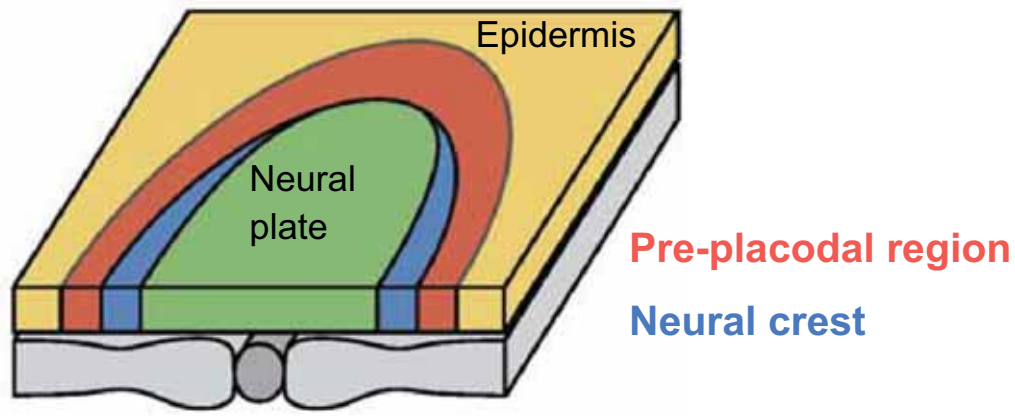

Figure 5.1 All placodes originate from a pre-placodal region immediately adjacent to the anterior neural plate. The positioning of the neural crest, pre-placodal region and the epidermis around the anterior neural plate. The pre-placodal region (red) develops exclusively from cranial ectoderm at the border of the anterior neural plate (green) early in gastrulation. Other regions include cranial neural crest (blue), cranial dorsolateral endomesoderm (light gray) and axial mesoderm (dark gray). Dorsal view, anterior to top. Figure reproduced from [210].

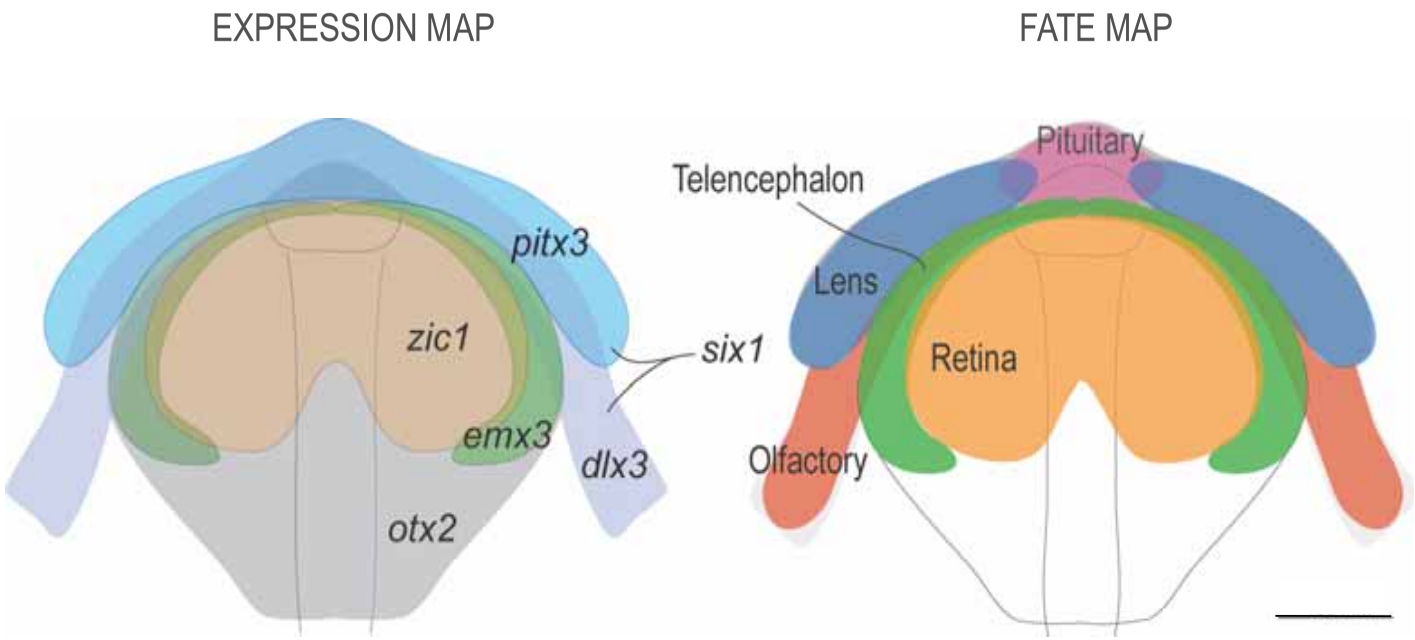

Figure 5.2 Schematic drawings showing expression map and fate map of the zebrafish anterior neural plate and pre-placodal field at the end of gastrulation (~8-9 hpf). The location of particular cell fates (right) in the anterior neural plate and pre-placodal field correlate to gene expression patterns (left). All placodal tissues express *six1* [210], and in addition express one (or a number of) other genes as listed; Adenohypophysis precursor cells (pituitary) express *dlx3b* and *pitx3*. Lens precursors express *pitx3* or *pitx3* and *dlx3b*. Olfactory precursors express *dlx3b* and *pitx3*, or only *dlx3b*. Anterior neural plate tissues, which are not derived from the pre-placodal region include: telencephalic precursor cells (expressing *emx3*, or *emx3* and *zic1*) and retinal precursors (expressing *zic1*). The *otx2* expression domain in the anterior neural plate is shown in grey and also is expressed within the *zic1* and *emx3* expressing regions. Figure adapted from [214], with reference to [210] and [216]. Dorsal view, anterior to top. Scale bar = 100 μm.

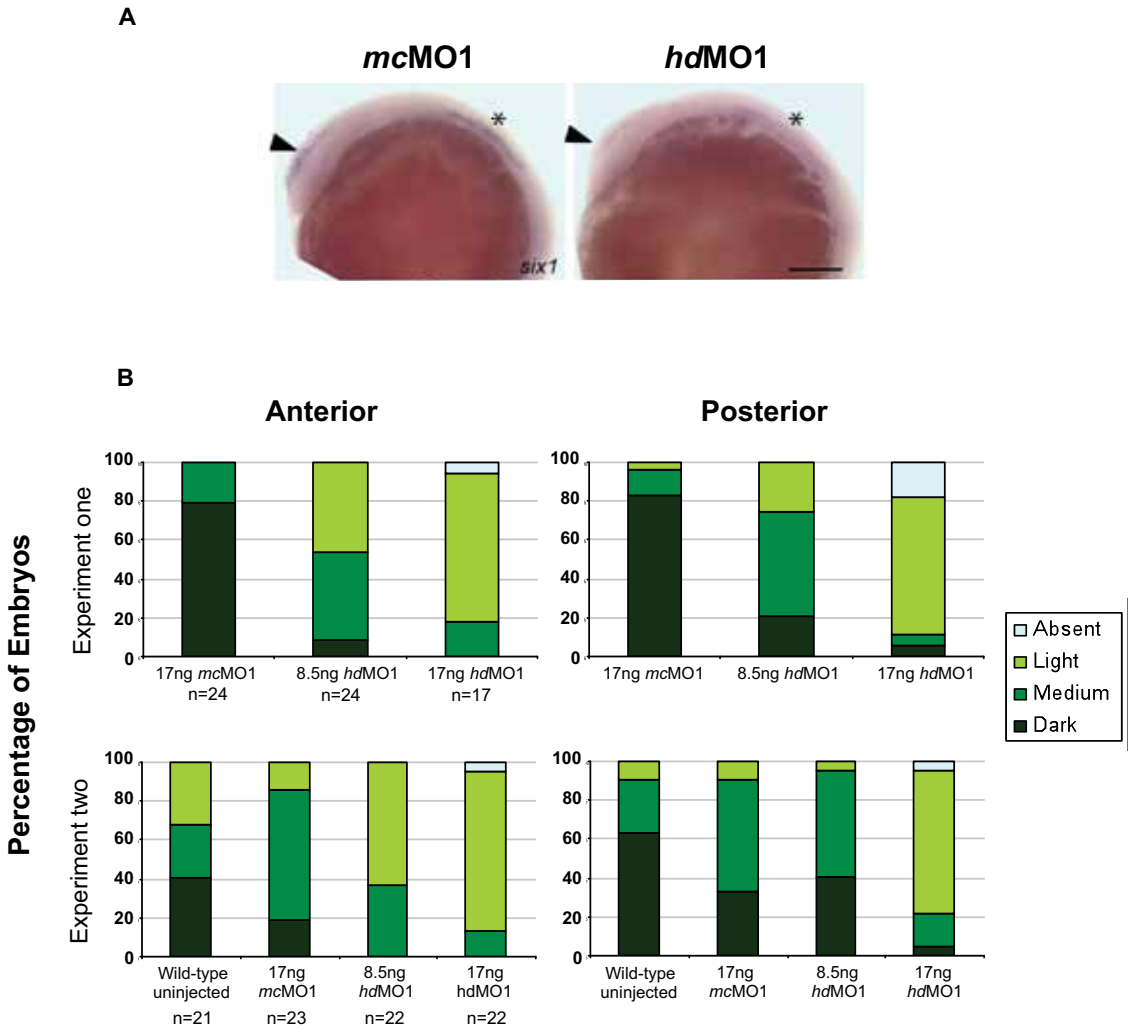

Figure 5.3 *hd*MO1 embryos show reduced expression of pan-placodal marker *six1*. (A) *In situ* hybridization analysis of *six1* expression at 12 hpf shows reduced expression in the pre-placodal region at the anterior end of the neural plate (arrow) and in the migrating lateral line and otic placodes (asterix). n= 27 wt, 23 *mc*MO, 29 *hd*MO1 embryos. (B) Results of the blinded scoring of *six1* expression compared to a standard embryo. Scoring was carried out on two independent experiments by Dr. Svanhild Nornes. These experiments demonstrate a trend towards reduced *six1* expression in *hd*MO1 embryos compared to *mc*MO1 and wild-type uninjected embryos. It also appears to demonstrate a dose dependent response to *hd*MO1 injection. All animals were at 12 hpf (6-somites). (A, B) 17 ng of morpholino injected per embryo. Lateral view, anterior toward the left. Representative embryos shown. Scale bar = 200 μm.

In order to quantitate the proportion of embryos showing a reduced level of *six1* expression, the level of *six1* mRNA expression (as shown by *in situ* hybridization) in each embryo was compared to a 'standard' embryo. This one 'standard' embryo was chosen from any group (either wt uninjected, *mc*MO1 or *hd*MO1) to represent an average level of staining over all groups (wt uninjected, *mc*MO1 and *hd*MO1). Each embryo from each group was compared to this one "standard' embryo. The standard embryo was scored as having a medium level of staining, whilst all other embryos were determined to have lighter, darker or an equal level of staining when compared to the chosen standard embryo. Absence of any staining within either of the two defined regions was also noted. Scoring was carried out by an independent researcher blinded to the treatment of each group of embryos and to the origin of the 'standard' embryo.

The graphs in Figure 5.3 B show that, using the above method, there is a distinct reduction in *six1* expression in both the anterior and posterior placodal cell groups in *hd*MO1 embryos. This observation also suggests a dose dependent response to injection of *hd*MO1 morpholino.

Quantitation of the overall level of *six1* mRNA expression was carried out by qPCR analysis on embryos of the same age as used above. Table 5.1 shows that *six1* expression was significantly reduced in *hd*MO1 zebrafish embryos in three independent experiments. This reduction was seen in both *hd*MO1 and *hd*MO2-injected embryos. qPCR analysis of a second marker of pre-placodal cells, *Drosophila distal-less* orthologue, *dlx3b* was used to confirm this finding. Dlx3 is a transcription factor expressed within the pre-placodal region primarily in cells of olfactory lineage [215, 216]. qPCR showed that expression of *dlx3b* is also significantly reduced in *hd*MO1 embryos (Table 5.1).

Together these results suggest that reduction in htt expression during development impairs formation of the pre-placodal region as evidenced by a reduction in *six1* and *dlx3b* expression. This result supports the theory that the observed reduction in sensory neurons of the olfactory and lateral line systems is due to perturbation in formation of the early pre-placodal precursor cells.

5.2.2 Neural plate formation in hdMO1 embryos

Like the pre-placodal region, forebrain tissue also arises at the anterior end of the neural plate. Fate maps show that some forebrain tissue lies in close proximity to the pre-placodal region such as telencephalic precursor cells, which arise in a region immediately

*hd*MO1 vs *mc*MO1

	Gene	Treatment	Estimate	Log_{10} Fold change	SE	T-Stat	DF	Adjusted P-value	Significance
1	*dlx3b*	*hd*MO1 vs *mc*MO1	-1.17221	-14.867	0.1684	-6.959	66	8.94E-09	***
2	*emx3*	*hd*MO1 vs *mc*MO1	-1.20867	-16.169	0.1257	-9.613	53	4.60E-12	***
3	*ntl*	*hd*MO1 vs *mc*MO1	-0.00583	-1.014	0.0610	-0.096	80	0.9238	
4	*omp*	*hd*MO1 vs *mc*MO1	-0.30378	-2.013	0.1105	-2.749	47	2.96E-02	***
5	*otx2*	*hd*MO1 vs *mc*MO1	-0.25161	-1.785	0.1213	-2.075	50	0.1007	
6	*six1*	*hd*MO1 vs *mc*MO1	-1.07600	-11.912	0.1437	-7.491	53	5.12E-09	***
7	*val*	*hd*MO1 vs *mc*MO1	-0.15320	-1.423	0.0736	-2.081	51	0.1007	

wt vs *mc*MO1

	Gene	Treatment	Estimate	Log_{10} Fold change	SE	T-Stat	DF	Adjusted P-value	Significance
1	*dlx3b*	wt vs *mc*MO1	-0.19321	-1.560	0.1667	-1.159	66	0.3900	
2	*emx3*	wt vs *mc*MO1	-0.12011	-1.319	0.1257	-0.955	53	0.4815	
3	*ntl*	wt vs *mc*MO1	0.11289	1.297	0.0604	1.870	80	0.1303	
4	*omp*	wt vs *mc*MO1	-0.13956	-1.379	0.1105	-1.263	47	0.3724	
5	*otx2*	wt vs *mc*MO1	-0.04433	-1.107	0.1193	-0.372	50	0.8153	
6	*six1*	wt vs *mc*MO1	0.04467	1.108	0.1437	0.311	53	0.8153	
7	*val*	wt vs *mc*MO1	-0.02317	-1.055	0.0723	-0.320	51	0.8153	

Table 5.1 Quantitative PCR analysis of various genes within the neural plate and derivative tissue, the olfactory receptor neurons. 'Estimate' column shows raw values representing arbitrary units of RNA transcript as determined by the standard curve, showing expression of each gene relative to expression of the control gene, *ef-1a* [139]. *** Significance is determined by P-value = < 0.001. For *hd*MO1 vs. *mc*MO1, *dlx3b, emx3, zOMP* and *six1* all show statistically significant evidence of differential regulation with P-value = < 0.001. *Ntl, otx2* and *val,* do not show statistically significant evidence of differential regulation. None of the wt vs. *mc*MO1 comparisons show any evidence of a significant effect due to *mc*MO1 injection. 8.5ng of morpholino injected per embryo. All embryos were analysed at 12 hpf except *omp* which was analysed at 48 hpf. A description of statistical analysis is included in Section 2.2.13. Abbreviations: DF, degrees of freedom; se, standard error.

adjacent to the pre-placodal region at the neural plate margin [217-219]. It was hypothesized that due to their close proximity to the pre-placodal region, neural ectoderm derived-telencephalic precursor cells could also be reduced in *hd*MO1 embryos. In an attempt to test this hypothesis, qPCR analysis was carried out on a gene called *empty spiracles homeobox 3* (*emx3),* which has high similarity to the mammalian gene *emx1*. Zebrafish *emx3* is expressed only in telencephalic precursor cells and not by cells with placodal fate [217-219].

qPCR analysis revealed reduced expression levels of *emx3* in *hd*MO1 embryos (Table 5.1) suggesting that in addition to pre-placodal tissue, htt is also required for formation of neural fated ectoderm. This result also correlates with reduced expression of the marker gene, *dlx2* within the subpallial telencephalon and diencephalon later in development (Figure 5.4 A and B). Interestingly, anterior neural plate expression of *orthodenticle homolog 2* (*otx2)* (slightly more posterior to *emx3*) was not significantly reduced in *hd*MO1 embryos by qPCR (Table 5.1) or by *in situ* hybridization analysis, with no change in the pattern of expression (Figure 5.4 C and D).

In an effort to identify the cellular location and developmental process(es) in the neural plate for which htt activity was rate-limiting, the expression level of a number of genes were examined. These genes are markers for known regions of the neural plate, neural plate derivative tissues, and also for notochord formation. As a first step, genes were selected that are expressed at specific locations along the neural plate from the forebrain to the hindbrain. As visualized by *in situ* hybridization, expression of *krox20* and *hoxd4a* genes within the hindbrain, (expressed in rhombomere 3 and 5, and rhombomere 7+ respectively) were not altered in *hd*MO1 embryos (Figure 4.2 I-N). In addition, expression of neural crest cell marker *dlx2* at 19hpf demonstrated that in *hd*MO1 embryos, cranial neural crest cells form in the same 3-group pattern in the hindbrain as seen in both *mc*MO1 and wild-type uninjected embryos (Figure 4.3 B-D).

The results described above suggest that the ectodermal deficiency seen in *hd*MO1 embryos is primarily evident in the anterior region of the embryo, specifically identifying a rate-limiting role for htt in formation of the pre-placodal region and telencephalic precursors at the anterior neural plate margin. It is also shown here that this rate-limiting role for htt does not extend to formation of the midbrain or hindbrain, or in anterior-posterior patterning of the neural plate at this reduced level of htt expression.

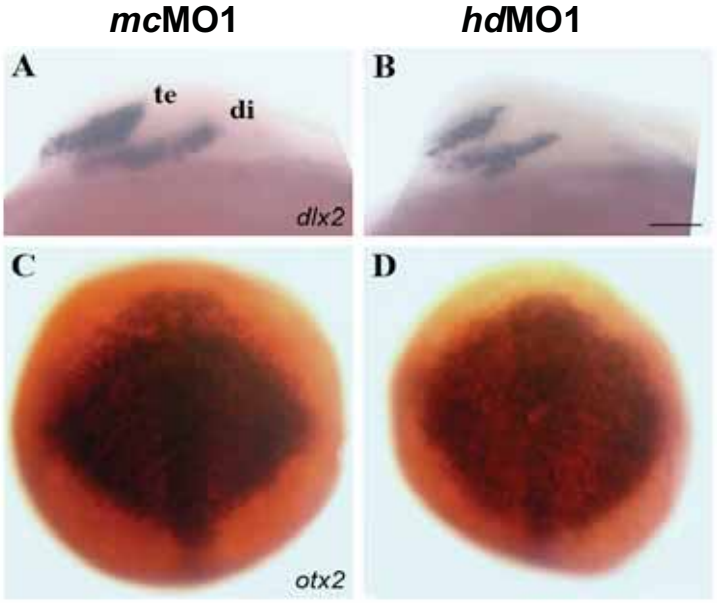

Figure 5.4 Neuronal specificity of *hd*MO1 anterior neural plate deficiency. The *hd*MO1 neural plate deficiency is limited to the anterior most region of the neural plate in *hd*MO1 embryos resulting in deficiency in formation of the telencephalon, but no significant change in anterior neural plate marker, *otx2*. (A, B) *hd*MO1 embryos have reduced expression of *dlx2*, particularly in the subpallial telencephalon (te), but also in the diencephalon (di). No change is seen in the expression pattern of anterior neural plate marker, *otx2* in *hd*MO1 embryos by *in situ* hybridization (C, D). (A, B) 19hpf, (C, D) 10hpf. (A, B) Lateral view, anterior to the left; (C, D) dorsal view, anterior to the top. Numbers of embryos displaying the described phenotypes were (A, B) wt uninjected, 0/12; *mc*MO1, 1/18; *hd*MO1, 15/18. Scoring was carried out in a blinded manner by an independent researcher. Representative embryos shown. Abbreviations: te, telencephalic *dlx2* streak; di, diencephalic *dlx2* streak. All embryos were injected with 17ng of morpholino. Scale bar = 100 μm.

5.2.3 Further investigation of hdMO1 anterior neural plate deficiency

In 2005, Woda *et al*. [83] carried out an investigation of very early stage htt deficient $Hdh^{ex4/5}$/ $Hdh^{ex4/5}$ mouse embryos (first characterized in 1997 [84]; see Section 1.5). At e6.5, these embryos have reduced neuroectoderm formation, and lack a morphological node. This is thought to be caused by a deficiency in formation of the anterior primitive streak (anterior blastoderm margin in zebrafish [220]). The blastoderm margin is required for formation of the germ layers; ectoderm, mesoderm and endoderm.

During gastrulation, the three germ layers are established by movement of epiblast cells through the blastopore margin, which is formed as a furrow in the embryo [220, 221] (Figure 5.5). To investigate whether a deficiency in the blastoderm margin gives rise to the anterior neural plate deficiency phenotype observed here, we examined mesoderm formation in *hd*MO1 embryos using *insitu* hybridisation. Analysis of $Hdh^{ex4/5}$/$Hdh^{ex4/5}$ embryos by Woda *et al*. showed an altered pattern of mesodermal marker, *T* with weaker expression in the anterior primitive streak. *In situ* hybridization of the zebrafish orthologue of the mouse *Brachyury* gene*, called no tail (ntl)* [126] showed no change in pattern of expression in the notochord of *hd*MO1 embryos compared to control embryos. However, lower expression within the tailbud was observed (Figure 5.6 A-D and Table 5.1). The tailbud is important for formation of posterior structures of the developing embryo, both axial and non-axial structures such as the notochord and the tail, respectively [222, 223]. With high doses of morpholino, *hd*MO1 embryos appear to have a curled tail [112], suggestive of a deficiency in non-axial mesoderm. Importantly within the tail bud, *hd*MO1 embryos still form the Kupffer's vesicle (KV), the zebrafish structure equivalent to the mouse node and required for left-right patterning [224].

During zebrafish development, somites are formed by segmentation of the paraxial mesoderm. *hd*MO1 embryos form ordered somites, which closely resemble those seen in wild-type uninjected and *mc*MO1-injected embryos. Appropriate formation of the notochord and the somites suggests that *hd*MO1 embryos are not deficient in mesoderm production. This therefore also suggests no deficiency in the blastoderm margin of *hd*MO1 embryos .

To further elucidate the mechanism of anterior ectoderm deficiency in *hd*MO1 embryos, investigation into embryonic tissues required for formation of this region was carried out. In zebrafish, the yolk syncytial layer (YSL) plays an important role in formation of the anterior neuroectoderm in a similar manner to the anterior visceral endoderm (AVE) in

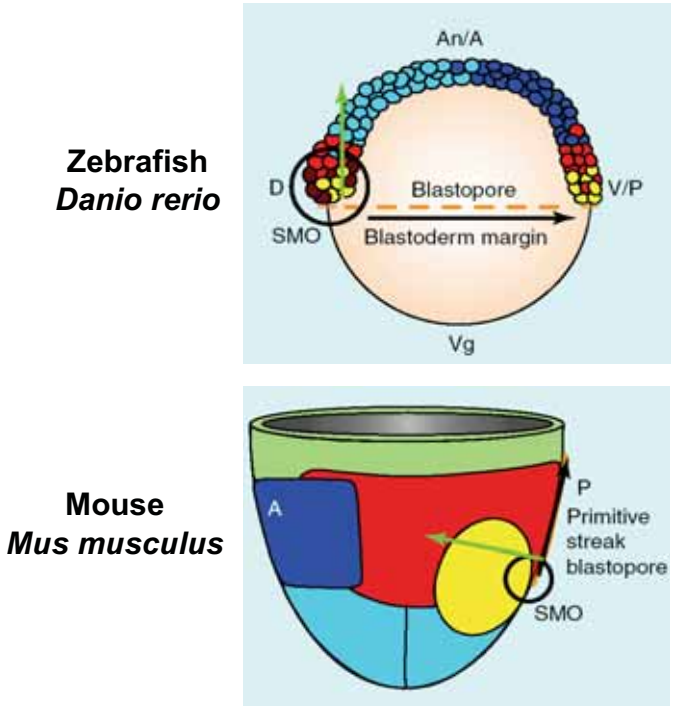

Figure 5.5 Location of the blastopore in zebrafish and mouse gastrulae. The blastopore of amniotes such as mouse and chick is called the primitive streak, while the blastopore of fish and frog is known as the blastoderm margin. The cartoons above shows the location of the blastopore in the zebrafish and mouse gastrulae using the location of the blastopore and the Spemann-Mangold organizer (SMO; shield) as reference points, which takes the axial blastopore position. This spatial organization enables comparison of gastrulation movements despite the distinct embryonic architecture of various vertebrate gastrulae. The proximodistal axis of the blastopore is indicated by the black arrow. Reference is also made to distance from the blastopore (blastoporal-ablastoporal axis; green arrow). Figure adapted from [220]. Abbreviations; A, anterior; An, animal; D, dorsal; P, posterior; V, ventral; Vg, vegetal; SMO, Spemann-Mangold organizer. Color code: red, mesoderm; yellow, endoderm; light blue, non-neural ectoderm; dark blue, neural ectoderm.

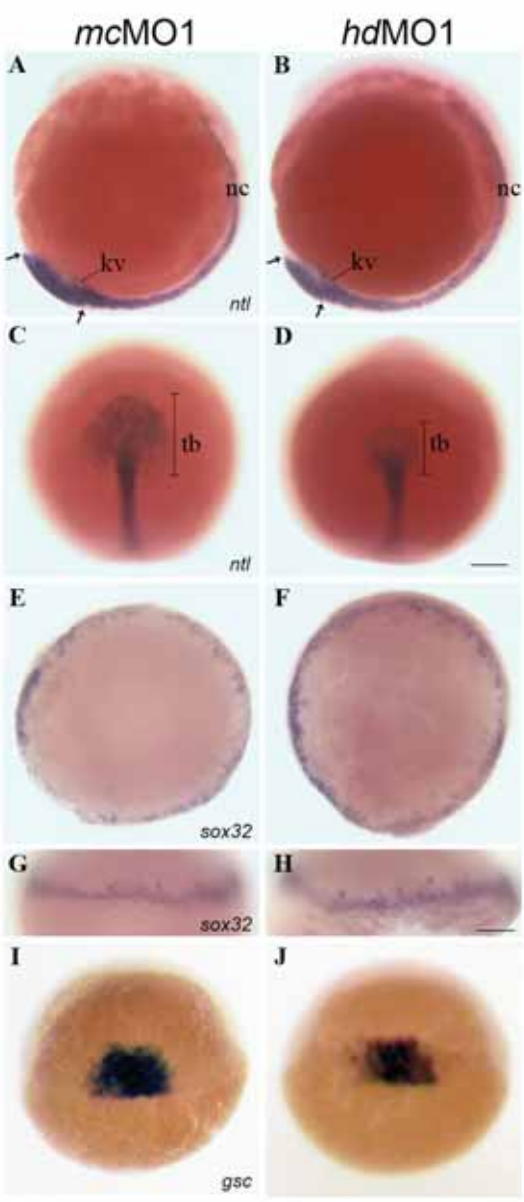

Figure 5.6 Further characterization of early *hd*MO1 embryo development. *hd*MO1 embryos show no significant change is mesoderm formation compared to *mc*MO1 embryos. (A, B) Reduction in htt expression does not affect formation of the notochord (nc) as shown by *in situ* hybridization of *ntl*. However *hd*MO1 embryos (B) have a noticeably smaller tail bud compared to *mc*MO1 embryos (A; compare distance between arrows in each image). Also compare length of bars in dorsal view; C, D). Kupffler's vesicle (kv) is present in both *mc*MO1 and *hd*MO1 embryos. (E-H) The yolk syncytial layer (YSL) of *hd*MO1 embryos is indistinguishable from that of *mc*MO1 embryos by *in situ* hybridization of *sox32*. (I, J) Reduction in htt expression does not alter formation of the node shown here by expression of *gsc*. (A, B) lateral views of embryos at 12 hpf, anterior to the left; (C, D) dorsal views of embryos at 12 hpf; (E, F) dorsal views of embryos at 30% epiboly; (G, H) lateral views of embryos at 30% epiboly, dorsal to the top; (I, J) lateral views of embryos at 60% epiboly, dorsal to the top. Numbers of embryos displaying the described phenotypes were (C, D) *c*MO1 8/47, *hd*MO1 27/35. Representative embryos shown. Abbreviations: kv, kupffler's vesicle; nc, notochord; tb, tail bud; YSL, yolk syncytial layer. All embryos in the left column are *mc*MO1 embryos. All embryos in the right column are *hd*MO1 embryos. All embryos were injected with 17ng of morpholino. All scale bars = 200 μm.

the mouse [225]. At 30% epiboly (4.7 hpf), *sox32* is expressed by cells of the YSL and presumptive endoderm. By *in situ* hybridization analysis, there appeared to be no change in the abundance or pattern of cells in the YSL in *hd*MO1 embryos (Figure 5.6 F and H) compared to the control embryos (Figure 5.6 E and G). This result suggests that reduction in htt expression does not alter the formation of the YSL and therefore does not give rise to the anterior ectoderm phenotype seen in *hd*MO1 embryos.

Like the node in mouse and chick, the zebrafish shield has an essential role in the induction of anterior neural plate tissue (reviewed in [226]). We analyzed the expression of the gene, *goosecoid* (*gsc*) that is normally expressed within the zebrafish organizer at shield stage (6 hpf) and plays an essential role in dorso-ventral patterning and formation of forebrain development [227]. We found that injection of *hd*MO1 did not affect the pattern or level of *gsc* expression in the organizer (Figure 5.6 I and J) suggesting that perturbation of shield formation does not play a role in the *hd*MO1 phenotype described herein.

5.3 Conclusion

This chapter outlines results of a detailed investigation into the sensory neuron deficiency in *hd*MO1 embryos. These phenotypes include a reduction in both the number of olfactory sensory neurons, and in the number of lateral line neuromasts (as first described in Chapter 3). The common placodal origin of these two sensory systems suggested that they could possibly be caused by a similar deficiency, resulting from reduced htt expression.

As described in this chapter, subsequent investigations demonstrated that *hd*MO1 embryos have impaired formation of the pre-placodal region as evidenced by reduced expression of pan-placodal genes *six1* and *dlx3b*. This deficiency also extends to the anterior region of the early neural plate shown by reduced expression of *emx3* normally expressed within telencephalic precursor cells.

While a significant reduction was observed in the level of anterior gene expression (for *six1*, *dlx3b* and *emx3*), no significant change was observed in the slightly more posterior marker, *otx2*. There was also no significant change in markers of midbrain and hindbrain tissue (*valentino (val)*, *krox20*, and *hoxd4a*), or the hindbrain-derived tissue, the cranial neural crest (*dlx2*). It therefore appears that the consequences of htt deficiency in *hd*MO1 embryos

are restricted to the most anterior regions of the neural plate and pre-placodal region, and do not affect anteroposterior patterning of the neural plate.

The anterior neural plate and cranial dorsolateral endomesoderm are important for induction of the pre-placodal region [228]. Given this, it is possible that the reduction in pre-placodal tissue occurs as a result of deficiency in the anterior neural plate *emx3* expressing cells, located at the anterior neural plate border region. It is therefore hypothesized that htt is specifically required for the formation or survival of the anterior neural plate margin, including *emx3* expressing telencephalic precursor cells.

Investigation of the possible cause of anterior neural plate deficiency showed no change in two structures known to be important in formation of the anterior neural plate, the shield (expressing *gsc*) and the yolk syncytial layer (expressing *sox32*). This result is in contrast to that observed by White *et al*., [84], and Woda *et al*., [83] where $Htt^{-/-}$ mice did not form a morphological node. The difference between *hd*MO1 zebrafish embryos and $Htt^{-/-}$ mice is likely to be due to the small amount of htt present in *hd*MO1 embryos as a result of the incomplete reduction of htt translation by *hd*MO1, and pre-injection translation of maternally deposited htt mRNA in 1-cell *hd*MO1 embryos [112]. This small level of htt expression is likely to be sufficient to allow formation of the node in *hd*MO1 embryos and supports that the anterior deficiency is not a result of perturbation in node formation.

Clinical observations of HD patients reveal some evidence of olfactory impairment (as mentioned in Chapter 3). This includes impaired olfactory detection, identification, memory, and discrimination of odors. Each of these symptoms is possibly caused by dysfunction of olfactory neurons and/or neurodegeneration within brain regions that are important for processing olfactory information. Due to htt's role in anterior neural plate formation shown here it is possible that either of these mechanisms results from perturbation of normal htt function. These findings therefore suggest that loss of normal functions of htt contributes to the impaired olfactory function seen in HD patients.

During the preparation of this thesis and associated manuscript [229], another description of brain morphology and apoptosis in zebrafish with reduced htt expression was published [195]. In this paper, Diekmann *et al*. (2009) noted that their *hd*MO1 embryos showed similar brain morphology to that described earlier in our lab [112]. They also described apoptosis within the midbrain and hindbrain of their *hd*MO1 embryos. While, research carried out within our lab has not revealed any increase in apoptosis within the hindbrain at anytime during development, a significant increase in apoptosis was observed within the optic tectum, in the midbrain, at 36-48 hpf (Figure 3.5). This result may also complement another observation by Diekmann *et al*. [195] showing significantly reduced

axonal innervation of this region by retinal axons. At approximately 36-48 hpf, retinal axons are required to make contact with the optic tectum. Any neurons in the optic tectum that are not contacted by retinal axons undergo apoptosis [158].

Although retinal precursors form within the anterior region of the neural plate, the anterior neural plate deficiency in *hd*MO1 embryos is not necessarily the cause of this retinal axon phenotype. Retinal precursor cells express *zic1*. This gene is expressed largely within the *otx2*-expressing domain, as shown in Figure 5.2. As *hd*MO1 embryos do not appear to be deficient in *otx2* expressing cells, it is unlikely that this phenotype is due to reduction of retinal precursor cell number. It is possible however that htt may play a role in retinal development after retinal cell formation, such as in survival, differentiation or axon guidance of the retinal cells. This possibility is supported by a *Drosophila htt* knockout model, in which absence of htt leads to retinal degeneration in adult flies [75]. The observed neurodegeneration is similar to that caused by over-expression of polyQ htt [75]. Retinal degeneration is also seen in an HD transgenic mouse model R6/2 [179, 180]. This evidence suggests a role for htt in survival of retinal cells, and for perturbation of htt function in the pathogenesis of HD.

In summary, the data presented here demonstrates a role for htt in formation of the anterior most region of the neural plate using a zebrafish model of reduced htt expression. The advantages of this system enable analysis of htt function at the earliest stages of development, a difficult task in mouse *Htt* knockout models. Research described within this thesis shows that despite the homogeneous expression of htt in the brain, htt functions specifically within the forebrain to enable formation of precursors of the telencephlon and pre-placodal cells. The downstream effect of this includes loss of placode-derived tissue including olfactory and lateral line sensory neurons, and reduction in telencephalic tissue. The observed sensory neuron requirement for htt in the *hd*MO model described here is consistent with the observation that HD patients show impaired olfactory function (first discussed in Section 3.3) [170-173, 175, 176]. This suggests that loss of the normal functions of htt contributes to at least some of the symptoms of HD pathology.

CHAPTER 6: DISCUSSION

Htt is a large 350 kDa protein that is ubiquitously expressed throughout development. Expansion of a polyglutamine repeat region in the amino terminus of htt is responsible for the devastating neurodegenerative condition, Huntington's disease (HD). Although it is widely accepted that the presence of the polyglutamine repeat beyond a threshold number imparts a toxic gain-of-function property to this protein, there is some compelling evidence to suggest that a loss of the normal function of htt contributes to HD pathology, especially its neuronal specificity (reviewed in [45]).

Presently, the normal functions of htt are unclear. The many binding partners and biological processes described to date suggest that the cellular functions of htt are numerous, including transcriptional regulation, vesicle trafficking, iron homeostasis, and cell survival (reviewed in [45]). It has been unclear which, if any, of these functions might be rate-limiting in neurons and therefore candidates for perturbation in HD.

Animal model systems are useful to identify the functions of htt in the complex developing organism. Previously, analysis of htt functions in the mouse model has been difficult due to the early embryonic lethality of homozygous knockout animals and the apparent lack of phenotype in heterozygous animals [80-82]. Embryonic lethality in these embryos demonstrates that htt plays a critical role in early embryonic development however it also makes analysis of the consequences of htt knockout in older embryos difficult.

Research included in this thesis has focused on the effects of morpholino-induced inhibition of htt translation in zebrafish embryos. The benefit of this approach is that the extent of inhibition of htt expression can be varied as can the resulting phenotype by adjusting the dosage of morpholino-injected. For research included in this thesis, a moderate level of morpholino was used in order to investigate the effects of a partial reduction of htt expression. The same approach has been used by our lab previously [112]. With partial htt reduction, *hd*MO1 embryos have disrupted craniofacial structure and impaired formation of the anterior region of the early neural plate, including the pre-placodal region and telencephalic presursors. The reduction in anterior neural plate precursor cells later results in a dose-

dependent reduction in the number of lateral line neuromasts and also reduction in olfactory sensory neurons and forebrain regions such as the subpallium and diencephalon.

The pre-placodal region is a homogeneous layer of embryonic ectoderm that becomes specified early in development to form a number of different placodal tissues. The olfactory and lateral line systems are among a number of placodal tissues that originate from this common precursor region. Others include adenohypophyseal, trigeminal, profundal, lens, otic, and a series of epibranchial and hypobranchial placodes. It is hypothesized that reduction of the pre-placodal domain will affect all tissues derived from these placodes including; the anterior lobe of the pituitary gland, ganglia of the trigeminal and profundal nerves, lens, otic vesicle and the sensory neurons of the distal ganglia of the face respectively [210]. The downstream affects of disruption in placode formation alone are wide ranging and, in addition to the loss of telencephalic precursor cells, have devastating consequences on embryo development.

Huntingtin's role in the developing brain - Differing requirements of neuronal cells for huntingtin function

A role for htt in brain development is suggested by the high level of htt expression in the brain early in development. Despite the limited knowledge of its function, htt has a known important role in neuronal survival, and has been shown to be required for formation or survival of neurons in specific regions of the brain. A conditional knockout system in mouse has previously shown that htt is required for survival of neurons within the postnatal forebrain [52]. While more specifically, *Htt*$^{-/-}$ ES cells injected into a wild-type blastocyst showed that htt expression was required for neuronal survival within the striatum, cortex, hippocampus and Purkinje cells of the cerebellum [53]. These results are complementary to that seen in our zebrafish model of morpholino-induced htt knockdown.

Research included in this thesis demonstrates that htt plays a role in formation of the anterior most region of the neural plate, specifically in formation of telencephalic progenitor cells and the pre-placodal tissue. Results obtained from this model system have demonstrated that neuronal cells have differing requirements for htt function. Given that perturbation of normal htt function is a component of HD pathogenesis, this differing requirement of particular neurons for htt function provides a mechanism that can account for the specificity of neuropathology in HD brains despite the widespread expression of htt in the brain.

Future work

Given the neuronal nature of pathology of HD, the anterior neural plate phenotype described in Chapter 5 has greater relevance to HD disease pathogenesis and will therefore provide a focus for future work.

A number of functions have been proposed for htt, which may affect brain formation and patterning contributing to a deficiency in anterior neural plate formation. Such functions include promotion of cell survival, differentiation and formation of progenitor cells. Neurotrophins, such as BDNF, are important in mammalian neurons for survival and differentiation. Htt is known to play an important role in regulating the production of BDNF [62, 95, 230] and in the transport of BDNF along microtubules [72]. Since completing this body or work, our lab has begun investigating a possible role for BDNF in the anterior neural plate phenotype described in this thesis. We have found that addition of exogenous recombinant BDNF to the fish water was able to partially rescue the number of lateral line neuromasts toward wild-type levels, suggesting that alteration in the production or supply of BDNF is responsible in part for the loss of lateral line neuromasts. It is currently not clear which step in the formation of lateral line neuromasts is rescued by BDNF - whether in the formation of the anterior neural ectoderm, in its survival or in differentiation of the sensory neurons, a known function of BDNF [231]. However, this finding further highlights the important developmental role for htt in regulation of BDNF signaling, and the likely participation of BDNF in HD pathology. This work is included in the attached manuscript.

Appendix A

A

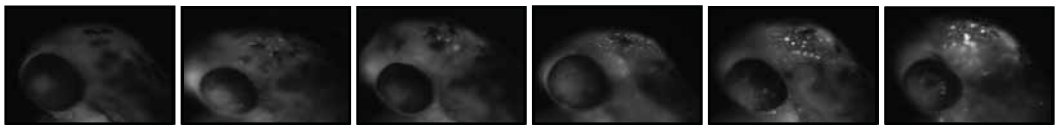

0 1 2 3 4 5

B

4.25ng MO		0	1	2	3	4	5	Total # of embryos
48hpf	WT uninj.	91.2	0	0	5.9	0	2.9	34
	cMO	85.7	4.8	9.5	0	0	0	21
	*hd*MO1	3.7	3.7	37.0	37.0	7.4	11.1	27
72hpf	WT uninj.	100	0	0	0	0	0	37
	cMO	95.0	5.0	0	0	0	0	20
	*hd*MO1	30.3	36.4	21.2	6.1	6.1	0	33
96hpf	WT uninj.	100	0	0	0	0	0	36
	cMO	100	0	0	0	0	0	25
	*hd*MO1	100	0	0	0	0	0	44

Appendix A: Apoptosis within the optic tectum. This appendix provides additional information to show a dose response to injection of half the amount of *hd*MO1 morpholino in the initial experiment (Figure 3.5). (B) Results of scoring are displayed as a percentage, with the total number of embryos observed shown in the right-hand column. Green boxes indicate the scoring level with the greatest number of embryos for each treatment group and each time point. *hd*MO1 embryos have an increased level of apoptosis at 48 and 72 hpf as evidenced by shift in green box to the right. The shift in the green box to the right is not as dramatic here as seen for 8.5ng morpholino injected embryos (Figure 3.5) indicating a dose response to *hd*MO1 injection. Results pooled from 2 independent experiments for each time point. 4.25ng morpholino injected per embryo. (A, B) Representative embryos shown for each group (0-5). Dorsal/lateral views of embryos, anterior to the left; 48 hpf. 4.25ng morpholino injected per embryo. Results pooled from 2 independent experiments for each time point.

REFERENCES

1 **Nakamura, K. J., S. Y., Uchihara, T., Anno, M., Nagashima, K., Nagashima, T., Ikeda, S., Tsuji, S. and Kanazawa, I.,** SCA17 a novel autosomal dominant cerebellar ataxia caused by an expanded polyglutamine in TATA-binding protein. *Hum Mol Genet* 2001. **10**: 1441-1448.

2 **Orr, H. T. and Zoghbi, H. Y.,** Trinucleotide repeat disorders. *Annu Rev Neurosci* 2007. **30**: 575-621.

3 **Duyao, M., Ambrose, C., Myers, R., Novelletto, A., Persichetti, F., Frontali, M., Folstein, S., Ross, C., Franz, M., Abbott, M. and et al.,** Trinucleotide repeat length instability and age of onset in Huntington's disease. *Nat Genet* 1993. **4**: 387-392.

4 **Harper, P. S.,** *Huntington's disease*. W.B.Saunders, London: 1991.

5 **HDCRG,** A novel gene containing a trinucleotide repeat that is expanded and unstable on Huntington's disease chromosomes. The Huntington's Disease Collaborative Research Group. *Cell* 1993. **72**: 971-983.

6 **HGNC, H. G. N. C.**, 06/28/2009 Edn. European Bioinformatics Institute 2009.

7 **Li, S. H. and Li, X. J.,** Huntingtin-protein interactions and the pathogenesis of Huntington's disease. *Trends Genet* 2004. **20**: 146-154.

8 **Ridley, R. M., Frith, C. D., Crow, T. J. and Conneally, P. M.,** Anticipation in Huntington's disease is inherited through the male line but may originate in the female. *J Med Genet* 1988. **25**: 589-595.

9 **Hoffmann, J.,** Uber Chorea chronica progressiva (Huntingtonsche Chorea, Chorea hereditaria). *Virchows Arch. A* 1888. **111**: 513-548.

10 **Myers, R. H., Marans, K.S., and MacDonald, M.E.,** Huntington's disease. In **Wells, R. D. a. W., S.T** (Ed.) *Genetic instabilities and hereditary neurological diseases*. Academic Press, California 1998, pp 302.

11 **Hedreen, J. C. and Folstein, S. E.,** Early loss of neostriatal striosome neurons in Huntington's disease. *J Neuropathol Exp Neurol* 1995. **54**: 105-120.

12 **Vonsattel, J. P., Myers, R. H., Stevens, T. J., Ferrante, R. J., Bird, E. D. and Richardson, E. P., Jr.,** Neuropathological classification of Huntington's disease. *J Neuropathol Exp Neurol* 1985. **44**: 559-577.

13 **Huq, A., Hackam, A., Graham, R., Wellington, C., Hayden, M.,** Molecular pathogenesis of Huntington's disease: Biochemical studies of Huntingtin. In **Wells, R. D. a. W., S.T** (Ed.) *Genetic Instabilities and Hereditory Neurological Diseases*. Academic Press, London 1998, pp 325-353.

14 **DiFiglia, M.,** Excitotoxic injury of the neostriatum: a model for Huntington's disease. *Trends Neurosci* 1990. **13**: 286-289.

15 **Zech, M., Roberts, G. W., Bogerts, B., Crow, T. J. and Polak, J. M.,** Neuropeptides in the amygdala of controls, schizophrenics and patients suffering from Huntington's chorea: an immunohistochemical study. *Acta Neuropathol (Berl)* 1986. **71**: 259-266.

16 **Kremer, H. P., Roos, R. A., Dingjan, G., Marani, E. and Bots, G. T.,** Atrophy of the hypothalamic lateral tuberal nucleus in Huntington's disease. *J Neuropathol Exp Neurol* 1990. **49**: 371-382.

17 **Fusco, F. R., Chen, Q., Lamoreaux, W. J., Figueredo-Cardenas, G., Jiao, Y., Coffman, J. A., Surmeier, D. J., Honig, M. G., Carlock, L. R. and Reiner, A.,** Cellular localization of huntingtin in striatal and cortical neurons in rats: lack of correlation with neuronal vulnerability in Huntington's disease. *J Neurosci* 1999. **19**: 1189-1202.

18 **Steffan, J. S., Kazantsev, A., Spasic-Boskovic, O., Greenwald, M., Zhu, Y. Z., Gohler, H., Wanker, E. E., Bates, G. P., Housman, D. E. and Thompson, L. M.,** The Huntington's disease protein interacts with p53 and CREB-binding protein and represses transcription. *Proc Natl Acad Sci U S A* 2000. **97**: 6763-6768.

19 **Bhide, P. G., Day, M., Sapp, E., Schwarz, C., Sheth, A., Kim, J., Young, A. B., Penney, J., Golden, J., Aronin, N. and DiFiglia, M.,** Expression of normal and mutant huntingtin in the developing brain. *J Neurosci* 1996. **16**: 5523-5535.

20 **Calabresi, P., Pisani, A., Mercuri, N. B. and Bernardi, G.,** The corticostriatal projection: from synaptic plasticity to dysfunctions of the basal ganglia. *Trends Neurosci* 1996. **19**: 19-24.

21 **Landwehrmeyer, G. B., McNeil, S. M., Dure, L. S. t., Ge, P., Aizawa, H., Huang, Q., Ambrose, C. M., Duyao, M. P., Bird, E. D., Bonilla, E. and et al.,** Huntington's disease gene: regional and cellular expression in brain of normal and affected individuals. *Ann Neurol* 1995. **37**: 218-230.

22 **Ferrante, R. J., Gutekunst, C. A., Persichetti, F., McNeil, S. M., Kowall, N. W., Gusella, J. F., MacDonald, M. E., Beal, M. F. and Hersch, S. M.,** Heterogeneous topographic and cellular distribution of huntingtin expression in the normal human neostriatum. *J Neurosci* 1997. **17**: 3052-3063.

23 **DiFiglia, M., Sapp, E., Chase, K., Schwarz, C., Meloni, A., Young, C., Martin, E., Vonsattel, J. P., Carraway, R., Reeves, S. A. and et al.,** Huntingtin is a cytoplasmic protein associated with vesicles in human and rat brain neurons. *Neuron* 1995. **14**: 1075-1081.

24 **Sharp, A. H., Loev, S. J., Schilling, G., Li, S. H., Li, X. J., Bao, J., Wagster, M. V., Kotzuk, J. A., Steiner, J. P., Lo, A. and et al.,** Widespread expression of Huntington's disease gene (IT15) protein product. *Neuron* 1995. **14**: 1065-1074.

25 **Wood, J. D., MacMillan, J. C., Harper, P. S., Lowenstein, P. R. and Jones, A. L.,** Partial characterisation of murine huntingtin and apparent variations in the subcellular localisation of huntingtin in human, mouse and rat brain. *Hum Mol Genet* 1996. **5**: 481-487.

26 **Gutekunst, C. A., Levey, A. I., Heilman, C. J., Whaley, W. L., Yi, H., Nash, N. R., Rees, H. D., Madden, J. J. and Hersch, S. M.,** Identification and localization of huntingtin in brain and human lymphoblastoid cell lines with anti-fusion protein antibodies. *Proc Natl Acad Sci U S A* 1995. **92**: 8710-8714.

27 **Perutz, M. F., Johnson, T., Suzuki, M. and Finch, J. T.,** Glutamine repeats as polar zippers: their possible role in inherited neurodegenerative diseases. *Proc Natl Acad Sci U S A* 1994. **91**: 5355-5358.

28 **Gerber, H. P., Seipel, K., Georgiev, O., Hofferer, M., Hug, M., Rusconi, S. and Schaffner, W.,** Transcriptional activation modulated by homopolymeric glutamine and proline stretches. *Science* 1994. **263**: 808-811.

29 **Harjes, P. and Wanker, E. E.,** The hunt for huntingtin function: interaction partners tell many different stories. *Trends Biochem Sci* 2003. **28**: 425-433.

30 **Goehler, H., Lalowski, M., Stelzl, U., Waelter, S., Stroedicke, M., Worm, U., Droege, A., Lindenberg, K. S., Knoblich, M., Haenig, C., Herbst, M., Suopanki, J., Scherzinger, E., Abraham, C., Bauer, B., Hasenbank, R., Fritzsche, A., Ludewig, A. H., Bussow, K., Coleman, S. H., Gutekunst, C. A., Landwehrmeyer, B. G., Lehrach, H. and Wanker, E. E.,** A protein interaction network links GIT1, an enhancer of huntingtin aggregation, to Huntington's disease. *Mol Cell* 2004. **15**: 853-865.

31 **Sun, Y., Savanenin, A., Reddy, P. H. and Liu, Y. F.,** Polyglutamine-expanded huntingtin promotes sensitization of N-methyl-D-aspartate receptors via post-synaptic density 95. *J Biol Chem* 2001. **276**: 24713-24718.

32 **Modregger, J., DiProspero, N. A., Charles, V., Tagle, D. A. and Plomann, M.,** PACSIN 1 interacts with huntingtin and is absent from synaptic varicosities in presymptomatic Huntington's disease brains. *Hum Mol Genet* 2002. **11**: 2547-2558.

33 **Gao, Y. G., Yan, X.Z., Song, A.X., Chang, Y.G., Jiang, N., Zhang, Q. and Hu, H.Y.,** Structural insights into the specific binding of huntingtin proline-rich region with the SH3 and WW domains. *Structure* 2006. **14**: 1755-1765.

34 **Sittler, A., Walter, S., Wedemeyer, N., Hasenbank, R., Scherzinger, E., Eickhoff, H., Bates, G. P., Lehrach, H. and Wanker, E. E.,** SH3GL3 associates with the Huntingtin exon 1 protein and promotes the formation of polygln-containing protein aggregates. *Mol Cell* 1998. **2**: 427-436.

35 **Andrade, M. A. and Bork, P.,** HEAT repeats in the Huntington's disease protein. *Nat Genet* 1995. **11**: 115-116.

36 **Andrade, M. A., Petosa, C., O'Donoghue, S. I., Muller, C. W. and Bork, P.,** Comparison of ARM and HEAT protein repeats. *J Mol Biol* 2001. **309**: 1-18.

37 **Li, W., Serpell, L.C, Carter, W.J., Rubinsztein, D.C. and Huntingtin, J.A.,** Expression and characterisation of the full-length human huntingtin, an elongated HEAT repeat protein. *J. Biol. Chem.* 2006. **281**: 15916-15922.

38 **Edwards, T. A., Pyle, S. E., Wharton, R. P. and Aggarwal, A. K.,** Structure of Pumilio reveals similarity between RNA and peptide binding motifs. *Cell* 2001. **105**: 281-289.

39 **Takano, H. and Gusella, J. F.,** The predominantly HEAT-like motif structure of huntingtin and its association and coincident nuclear entry with dorsal, an NF-kB/Rel/dorsal family transcription factor. *BMC Neurosci* 2002. **3**: 15.

40 **Andrade, M. A., Ponting, C. P., Gibson, T. J. and Bork, P.,** Homology-based method for identification of protein repeats using statistical significance estimates. *J Mol Biol* 2000. **298**: 521-537.

41 **Singaraja, R. R., Hadano, S., Metzler, M., Givan, S., Wellington, C. L., Warby, S., Yanai, A., Gutekunst, C. A., Leavitt, B. R., Yi, H., Fichter, K., Gan, L., McCutcheon, K., Chopra, V., Michel, J., Hersch, S. M., Ikeda, J. E. and Hayden, M. R.,** HIP14, a novel ankyrin domain-containing protein, links huntingtin to intracellular trafficking and endocytosis. *Hum Mol Genet* 2002. **11**: 2815-2828.

42 **Wanker, E. E., Rovira, C., Scherzinger, E., Hasenbank, R., Walter, S., Tait, D., Colicelli, J. and Lehrach, H.,** HIP-I: a huntingtin interacting protein isolated by the yeast two-hybrid system. *Hum Mol Genet* 1997. **6**: 487-495.

43 **Kalchman, M. A., Koide, H. B., McCutcheon, K., Graham, R. K., Nichol, K., Nishiyama, K., Kazemi-Esfarjani, P., Lynn, F. C., Wellington, C., Metzler, M., Goldberg, Y. P., Kanazawa, I., Gietz, R. D. and Hayden, M. R.,** HIP1, a human homologue of S. cerevisiae Sla2p, interacts with membrane-associated huntingtin in the brain. *Nat Genet* 1997. **16**: 44-53.

44 **Li, X. J., Li, S. H., Sharp, A. H., Nucifora, F. C., Jr., Schilling, G., Lanahan, A., Worley, P., Snyder, S. H. and Ross, C. A.,** A huntingtin-associated protein enriched in brain with implications for pathology. *Nature* 1995. **378**: 398-402.

45 **Imarisio, S., Carmichael, J., Korolchuk, V., Chen, C. W., Saiki, S., Rose, C., Krishna, G., Davies, J. E., Ttofi, E., Underwood, B. R. and Rubinsztein, D. C.,** Huntington's disease: from pathology and genetics to potential therapies. *Biochem J* 2008. **412**: 191-209.

46 **Gil, J. M. and Rego, A. C.,** Mechanisms of neurodegeneration in Huntington's disease. *Eur J Neurosci* 2008. **27**: 2803-2820.

47 **Rigamonti, D., Bauer, J. H., De-Fraja, C., Conti, L., Sipione, S., Sciorati, C., Clementi, E., Hackam, A., Hayden, M. R., Li, Y., Cooper, J. K., Ross, C. A., Govoni, S., Vincenz, C. and**

Cattaneo, E., Wild-type huntingtin protects from apoptosis upstream of caspase-3. *J Neurosci* 2000. **20**: 3705-3713.

48 **Hackam, A. S., Yassa, A. S., Singaraja, R., Metzler, M., Gutekunst, C. A., Gan, L., Warby, S., Wellington, C. L., Vaillancourt, J., Chen, N., Gervais, F. G., Raymond, L., Nicholson, D. W. and Hayden, M. R.,** Huntingtin interacting protein 1 induces apoptosis via a novel caspase-dependent death effector domain. *J Biol Chem* 2000. **275**: 41299-41308.

49 **Liu, Y. F., Dorow, D. and Marshall, J.,** Activation of MLK2-mediated signaling cascades by polyglutamine-expanded huntingtin. *J Biol Chem* 2000. **275**: 19035-19040.

50 **Marcora, E., Gowan, K. and Lee, J. E.,** Stimulation of NeuroD activity by huntingtin and huntingtin-associated proteins HAP1 and MLK2. *Proc Natl Acad Sci U S A* 2003. **100**: 9578-9583.

51 **Luo, S. and Rubinsztein, D. C.,** Huntingtin promotes cell survival by preventing Pak2 cleavage. *J Cell Sci* 2009. **122**: 875-885.

52 **Dragatsis, I., Levine, M. S. and Zeitlin, S.,** Inactivation of Hdh in the brain and testis results in progressive neurodegeneration and sterility in mice. *Nat Genet* 2000. **26**: 300-306.

53 **Reiner, A., Del Mar, N., Meade, C. A., Yang, H., Dragatsis, I., Zeitlin, S. and Goldowitz, D.,** Neurons lacking huntingtin differentially colonize brain and survive in chimeric mice. *J Neurosci* 2001. **21**: 7608-7619.

54 **Leavitt, B. R., Guttman, J. A., Hodgson, J. G., Kimel, G. H., Singaraja, R., Vogl, A. W. and Hayden, M. R.,** Wild-type huntingtin reduces the cellular toxicity of mutant huntingtin in vivo. *Am J Hum Genet* 2001. **68**: 313-324.

55 **Leavitt, B. R., van Raamsdonk, J. M., Shehadeh, J., Fernandes, H., Murphy, Z., Graham, R. K., Wellington, C. L., Raymond, L. A. and Hayden, M. R.,** Wild-type huntingtin protects neurons from excitotoxicity. *J Neurochem* 2006. **96**: 1121-1129.

56 **Boutell, J. M., Thomas, P., Neal, J. W., Weston, V. J., Duce, J., Harper, P. S. and Jones, A. L.,** Aberrant interactions of transcriptional repressor proteins with the Huntington's disease gene product, huntingtin. *Hum Mol Genet* 1999. **8**: 1647-1655.

57 **Kegel, K. B., Meloni, A. R., Yi, Y., Kim, Y. J., Doyle, E., Cuiffo, B. G., Sapp, E., Wang, Y., Qin, Z. H., Chen, J. D., Nevins, J. R., Aronin, N. and DiFiglia, M.,** Huntingtin is present in the nucleus, interacts with the transcriptional corepressor C-terminal binding protein, and represses transcription. *J Biol Chem* 2002. **277**: 7466-7476.

58 **McCampbell, A., Taylor, J. P., Taye, A. A., Robitschek, J., Li, M., Walcott, J., Merry, D., Chai, Y., Paulson, H., Sobue, G. and Fischbeck, K. H.,** CREB-binding protein sequestration by expanded polyglutamine. *Hum Mol Genet* 2000. **9**: 2197-2202.

59 **Holbert, S., Denghien, I., Kiechle, T., Rosenblatt, A., Wellington, C., Hayden, M. R., Margolis, R. L., Ross, C. A., Dausset, J., Ferrante, R. J. and Neri, C.,** The Gln-Ala repeat transcriptional activator CA150 interacts with huntingtin: neuropathologic and genetic evidence for a role in Huntington's disease pathogenesis. *Proc Natl Acad Sci U S A* 2001. **98**: 1811-1816.

60 **Li, S. H., Cheng, A. L., Zhou, H., Lam, S., Rao, M., Li, H. and Li, X. J.,** Interaction of Huntington disease protein with transcriptional activator Sp1. *Mol Cell Biol* 2002. **22**: 1277-1287.

61 **Dunah, A. W., Jeong, H., Griffin, A., Kim, Y. M., Standaert, D. G., Hersch, S. M., Mouradian, M. M., Young, A. B., Tanese, N. and Krainc, D.,** Sp1 and TAFII130 transcriptional activity disrupted in early Huntington's disease. *Science* 2002. **296**: 2238-2243.

62 **Zuccato, C., Tartari, M., Crotti, A., Goffredo, D., Valenza, M., Conti, L., Cataudella, T., Leavitt, B. R., Hayden, M. R., Timmusk, T., Rigamonti, D. and Cattaneo, E.,** Huntingtin interacts with REST/NRSF to modulate the transcription of NRSE-controlled neuronal genes. *Nat Genet* 2003. **35**: 76-83.

63 **Schoenherr, C. J., Levorse, J. M. and Tilghman, S. M.,** CTCF maintains differential methylation at the Igf2/H19 locus. *Nat Genet* 2003. **33**: 66-69.

64 **Bruce, A. W., Donaldson, I. J., Wood, I. C., Yerbury, S. A., Sadowski, M. I., Chapman, M., Gottgens, B. and Buckley, N. J.,** Genome-wide analysis of repressor element 1 silencing transcription factor/neuron-restrictive silencing factor (REST/NRSF) target genes. *Proc Natl Acad Sci U S A* 2004. **101**: 10458-10463.

65 **Thompson, L. M.,** An expanded role for wild-type huntingtin in neuronal transcription. *Nat Genet* 2003. **35**: 13-14.

66 **Tukamoto, T., Nukina, N., Ide, K. and Kanazawa, I.,** Huntington's disease gene product, huntingtin, associates with microtubules in vitro. *Brain Res Mol Brain Res* 1997. **51**: 8-14.

67 **Li, X. J. and Li, S. H.,** HAP1 and intracellular trafficking. *Trends Pharmacol Sci* 2005. **26**: 1-3.

68 **Engqvist-Goldstein, A. E., Warren, R. A., Kessels, M. M., Keen, J. H., Heuser, J. and Drubin, D. G.,** The actin-binding protein Hip1R associates with clathrin during early stages of endocytosis and promotes clathrin assembly in vitro. *J Cell Biol* 2001. **154**: 1209-1223.

69 **Block-Galarza, J., Chase, K. O., Sapp, E., Vaughn, K. T., Vallee, R. B., DiFiglia, M. and Aronin, N.,** Fast transport and retrograde movement of huntingtin and HAP 1 in axons. *Neuroreport* 1997. **8**: 2247-2251.

70 **McGuire, J. R., Rong, J., Li, S. H. and Li, X. J.,** Interaction of Huntingtin-associated protein-1 with kinesin light chain: implications in intracellular trafficking in neurons. *J Biol Chem* 2006. **281**: 3552-3559.

71 **Rong, J., McGuire, J. R., Fang, Z. H., Sheng, G., Shin, J. Y., Li, S. H. and Li, X. J.,** Regulation of intracellular trafficking of huntingtin-associated protein-1 is critical for TrkA protein levels and neurite outgrowth. *J Neurosci* 2006. **26**: 6019-6030.

72 **Gauthier, L. R., Charrin, B. C., Borrell-Pages, M., Dompierre, J. P., Rangone, H., Cordelieres, F. P., De Mey, J., MacDonald, M. E., Lessmann, V., Humbert, S. and Saudou, F.,** Huntingtin controls neurotrophic support and survival of neurons by enhancing BDNF vesicular transport along microtubules. *Cell* 2004. **118**: 127-138.

73 **Morfini, G. A., You, Y. M., Pollema, S. L., Kaminska, A., Liu, K., Yoshioka, K., Bjorkblom, B., Coffey, E. T., Bagnato, C., Han, D., Huang, C. F., Banker, G., Pigino, G. and Brady, S. T.,** Pathogenic huntingtin inhibits fast axonal transport by activating JNK3 and phosphorylating kinesin. *Nat Neurosci* 2009. **12**: 864-871.

74 **Smith, R., Bacos, K., Fedele, V., Soulet, D., Walz, H. A., Obermuller, S., Lindqvist, A., Bjorkqvist, M., Klein, P., Onnerfjord, P., Brundin, P., Mulder, H. and Li, J. Y.,** Mutant huntingtin interacts with {beta}-tubulin and disrupts vesicular transport and insulin secretion. *Hum Mol Genet* 2009.

75 **Gunawardena, S., Her, L. S., Brusch, R. G., Laymon, R. A., Niesman, I. R., Gordesky-Gold, B., Sintasath, L., Bonini, N. M. and Goldstein, L. S.,** Disruption of axonal transport by loss of huntingtin or expression of pathogenic polyQ proteins in Drosophila. *Neuron* 2003. **40**: 25-40.

76 **Li, S. H., Gutekunst, C. A., Hersch, S. M. and Li, X. J.,** Interaction of huntingtin-associated protein with dynactin P150Glued. *J Neurosci* 1998. **18**: 1261-1269.

77 **Scannevin, R. H. and Huganir, R. L.,** Postsynaptic organization and regulation of excitatory synapses. *Nat Rev Neurosci* 2000. **1**: 133-141.

78 **Spires, T. L., Grote, H. E., Garry, S., Cordery, P. M., Van Dellen, A., Blakemore, C. and Hannan, A. J.,** Dendritic spine pathology and deficits in experience-dependent dendritic plasticity in R6/1 Huntington's disease transgenic mice. *Eur J Neurosci* 2004. **19**: 2799-2807.

79 **Gaudilliere, B., Konishi, Y., de la Iglesia, N., Yao, G. and Bonni, A.,** A CaMKII-NeuroD signaling pathway specifies dendritic morphogenesis. *Neuron* 2004. **41**: 229-241.

80 **Duyao, M. P., Auerbach, A. B., Ryan, A., Persichetti, F., Barnes, G. T., McNeil, S. M., Ge, P., Vonsattel, J. P., Gusella, J. F., Joyner, A. L. and et al.,** Inactivation of the mouse Huntington's disease gene homolog Hdh. *Science* 1995. **269**: 407-410.

81 **Zeitlin, S., Liu, J. P., Chapman, D. L., Papaioannou, V. E. and Efstratiadis, A.,** Increased apoptosis and early embryonic lethality in mice nullizygous for the Huntington's disease gene homologue. *Nat Genet* 1995. **11**: 155-163.

82 **Nasir, J., Floresco, S. B., O'Kusky, J. R., Diewert, V. M., Richman, J. M., Zeisler, J., Borowski, A., Marth, J. D., Phillips, A. G. and Hayden, M. R.,** Targeted disruption of the Huntington's disease gene results in embryonic lethality and behavioral and morphological changes in heterozygotes. *Cell* 1995. **81**: 811-823.

83 **Woda, J. M., Calzonetti, T., Hilditch-Maguire, P., Duyao, M. P., Conlon, R. A. and MacDonald, M. E.,** Inactivation of the Huntington's disease gene (Hdh) impairs anterior streak formation and early patterning of the mouse embryo. *BMC Dev Biol* 2005. **5**: 17.

84 **White, J. K., Auerbach, W., Duyao, M. P., Vonsattel, J. P., Gusella, J. F., Joyner, A. L. and MacDonald, M. E.,** Huntingtin is required for neurogenesis and is not impaired by the Huntington's disease CAG expansion. *Nat Genet* 1997. **17**: 404-410.

85 **Sipione, S. and Cattaneo, E.,** Modeling Huntington's disease in cells, flies, and mice. *Mol Neurobiol* 2001. **23**: 21-51.

86 **Bates, G., Harper, P., Jones, L.,** *Huntington's disease*, 3rd edition Edn. Oxford University Press, Oxford, UK: 2002.

87 **Gottfried, M., Lavine, L. and Roessmann, U.,** Neuropathological findings in Wolf-Hirschhorn (4p-) syndrome. *Acta Neuropathol (Berl)* 1981. **55**: 163-165.

88 **Gusella, J. F. and MacDonald, M. E.,** Trinucleotide instability: a repeating theme in human inherited disorders. *Annu Rev Med* 1996. **47**: 201-209.

89 **Myers, R. H., Leavitt, J., Farrer, L. A., Jagadeesh, J., McFarlane, H., Mastromauro, C. A., Mark, R. J. and Gusella, J. F.,** Homozygote for Huntington disease. *Am J Hum Genet* 1989. **45**: 615-618.

90 **Wexler, N. S., Young, A. B., Tanzi, R. E., Travers, H., Starosta-Rubinstein, S., Penney, J. B., Snodgrass, S. R., Shoulson, I., Gomez, F., Ramos Arroyo, M. A. and et al.,** Homozygotes for Huntington's disease. *Nature* 1987. **326**: 194-197.

91 **Ordway, J. M., Tallaksen-Greene, S., Gutekunst, C. A., Bernstein, E. M., Cearley, J. A., Wiener, H. W., Dure, L. S. t., Lindsey, R., Hersch, S. M., Jope, R. S., Albin, R. L. and Detloff, P. J.,** Ectopically expressed CAG repeats cause intranuclear inclusions and a progressive late onset neurological phenotype in the mouse. *Cell* 1997. **91**: 753-763.

92 **Narain, Y., Wyttenbach, A., Rankin, J., Furlong, R. A. and Rubinsztein, D. C.,** A molecular investigation of true dominance in Huntington's disease. *J Med Genet* 1999. **36**: 739-746.

93 **Cattaneo, E., Rigamonti, D., Goffredo, D., Zuccato, C., Squitieri, F. and Sipione, S.,** Loss of normal huntingtin function: new developments in Huntington's disease research. *Trends Neurosci* 2001. **24**: 182-188.

94 **Auerbach, W., Hurlbert, M. S., Hilditch-Maguire, P., Wadghiri, Y. Z., Wheeler, V. C., Cohen, S. I., Joyner, A. L., MacDonald, M. E. and Turnbull, D. H.,** The HD mutation causes progressive lethal neurological disease in mice expressing reduced levels of huntingtin. *Hum Mol Genet* 2001. **10**: 2515-2523.

95 **Zuccato, C., Ciammola, A., Rigamonti, D., Leavitt, B. R., Goffredo, D., Conti, L., MacDonald, M. E., Friedlander, R. M., Silani, V., Hayden, M. R., Timmusk, T., Sipione, S. and Cattaneo, E.,** Loss of huntingtin-mediated BDNF gene transcription in Huntington's disease. *Science* 2001. **293**: 493-498.

96 **Zhang, Y., Li, M., Drozda, M., Chen, M., Ren, S., Mejia Sanchez, R. O., Leavitt, B. R., Cattaneo, E., Ferrante, R. J., Hayden, M. R. and Friedlander, R. M.,** Depletion of wild-type huntingtin in mouse models of neurologic diseases. *J Neurochem* 2003. **87**: 101-106.

97 **Gines, S., Seong, I. S., Fossale, E., Ivanova, E., Trettel, F., Gusella, J. F., Wheeler, V. C., Persichetti, F. and MacDonald, M. E.,** Specific progressive cAMP reduction implicates energy deficit in presymptomatic Huntington's disease knock-in mice. *Hum Mol Genet* 2003. **12**: 497-508.

98 **Duan, W., Guo, Z., Jiang, H., Ware, M., Li, X. J. and Mattson, M. P.,** Dietary restriction normalizes glucose metabolism and BDNF levels, slows disease progression, and increases survival in huntingtin mutant mice. *Proc Natl Acad Sci U S A* 2003. **100**: 2911-2916.

99 **Luthi-Carter, R., Hanson, S. A., Strand, A. D., Bergstrom, D. A., Chun, W., Peters, N. L., Woods, A. M., Chan, E. Y., Kooperberg, C., Krainc, D., Young, A. B., Tapscott, S. J. and Olson, J. M.,** Dysregulation of gene expression in the R6/2 model of polyglutamine disease: parallel changes in muscle and brain. *Hum Mol Genet* 2002. **11**: 1911-1926.

100 **Hermel, E., Gafni, J., Propp, S. S., Leavitt, B. R., Wellington, C. L., Young, J. E., Hackam, A. S., Logvinova, A. V., Peel, A. L., Chen, S. F., Hook, V., Singaraja, R., Krajewski, S., Goldsmith, P. C., Ellerby, H. M., Hayden, M. R., Bredesen, D. E. and Ellerby, L. M.,** Specific caspase interactions and amplification are involved in selective neuronal vulnerability in Huntington's disease. *Cell Death Differ* 2004. **11**: 424-438.

101 **Gusella, J. F. and MacDonald, M. E.,** Molecular genetics: unmasking polyglutamine triggers in neurodegenerative disease. *Nat Rev Neurosci* 2000. **1**: 109-115.

102 **Kimmel, C. B., Ballard, W.W., Kimmel, S.R., Ullmann, B., and Schilling, T. F.,** Stages of embryonic development of the zebrafish. *Dev. Dyn.* 1995. **203**: 253-310.

103 **Zon, L. I.,** Zebrafish: a new model for human disease. *Genome Res* 1999. **9**: 99-100.

104 **Geisler, R., Rauch, G. J., Geiger-Rudolph, S., Albrecht, A., van Bebber, F., Berger, A., Busch-Nentwich, E., Dahm, R., Dekens, M. P., Dooley, C., Elli, A. F., Gehring, I., Geiger, H., Geisler, M., Glaser, S., Holley, S., Huber, M., Kerr, A., Kirn, A., Knirsch, M., Konantz, M., Kuchler, A. M., Maderspacher, F., Neuhauss, S. C., Nicolson, T., Ober, E. A., Praeg, E., Ray, R., Rentzsch, B., Rick, J. M., Rief, E., Schauerte, H. E., Schepp, C. P., Schonberger, U., Schonthaler, H. B., Seiler, C., Sidi, S., Sollner, C., Wehner, A., Weiler, C. and Nusslein-Volhard, C.,** Large-scale mapping of mutations affecting zebrafish development. *BMC Genomics* 2007. **8**: 11.

105 **Golling, G., Amsterdam, A., Sun, Z., Antonelli, M., Maldonado, E., Chen, W., Burgess, S., Haldi, M., Artzt, K., Farrington, S., Lin, S. Y., Nissen, R. M. and Hopkins, N.,** Insertional mutagenesis in zebrafish rapidly identifies genes essential for early vertebrate development. *Nat Genet* 2002. **31**: 135-140.

106 **Haffter, P., Granato, M., Brand, M., Mullins, M. C., Hammerschmidt, M., Kane, D. A., Odenthal, J., van Eeden, F. J., Jiang, Y. J., Heisenberg, C. P., Kelsh, R. N., Furutani-Seiki, M., Vogelsang, E., Beuchle, D., Schach, U., Fabian, C. and Nusslein-Volhard, C.,** The identification of genes with unique and essential functions in the development of the zebrafish, Danio rerio. *Development* 1996. **123**: 1-36.

107 **Driever, W., Solnica-Krezel, L., Schier, A. F., Neuhauss, S. C., Malicki, J., Stemple, D. L., Stainier, D. Y., Zwartkruis, F., Abdelilah, S., Rangini, Z., Belak, J. and Boggs, C.,** A genetic screen for mutations affecting embryogenesis in zebrafish. *Development* 1996. **123**: 37-46.

108 **Barbazuk, W. B., Korf, I., Kadavi, C., Heyen, J., Tate, S., Wun, E., Bedell, J. A., McPherson, J. D. and Johnson, S. L.,** The syntenic relationship of the zebrafish and human genomes. *Genome Res* 2000. **10**: 1351-1358.

109 **Karlovich, C. A., John, R. M., Ramirez, L., Stainier, D. Y. and Myers, R. M.,** Characterization of the Huntington's disease (HD) gene homologue in the zebrafish Danio rerio. *Gene* 1998. **217**: 117-125.

110 **Dragatsis, I., Efstratiadis, A. and Zeitlin, S.,** Mouse mutant embryos lacking huntingtin are rescued from lethality by wild-type extraembryonic tissues. *Development* 1998. **125**: 1529-1539.

111 **Schmitt, I., Bachner, D., Megow, D., Henklein, P., Hameister, H., Epplen, J. T. and Riess, O.,** Expression of the Huntington disease gene in rodents: cloning the rat homologue and evidence for downregulation in non-neuronal tissues during development. *Hum Mol Genet* 1995. **4**: 1173-1182.

112 **Lumsden, A. L., Henshall, T. L., Dayan, S., Lardelli, M. T. and Richards, R. I.,** Huntingtin-deficient zebrafish exhibit defects in iron utilization and development. *Hum Mol Genet* 2007.

113 **Roush, W.,** Nobel prizes: fly development work bears prize-winning fruit. *Science* 1995. **270**: 380-381.

114 **Nusslein-Volhard, C. and Wieschaus, E.,** Mutations affecting segment number and polarity in Drosophila. *Nature* 1980. **287**: 795-801.

115 **Hekimi, S., Boutis, P. and Lakowski, B.,** Viable maternal-effect mutations that affect the development of the nematode Caenorhabditis elegans. *Genetics* 1995. **141**: 1351-1364.

116 **De Robertis, E. M. and Sasai, Y.,** A common plan for dorsoventral patterning in Bilateria. *Nature* 1996. **380**: 37-40.

117 **Ingham, P. W.,** Signalling by hedgehog family proteins in Drosophila and vertebrate development. *Curr Opin Genet Dev* 1995. **5**: 492-498.

118 **Henshall, T. L., Tucker, B., Lumsden, A. L., Nornes, S., Lardelli, M. T. and Richards, R. I.,** Selective neuronal requirement for Huntingtin in the developing zebrafish. *Hum Mol Genet* 2009.

119 **Turner, D. L. and Weintraub, H.,** Expression of achaete-scute homolog 3 in Xenopus embryos converts ectodermal cells to a neural fate. *Genes Dev* 1994. **8**: 1434-1447.

120 **Oxtoby, E. and Jowett, T.,** Cloning of the zebrafish krox-20 gene (krx-20) and its expression during hindbrain development. *Nucleic Acids Res* 1993. **21**: 1087-1095.

121 **Moens, C. B., Yan, Y. L., Appel, B., Force, A. G. and Kimmel, C. B.,** valentino: a zebrafish gene required for normal hindbrain segmentation. *Development* 1996. **122**: 3981-3990.

122 **Mori, H., Miyazaki, Y., Morita, T., Nitta, H. and Mishina, M.,** Different spatio-temporal expressions of three otx homeoprotein transcripts during zebrafish embryogenesis. *Brain Res Mol Brain Res* 1994. **27**: 221-231.

123 **Akimenko, M. A., Ekker, M., Wegner, J., Lin, W. and Westerfield, M.,** Combinatorial expression of three zebrafish genes related to distal-less: part of a homeobox gene code for the head. *J Neurosci* 1994. **14**: 3475-3486.

124 **Bessarab, D. A., Chong, S. W. and Korzh, V.,** Expression of zebrafish six1 during sensory organ development and myogenesis. *Dev Dyn* 2004. **230**: 781-786.

125 **Schulte-Merker, S., Hammerschmidt, M., Beuchle, D., Cho, K. W., De Robertis, E. M. and Nusslein-Volhard, C.,** Expression of zebrafish goosecoid and no tail gene products in wild-type and mutant no tail embryos. *Development* 1994. **120**: 843-852.

126 **Schulte-Merker, S., Ho, R. K., Herrmann, B. G. and Nusslein-Volhard, C.,** The protein product of the zebrafish homologue of the mouse T gene is expressed in nuclei of the germ ring and the notochord of the early embryo. *Development* 1992. **116**: 1021-1032.

127 **Yan, Y. L., Hatta, K., Riggleman, B. and Postlethwait, J. H.,** Expression of a type II collagen gene in the zebrafish embryonic axis. *Dev Dyn* 1995. **203**: 363-376.

128 **Maves, L. and Kimmel, C. B.,** Dynamic and sequential patterning of the zebrafish posterior hindbrain by retinoic acid. *Dev Biol* 2005. **285**: 593-605.

129 **Nasevicius, A., Ekker, S,** Effective targeted gene 'knockdown' in zebrafish. *Nature genetics* 2000. **26**: 216-220.

130 **Westerfield, M.,** *The Zebrafish Book: A guide to the laboratory use of Zebrafish (Danio rerio)*, 3rd Edn. University of Oregon Press,, Eugene: 1995.

131 **Sambrook, J., Fritsch, E. and Maniatis, T,** *Molecular cloning: A laboratory manual*, 2nd Edn. Cold spring harbour laboratory press: 1989.

132 **Abrams, J. M., White, K., Fessler, L. I. and Steller, H.,** Programmed cell death during Drosophila embryogenesis. *Development* 1993. **117**: 29-43.

133 **Li, L. and Dowling, J. E.,** A dominant form of inherited retinal degeneration caused by a non-photoreceptor cell-specific mutation. *Proc Natl Acad Sci U S A* 1997. **94**: 11645-11650.

134 **Whitlock, K. E. and Westerfield, M.,** A transient population of neurons pioneers the olfactory pathway in the zebrafish. *J Neurosci* 1998. **18**: 8919-8927.

135 **Collazo, A., Fraser, S. E. and Mabee, P. M.,** A dual embryonic origin for vertebrate mechanoreceptors. *Science* 1994. **264**: 426-430.

136 **Whitfield, T. T., Granato, M., van Eeden, F. J., Schach, U., Brand, M., Furutani-Seiki, M., Haffter, P., Hammerschmidt, M., Heisenberg, C. P., Jiang, Y. J., Kane, D. A., Kelsh, R. N., Mullins, M. C., Odenthal, J. and Nusslein-Volhard, C.,** Mutations affecting development of the zebrafish inner ear and lateral line. *Development* 1996. **123**: 241-254.

137 **Harris, J. A., Cheng, A. G., Cunningham, L. L., MacDonald, G., Raible, D. W. and Rubel, E. W.,** Neomycin-induced hair cell death and rapid regeneration in the lateral line of zebrafish (Danio rerio). *J Assoc Res Otolaryngol* 2003. **4**: 219-234.

138 **Jowett, T.,** Double in situ hybridization techniques in zebrafish. *Methods* 2001. **23**: 345-358.

139 **Tang, R., Dodd, A., Lai, D., McNabb, W. C. and Love, D. R.,** Validation of zebrafish (Danio rerio) reference genes for quantitative real-time RT-PCR normalization. *Acta Biochim Biophys Sin (Shanghai)* 2007. **39**: 384-390.

140 **Ekker, S. C. and Larson, J. D.,** Morphant technology in model developmental systems. *Genesis* 2001. **30**: 89-93.

141 **Summerton, J.,** Morpholino antisense oligomers: the case for an RNase H-independent structural type. *Biochim Biophys Acta* 1999. **1489**: 141-158.

142 **Stein, D., Foster, E., Huang, S. B., Weller, D. and Summerton, J.,** A specificity comparison of four antisense types: morpholino, 2'-O-methyl RNA, DNA, and phosphorothioate DNA. *Antisense Nucleic Acid Drug Dev* 1997. **7**: 151-157.

143 **Summerton, J., Stein, D., Huang, S. B., Matthews, P., Weller, D. and Partridge, M.,** Morpholino and phosphorothioate antisense oligomers compared in cell-free and in-cell systems. *Antisense Nucleic Acid Drug Dev* 1997. **7**: 63-70.

144 **Summerton, J. and Weller, D.,** Morpholino antisense oligomers: design, preparation, and properties. *Antisense Nucleic Acid Drug Dev* 1997. **7**: 187-195.

145 **Heasman, J.,** Morpholino oligos: making sense of antisense? *Dev Biol* 2002. **243**: 209-214.

146 **Borrell-Pages, M., Zala, D., Humbert, S. and Saudou, F.,** Huntington's disease: from huntingtin function and dysfunction to therapeutic strategies. *Cell Mol Life Sci* 2006. **63**: 2642-2660.

147 **Kawakami, K., Takeda, H., Kawakami, N., Kobayashi, M., Matsuda, N. and Mishina, M.,** A transposon-mediated gene trap approach identifies developmentally regulated genes in zebrafish. *Dev Cell* 2004. **7**: 133-144.

148 **Urasaki, A., Morvan, G. and Kawakami, K.,** Functional dissection of the Tol2 transposable element identified the minimal cis-sequence and a highly repetitive sequence in the subterminal region essential for transposition. *Genetics* 2006. **174**: 639-649.

149 **Darzynkiewicz, Z., Bruno, S., Del Bino, G., Gorczyca, W., Hotz, M. A., Lassota, P. and Traganos, F.,** Features of apoptotic cells measured by flow cytometry. *Cytometry* 1992. **13**: 795-808.

150 **Rodriguez, M. and Driever, W.,** Mutations resulting in transient and localized degeneration in the developing zebrafish brain. *Biochem Cell Biol* 1997. **75**: 579-600.

151 **Barrallo-Gimeno, A., Holzschuh, J., Driever, W. and Knapik, E. W.,** Neural crest survival and differentiation in zebrafish depends on mont blanc/tfap2a gene function. *Development* 2004. **131**: 1463-1477.

152 **Hill, A., Howard, C. V., Strahle, U. and Cossins, A.,** Neurodevelopmental defects in zebrafish (Danio rerio) at environmentally relevant dioxin (TCDD) concentrations. *Toxicol Sci* 2003. **76**: 392-399.

153 **Furutani-Seiki, M., Jiang, Y. J., Brand, M., Heisenberg, C. P., Houart, C., Beuchle, D., van Eeden, F. J., Granato, M., Haffter, P., Hammerschmidt, M., Kane, D. A., Kelsh, R. N., Mullins, M. C., Odenthal, J. and Nusslein-Volhard, C.,** Neural degeneration mutants in the zebrafish, Danio rerio. *Development* 1996. **123**: 229-239.

154 **Guo, Y., Cheong, N., Zhang, Z., De Rose, R., Deng, Y., Farber, S. A., Fernandes-Alnemri, T. and Alnemri, E. S.,** Tim50, a component of the mitochondrial translocator, regulates mitochondrial integrity and cell death. *J Biol Chem* 2004. **279**: 24813-24825.

155 **Parng, C.,** In vivo zebrafish assays for toxicity testing. *Curr Opin Drug Discov Devel* 2005. **8**: 100-106.

156 **Parng, C., Anderson, N., Ton, C. and McGrath, P.,** Zebrafish apoptosis assays for drug discovery. *Methods Cell Biol* 2004. **76**: 75-85.

157 **Ton, C., Lin, Y. and Willett, C.,** Zebrafish as a model for developmental neurotoxicity testing. *Birth Defects Res A Clin Mol Teratol* 2006. **76**: 553-567.

158 **Cole, L. K. and Ross, L. S.,** Apoptosis in the developing zebrafish embryo. *Dev Biol* 2001. **240**: 123-142.

159 **Stein, B. E., Meredith, M.A.,** *The Merging of the Senses*. MIT Press, Cambridge, Massachusetts: 1993.

160 **Knudsen, E. I.,** Auditory and visual maps of space in the optic tectum of the owl. *J Neurosci* 1982. **2**: 1177-1194.

161 **Farbman, A. I.,** Developmental biology of olfactory sensory neurons. *Semin Cell Biol* 1994. **5**: 3-10.

162 **Celik, A., Fuss, S. H. and Korsching, S. I.,** Selective targeting of zebrafish olfactory receptor neurons by the endogenous OMP promoter. *Eur J Neurosci* 2002. **15**: 798-806.

163 **Dambly-Chaudiere, C., Sapede, D., Soubiran, F., Decorde, K., Gompel, N. and Ghysen, A.,** The lateral line of zebrafish: a model system for the analysis of morphogenesis and neural development in vertebrates. *Biol Cell* 2003. **95**: 579-587.

164 **Williams, J. A. and Holder, N.,** Cell turnover in neuromasts of zebrafish larvae. *Hear Res* 2000. **143**: 171-181.

165 **Piotrowski, T., Schilling, T. F., Brand, M., Jiang, Y. J., Heisenberg, C. P., Beuchle, D., Grandel, H., van Eeden, F. J., Furutani-Seiki, M., Granato, M., Haffter, P., Hammerschmidt, M., Kane, D. A., Kelsh, R. N., Mullins, M. C., Odenthal, J., Warga, R. M. and Nusslein-Volhard, C.,** Jaw and

branchial arch mutants in zebrafish II: anterior arches and cartilage differentiation. *Development* 1996. **123**: 345-356.

166 **Neuhauss, S. C., Solnica-Krezel, L., Schier, A. F., Zwartkruis, F., Stemple, D. L., Malicki, J., Abdelilah, S., Stainier, D. Y. and Driever, W.,** Mutations affecting craniofacial development in zebrafish. *Development* 1996. **123**: 357-367.

167 **Schilling, T. F., Piotrowski, T., Grandel, H., Brand, M., Heisenberg, C. P., Jiang, Y. J., Beuchle, D., Hammerschmidt, M., Kane, D. A., Mullins, M. C., van Eeden, F. J., Kelsh, R. N., Furutani-Seiki, M., Granato, M., Haffter, P., Odenthal, J., Warga, R. M., Trowe, T. and Nusslein-Volhard, C.,** Jaw and branchial arch mutants in zebrafish I: branchial arches. *Development* 1996. **123**: 329-344.

168 **Metzler, M., Helgason, C. D., Dragatsis, I., Zhang, T., Gan, L., Pineault, N., Zeitlin, S. O., Humphries, R. K. and Hayden, M. R.,** Huntingtin is required for normal hematopoiesis. *Hum Mol Genet* 2000. **9**: 387-394.

169 **Metzler, M., Chen, N., Helgason, C. D., Graham, R. K., Nichol, K., McCutcheon, K., Nasir, J., Humphries, R. K., Raymond, L. A. and Hayden, M. R.,** Life without huntingtin: normal differentiation into functional neurons. *J Neurochem* 1999. **72**: 1009-1018.

170 **Nordin, S., Paulsen, J. S. and Murphy, C.,** Sensory- and memory-mediated olfactory dysfunction in Huntington's disease. *J Int Neuropsychol Soc* 1995. **1**: 281-290.

171 **Moberg, P. J. and Doty, R. L.,** Olfactory function in Huntington's disease patients and at-risk offspring. *Int J Neurosci* 1997. **89**: 133-139.

172 **Hamilton, J. M., Murphy, C. and Paulsen, J. S.,** Odor detection, learning, and memory in Huntington's disease. *J Int Neuropsychol Soc* 1999. **5**: 609-615.

173 **Pirogovsky, E., Gilbert, P. E., Jacobson, M., Peavy, G., Wetter, S., Goldstein, J., Corey-Bloom, J. and Murphy, C.,** Impairments in source memory for olfactory and visual stimuli in preclinical and clinical stages of Huntington's disease. *J Clin Exp Neuropsychol* 2007. **29**: 395-404.

174 **Moberg, P. J., Pearlson, G. D., Speedie, L. J., Lipsey, J. R., Strauss, M. E. and Folstein, S. E.,** Olfactory recognition: differential impairments in early and late Huntington's and Alzheimer's diseases. *J Clin Exp Neuropsychol* 1987. **9**: 650-664.

175 **Bylsma, F. W., Moberg, P. J., Doty, R. L. and Brandt, J.,** Odor identification in Huntington's disease patients and asymptomatic gene carriers. *J Neuropsychiatry Clin Neurosci* 1997. **9**: 598-600.

176 **Lazic, S. E., Goodman, A. O., Grote, H. E., Blakemore, C., Morton, A. J., Hannan, A. J., van Dellen, A. and Barker, R. A.,** Olfactory abnormalities in Huntington's disease: decreased plasticity in the primary olfactory cortex of R6/1 transgenic mice and reduced olfactory discrimination in patients. *Brain Res* 2007. **1151**: 219-226.

177 **Hardt, P.,** Is Loss of Hearing Caused by HD? Huntington's Disease Advocacy Centre 2005.

178 **NINDS,** Huntington's Disease: Hope Through Research. National Institute of Neurological Disorders and Stroke, National Institutes of Health, Bethesda, MD 2007.

179 **Petrasch-Parwez, E., Habbes, H. W., Weickert, S., Lobbecke-Schumacher, M., Striedinger, K., Wieczorek, S., Dermietzel, R. and Epplen, J. T.,** Fine-structural analysis and connexin expression in the retina of a transgenic model of Huntington's disease. *J Comp Neurol* 2004. **479**: 181-197.

180 **Helmlinger, D., Yvert, G., Picaud, S., Merienne, K., Sahel, J., Mandel, J. L. and Devys, D.,** Progressive retinal degeneration and dysfunction in R6 Huntington's disease mice. *Hum Mol Genet* 2002. **11**: 3351-3359.

181 **Petrasch-Parwez, E., Saft, C., Schlichting, A., Andrich, J., Napirei, M., Arning, L., Wieczorek, S., Dermietzel, R. and Epplen, J. T.,** Is the retina affected in Huntington disease? *Acta Neuropathol (Berl)* 2005. **110**: 523-525.

182 **Farrer, L. A. and Meaney, F. J.,** An anthropometric assessment of Huntington's disease patients and families. *Am J Phys Anthropol* 1985. **67**: 185-194.

183 **Grandel, H., Lun, K., Rauch, G. J., Rhinn, M., Piotrowski, T., Houart, C., Sordino, P., Kuchler, A. M., Schulte-Merker, S., Geisler, R., Holder, N., Wilson, S. W. and Brand, M.,** Retinoic acid signalling in the zebrafish embryo is necessary during pre-segmentation stages to pattern the anterior-posterior axis of the CNS and to induce a pectoral fin bud. *Development* 2002. **129**: 2851-2865.

184 **Depew, M. J., Simpson, C. A., Morasso, M. and Rubenstein, J. L.,** Reassessing the Dlx code: the genetic regulation of branchial arch skeletal pattern and development. *J Anat* 2005. **207**: 501-561.

185 **Yohrling, G. J., Farrell, L. A., Hollenberg, A. N. and Cha, J. H.,** Mutant huntingtin increases nuclear corepressor function and enhances ligand-dependent nuclear hormone receptor activation. *Mol Cell Neurosci* 2003. **23**: 28-38.

186 **Basch, M. L., Garcia-Castro, M. I. and Bronner-Fraser, M.,** Molecular mechanisms of neural crest induction. *Birth Defects Res C Embryo Today* 2004. **72**: 109-123.

187 **Le Douarin, N. M. a. K., C.,** *The Neural crest*, 2 Edn. Cambridge University Press, New York, N.Y.: 1999.

188 **Noden, D. M.,** The role of the neural crest in patterning of avian cranial skeletal, connective, and muscle tissues. *Dev Biol* 1983. **96**: 144-165.

189 **Couly, G. F., Coltey, P. M. and Le Douarin, N. M.,** The triple origin of skull in higher vertebrates: a study in quail-chick chimeras. *Development* 1993. **117**: 409-429.

190 **Couly, G. F., Coltey, P. M. and Le Douarin, N. M.,** The developmental fate of the cephalic mesoderm in quail-chick chimeras. *Development* 1992. **114**: 1-15.

191 **Trainor, P. A., Tan, S. S. and Tam, P. P.,** Cranial paraxial mesoderm: regionalisation of cell fate and impact on craniofacial development in mouse embryos. *Development* 1994. **120**: 2397-2408.

192 **McKeown, S. J., Newgreen, D. F. and Farlie, P. G.,** Dlx2 over-expression regulates cell adhesion and mesenchymal condensation in ectomesenchyme. *Dev Biol* 2005. **281**: 22-37.

193 **Vandenberg, P., Khillan, J. S., Prockop, D. J., Helminen, H., Kontusaari, S. and Ala-Kokko, L.,** Expression of a partially deleted gene of human type II procollagen (COL2A1) in transgenic mice produces a chondrodysplasia. *Proc Natl Acad Sci U S A* 1991. **88**: 7640-7644.

194 **Yan, Y. L., Miller, C. T., Nissen, R. M., Singer, A., Liu, D., Kirn, A., Draper, B., Willoughby, J., Morcos, P. A., Amsterdam, A., Chung, B. C., Westerfield, M., Haffter, P., Hopkins, N., Kimmel, C. and Postlethwait, J. H.,** A zebrafish sox9 gene required for cartilage morphogenesis. *Development* 2002. **129**: 5065-5079.

195 **Diekmann, H., Anichtchik, O., Fleming, A., Futter, M., Goldsmith, P., Roach, A. and Rubinsztein, D. C.,** Decreased BDNF levels are a major contributor to the embryonic phenotype of huntingtin knockdown zebrafish. *J Neurosci* 2009. **29**: 1343-1349.

196 **Lumsden, A., Sprawson, N. and Graham, A.,** Segmental origin and migration of neural crest cells in the hindbrain region of the chick embryo. *Development* 1991. **113**: 1281-1291.

197 **Trainor, P. A. and Krumlauf, R.,** Hox genes, neural crest cells and branchial arch patterning. *Curr Opin Cell Biol* 2001. **13**: 698-705.

198 **Hall, B. K.,** Development of the mandibular skeleton in the embryonic chick as evaluated using the DNA-inhibiting agent 5-fluoro-2'-deoxyuridine. *J Craniofac Genet Dev Biol* 1987. **7**: 145-159.

199 **Hall, B. K.,** Tissue interactions and the initiation of osteogenesis and chondrogenesis in the neural crest-derived mandibular skeleton of the embryonic mouse as seen in isolated murine tissues and in recombinations of murine and avian tissues. *J Embryol Exp Morphol* 1980. **58**: 251-264.

200 **Epperlein, H. H.,** The ectomesenchymal-endodermal interaction-system (EEIS) of Triturus alpestris in tissue culture. I. Observations on attachment, migration and differentiation of neural crest cells. *Differentiation* 1974. **2**: 151-168.

201 **Trevarrow, B., Marks, D. L. and Kimmel, C. B.,** Organization of hindbrain segments in the zebrafish embryo. *Neuron* 1990. **4**: 669-679.

202 **Piotrowski, T. and Nusslein-Volhard, C.,** The endoderm plays an important role in patterning the segmented pharyngeal region in zebrafish (Danio rerio). *Dev Biol* 2000. **225**: 339-356.

203 **Bhattacharyya, S., Bailey, A. P., Bronner-Fraser, M. and Streit, A.,** Segregation of lens and olfactory precursors from a common territory: cell sorting and reciprocity of Dlx5 and Pax6 expression. *Dev Biol* 2004. **271**: 403-414.

204 **Carpenter, E.,** The head pattern in *Amblystoma* studied by vital staining and transplantation methods. *Journal of Experimental Zoology* 1937. **75**: 103-126.

205 **Kozlowski, D. J., Murakami, T., Ho, R. K. and Weinberg, E. S.,** Regional cell movement and tissue patterning in the zebrafish embryo revealed by fate mapping with caged fluorescein. *Biochem Cell Biol* 1997. **75**: 551-562.

206 **Streit, A.,** Extensive cell movements accompany formation of the otic placode. *Dev Biol* 2002. **249**: 237-254.

207 **Baker, C. V. and Bronner-Fraser, M.,** Vertebrate cranial placodes I. Embryonic induction. *Dev Biol* 2001. **232**: 1-61.

208 **Schlosser, G.,** Development and evolution of lateral line placodes in amphibians I. Development. *Zoology (Jena)* 2002. **105**: 119-146.

209 **Schlosser, G.,** Evolutionary origins of vertebrate placodes: insights from developmental studies and from comparisons with other deuterostomes. *J Exp Zoolog B Mol Dev Evol* 2005. **304**: 347-399.

210 **Schlosser, G.,** Induction and specification of cranial placodes. *Dev Biol* 2006. **294**: 303-351.

211 **Streit, A.,** Early development of the cranial sensory nervous system: from a common field to individual placodes. *Dev Biol* 2004. **276**: 1-15.

212 **Brugmann, S. A. and Moody, S. A.,** Induction and specification of the vertebrate ectodermal placodes: precursors of the cranial sensory organs. *Biol Cell* 2005. **97**: 303-319.

213 **Bailey, A. P. and Streit, A.,** Sensory organs: making and breaking the pre-placodal region. *Curr Top Dev Biol* 2006. **72**: 167-204.

214 **Toro, S. and Varga, Z. M.,** Equivalent progenitor cells in the zebrafish anterior preplacodal field give rise to adenohypophysis, lens, and olfactory placodes. *Semin Cell Dev Biol* 2007. **18**: 534-542.

215 **Dutta, S., Dietrich, J. E., Aspock, G., Burdine, R. D., Schier, A., Westerfield, M. and Varga, Z. M.,** pitx3 defines an equivalence domain for lens and anterior pituitary placode. *Development* 2005. **132**: 1579-1590.

216 **Whitlock, K. E. and Westerfield, M.,** The olfactory placodes of the zebrafish form by convergence of cellular fields at the edge of the neural plate. *Development* 2000. **127**: 3645-3653.

217 **Simeone, A., Gulisano, M., Acampora, D., Stornaiuolo, A., Rambaldi, M. and Boncinelli, E.,** Two vertebrate homeobox genes related to the Drosophila empty spiracles gene are expressed in the embryonic cerebral cortex. *Embo J* 1992. **11**: 2541-2550.

218 **Morita, T., Nitta, H., Kiyama, Y., Mori, H. and Mishina, M.,** Differential expression of two zebrafish emx homeoprotein mRNAs in the developing brain. *Neurosci Lett* 1995. **198**: 131-134.

219 **Kawahara, A. and Dawid, I. B.,** Developmental expression of zebrafish emx1 during early embryogenesis. *Gene Expr Patterns* 2002. **2**: 201-206.

220 **Solnica-Krezel, L.,** Conserved patterns of cell movements during vertebrate gastrulation. *Curr Biol* 2005. **15**: R213-228.

221 **Stern, B.** (Ed.) *From Cells to Embryo*, 1 Edn. Cold Spring Harbour Laboratory, New York 2004.

222 **Kanki, J. P. and Ho, R. K.,** The development of the posterior body in zebrafish. *Development* 1997. **124**: 881-893.

223 **Agathon, A., Thisse, C. and Thisse, B.,** The molecular nature of the zebrafish tail organizer. *Nature* 2003. **424**: 448-452.

224 **Essner, J. J., Amack, J. D., Nyholm, M. K., Harris, E. B. and Yost, H. J.,** Kupffer's vesicle is a ciliated organ of asymmetry in the zebrafish embryo that initiates left-right development of the brain, heart and gut. *Development* 2005. **132**: 1247-1260.

225 **Thomas, P. and Beddington, R.,** Anterior primitive endoderm may be responsible for patterning the anterior neural plate in the mouse embryo. *Curr Biol* 1996. **6**: 1487-1496.

226 **Brewster, R. and Dahmane, N.,** Getting a-head of the organizer: anterior-posterior patterning of the forebrain. *Bioessays* 1999. **21**: 631-636.

227 **Thisse, C., Thisse, B., Halpern, M. E. and Postlethwait, J. H.,** Goosecoid expression in neurectoderm and mesendoderm is disrupted in zebrafish cyclops gastrulas. *Dev Biol* 1994. **164**: 420-429.

228 **Ahrens, K. and Schlosser, G.,** Tissues and signals involved in the induction of placodal Six1 expression in Xenopus laevis. *Dev Biol* 2005. **288**: 40-59.

229 **Henshall, T. L., Tucker, B., Lumsden, A. L., Nornes, S., Lardelli, M. T. and Richards, R. I.,** Selective neuronal requirement for huntingtin in the developing zebrafish. *Hum Mol Genet* 2009. **18**: 4830-4842.

230 **Hodgson, J. G., Agopyan, N., Gutekunst, C. A., Leavitt, B. R., LePiane, F., Singaraja, R., Smith, D. J., Bissada, N., McCutcheon, K., Nasir, J., Jamot, L., Li, X. J., Stevens, M. E., Rosemond, E., Roder, J. C., Phillips, A. G., Rubin, E. M., Hersch, S. M. and Hayden, M. R.,** A YAC mouse model for Huntington's disease with full-length mutant huntingtin, cytoplasmic toxicity, and selective striatal neurodegeneration. *Neuron* 1999. **23**: 181-192.

231 **Hall, B. K. and Ekanayake, S.,** Effects of growth factors on the differentiation of neural crest cells and neural crest cell-derivatives. *Int J Dev Biol* 1991. **35**: 367-387.

STATEMENT OF AUTHORSHIP

SELECTIVE NEURONAL REQUIREMENT FOR HUNTINGTIN IN THE DEVELOPING ZEBRAFISH

Tanya L. Henshall, Ben Tucker, Amanda L. Lumsden, Svanhild Nornes, Michael T. Lardelli and Robert I. Richards

ARC Special Research Centre for the Molecular Genetics of Development and Discipline of Genetics, School of Molecular and Biomedical Sciences, The University of Adelaide, Adelaide SA, 5005, Australia

Human Molecular Genetics – 2009, 18: 4830-4842

Tanya Henshall (Candidate)

Performed analysis on all samples, and all data interpretation (except BDNF rescue of lateral line neuromast phenotype). Wrote manuscript.

Certification that the statement of contribution is accurate.

Signed……Date……

Ben Tucker

Carried out BDNF rescue of lateral line neuromast phenotype and its associated data analysis. Drew fate and expression maps included in Figure 2.

Certification that the statement of contribution is accurate and permission is given for the inclusion of the paper in the thesis.

Signed.....*Date*.....

Ben Tucker

Carried out BDNF rescue of lateral line neuromast phenotype and its associated data analysis. Drew fate and expression maps included in Figure 2.

Certification that the statement of contribution is accurate and permission is given for the inclusion of the paper in the thesis.

Signed.....*Date*.....

Amanda Lumsden

Helped in data interpretation and provided critical evaluation of the manuscript.

Certification that the statement of contribution is accurate and permission is given for the inclusion of the paper in the thesis.

Signed.....*Date*.....

Amanda Lumsden

Helped in data interpretation and provided critical evaluation of the manuscript.

Certification that the statement of contribution is accurate and permission is given for the inclusion of the paper in the thesis.

Signed.....*Date*.....

Svanhild Nornes

Carried out data analysis and provided critical evaluation of the manuscript.

Certification that the statement of contribution is accurate and permission is given for the inclusion of the paper in the thesis.

Signed.....*Date*.....

Svanhild Nornes

Carried out data analysis and provided critical evaluation of the manuscript.

Certification that the statement of contribution is accurate and permission is given for the inclusion of the paper in the thesis.

Signed.....*Date*.....

Michael Lardelli

Supervised development of work, and helped in data interpretation and manuscript evaluation.

Certification that the statement of contribution is accurate and permission is given for the inclusion of the paper in the thesis.

Signed……Date……

Robert Richards

Supervised development of work, and helped in data interpretation and manuscript evaluation.

Acted as corresponding author.

Certification that the statement of contribution is accurate and permission is given for the inclusion of the paper in the thesis.

Signed……Date……

Henshall, T.L., Tucker, B., Lumsden, A.L., Nornes, S., Lardelli, M.T. and Richards, R.I. (2009) Selective neuronal requirement for huntingtin in the developing zebrafish.
Human Molecular Genetics, v.18 (24), pp. 4830-4842, September 2009

Love to my two beautiful nephews,(one of whom I am yet to meet).

Jordan, sweety, its done! Thank you for being patient with me.

AMENDMENTS TO THESIS

Page 11 Line 20

To provide a more accurate description of Wolf-Hirschhorn syndrome and the associated balanced translocation often found in parents of Wolf-Hirschhorn patients, the following sentence should be deleted:
'Deletion of one allele of *HTT* (as seen in Wolf-Hirschhorn syndrome) does not result in HD-like pathology in humans'.

The below passage then should be inserted in place of the deleted sentence:
'It has been observed that, in humans, hemizygous inactivation of one of the two *HTT* genes does not cause an HD phenotype. Loss of one allele of *HTT* has been known to occur as a result of either a terminal deletion of one copy of chromosome 4 (which includes the *HTT* gene) in patients with Wolf-Hirschhorn syndrome [232], or of a balanced translocation with a break point between exons 40 and 41, physically disrupting one of the *HTT* gene copies in one female [233, 234]. In these cases, loss of one allele of *HTT* does not result in HD-like pathology in humans'.

References:

232 **Harper, P. S.,** *Huntington's Disease*: W. B. Saunders, London, ed. 2: 1996.

233 **Ambrose, C. M., Duyao, M. P., Barnes, G., Bates, G. P., Lin, C. S., Srinidhi, J., Baxendale, S., Hummerich, H., Lehrach, H., Altherr, M., Wasmuth, J., Buckler, A., Church, D., Housman, D., Berks, M., Micklem, G., Durbin, R., Dodge, A., Read, A., Gusella, J. and MacDonald, M. E.,** Structure and expression of the Huntington's Disease gene: Evidence against simple inactivation due to an expanded CAG repeat. *Somat Cell Mol Genet* 1994. **20**: 27-38.

234 **Rubinsztein, D. C.,** How does the Huntington's disease mutation damage cells? *Sci Aging Knowledge Environ* 2003. **2003**: PE26.

Page 2 Line 4

A recent description of CAG repeat length instability and HD penetrance has become available. This reference attempts to predict the rate of *de novo* cases of HD arising from paternal transmission of a high normal allele with 27-35 CAG repeats [235].

Reference:

235 **Hendricks, A. E., Latourelle, J. C., Lunetta, K. L., Cupples, L. A., Wheeler, V., MacDonald, M. E., Gusella, J. F. and Myers R. H.,** Estimating the probability of de novo HD cases from transmissions of expanded penetrant CAG alleles in the Huntington disease gene from male carriers of high normal alleles (27-35 CAG). *Am J Med Genet Part A* 2009. **149A**: 1375-1381.